International Journal of Antennas and Propagation

RFID Technology and Applications

Guest Editors: Xiaodong Chen, Junsheng Yu, Yuan Yao, Chaowei Wang, and Daniel Valderas

RFID Technology and Applications

International Journal of Antennas and Propagation

RFID Technology and Applications

Guest Editors: Xiaodong Chen, Junsheng Yu, Yuan Yao, Chaowei Wang, and Daniel Valderas

Editorial Board

Contents

Hindawi Publishing Corporation
International Journal of Antennas and Propagation
Volume 2014, Article ID 184934, 1 page
http://dx.doi.org/10.1155/2014/184934

Editorial
RFID Technology and Applications

Xiaodong Chen,[1] Junsheng Yu,[2] Yuan Yao,[2] Chaowei Wang,[2] and Daniel Valderas[3]

[1] *School of Electronic Engineering and Computer Science, Queen Mary University of London, London E14NS, UK*
[2] *School of Electronic Engineering, Beijing University of Posts and Telecommunications, Beijing 100876, China*
[3] *Department of Electronics and Communications, University of Navarra, 31080 Navarra, Spain*

Correspondence should be addressed to Xiaodong Chen; xiaodong.chen@eecs.qmul.ac.uk

Received 9 April 2014; Accepted 9 April 2014; Published 28 April 2014

RFID is emerging as one of most fundamental technologies to Internet of Things due to its attractive features such as good reading ranges, high data rates, and low cost. RFID has achieved a widespread success in various applications, ranging from asset tracking, highway toll collection, supply chain management, animal identification to surveillance systems. Moreover, there has been a wide scope of development in RFID standards, protocols, and middleware. However, a series of challenging issues should be properly addressed before a massive adaptation of RFID technology.

In this special issue, we have received 24 paper submissions and accepted 9 papers finally according to the reviewers' comment and associate editors' suggestion. These accepted papers include RFID reader antenna design, RFID tag antenna design, RFID passive transponders, tag collision algorithm, and RFID application systems.

B. Lee et al. from Kwangwoon University of Korea proposed a novel structure of an NFC loop antenna for mobile handset applications by improving the performance of an NFC loop antenna when a ferrite-polymer composite is attached between the embedded NFC loop antenna and the phone battery. The proposed loop antenna gives better performance than that of a conventional NFC loop antenna.

L. X. Zheng et al. from South China University of Technology proposed a compact RFID reader antenna for UHF near-field and far-field operations. The structure of the antenna is a novel folded-dipole loop and is formed by a concentric metal ring with a split. It can provide uniform magnetic near-field distribution and available far-field gain. Y. Yao et al. from Beijing University of Posts and Telecommunications also proposed a novel RFID reader antenna. This antenna was fabricated using indium tin oxide film; thus, it has optically transparent characteristic. This kind of antenna can be used in clothing stores.

P. Jankowski-Mihulowicz et al. from Rzeszów University of Technology proposed novel RFID passive transponders with additional energy harvester. They can recover energy from the electromagnetic field of read device and the harvested energy was utilized to supply a microprocessor acquisition block for developed LTCC pressure sensor.

C. Wang et al. from Beijing University of Posts and Telecommunications proposed an advanced dynamic framed-slotted ALOHA algorithm based on Bayesian estimation and probability response to solve the tag collision problem of RFID system. The simulation results show that the proposed algorithm has better performance.

We sincerely hope that this special issue can further help the readers to understand RFID antenna design and applications and explore the future development of the system.

Xiaodong Chen
Junsheng Yu
Yuan Yao
Chaowei Wang
Daniel Valderas

Hindawi Publishing Corporation
International Journal of Antennas and Propagation
Volume 2014, Article ID 197437, 8 pages
http://dx.doi.org/10.1155/2014/197437

Research Article

RFID Presenter: A New Way to Feel a Talk

Jonathan Ruiz-de-Garibay, Jon Legarda, Szilárd A. Kados, and Xabier Eguiluz

Deusto Institute of Technology, DeustoTech, University of Deusto, 48007 Bilbao, Spain

Correspondence should be addressed to Jonathan Ruiz-de-Garibay; jonathan.garibay@deusto.es

Received 15 November 2013; Accepted 16 January 2014; Published 10 April 2014

Academic Editor: Yuan Yao

RFID is a key which enables technology for the Internet of Things paradigm, allowing the virtualization of the physical objects into the Internet. There are uncountable applications whereby these connected objects can be a breakthrough for new business models, and this work shows a good example of that. We present the RFID Presenter as the evolution of a classical consumer electronic product to a novel connected Internet product with the addition of the RFID technology. It supposes a new way to manage the conference talks in a personalization way, improving the end-user interaction and providing services that were impossible before. The design, implementation, and validation of a real gadget are well explained in order to give a real example of how the Internet of Things can be integrated into daily objects and enhance the end-user experiences.

1. Introduction

This work introduces the design and validation of the RFID Presenter, a new concept of presenter that integrates the radiofrequency identification (RFID) technology into a traditional remote wireless controller for conference and lecture talks. The aim is the addition of new services to the basic presenter functions, keeping the same ergonomic performance without decreasing the usability and enhancing the end-user experience.

The system consists of a conference manager (CM) installed in a personal computer that runs typical desktop applications and the wireless RFID Presenter. It identifies the end-user with a RFID conference card and the CM immediately launches the desktop applications associated with the documents or the multimedia that each user has previously remotely uploaded. The remote file allocation allows the end-user to manage until the last time the required documents and their sharing with the conference audience if it is necessary.

The RFID Presenter controls every action needed for the execution of the applications, the switching between applications, and the end-up of the conference presentation.

The conference manager will be usually installed in a personal computer that makes the gateway between the video projector, the files repository, and the RFID Presenter.

The proposed system architecture is simple and flexible, as it requires a minimum number of elements to maximize the user experience and it is designed to work together with the CM application.

This paper is organized as follows. Section 1 introduces the main scope of the work and the basic characteristics of the proposed solution. A brief related work shows the current presenters and their typical functionalities in Section 2, before describing the system architecture in Section 3. Section 4 goes deep into the hardware, software, and mechanic design of the RFID Presenter and Section 5 does the same with the conference manager application. Finally, Section 6 shows the system validation and the final result discussion, before presenting some conclusions and the proposal of some future work.

2. Related Work

The radio frequency identification emerged as a new contactless identification technology mainly focused on logistic processes, in order to improve their efficiency and cost reduction [1], but it has become the seed of the Internet of Things concept as it has facilitated the presence of the physical world into the digital world [2, 3].

The Internet of Things covers a wide range of applications and technologies, but all of them need some communication

Figure 1: Genius ring presenter.

capability to upload, at least, their ID to the Internet [4]. In the recent years, there have been a large number of gadgets based on RFID that try to break the market, and their acceptance by end-user becomes a priority requirement. The addition of new functionalities to any existing or new gadget must not compromise its usability; otherwise it will not succeed. That is why the design [5] and interaction [6] aspects have become relevant for the research community. Some examples show how to increase the added value of a product personalizing it to the end-user with the use of RFID technology but keeping the usability equal or even improving it [7, 8].

2.1. Presenters. The market offers a wide range of presenters, most of them based on a specific radiofrequency receptor. The complexity of these devices has evolved from multibutton and multifunction gadgets to more simple and user-friendly devices, whereby only the most used actions are available [9–13]. Some curiosities can be found, like the control of the scrolls, the display of the presentation time, or more ergonomic shapes, like in Figure 1.

However, all of them work with traditional presentation tools (i.e., Microsoft PowerPoint), they cannot be configured by the end-user, they have to be launched directly in the computer and above all, and none of them identifies the end-user who holds it.

3. System Architecture

The RFID Presenter is based on the system architecture described in Figure 2 in order to fulfill the functional requirements defined by the use cases described in Figure 3.

The presenter is wirelessly connected to the CM that is allocated in a personal computer (PC), which in turn is connected to a video projector. The document that is going to be used in the presentation can be both in a local or in a remote repository, whatever suits better, despite the fact that this work is validated only in the local use case.

3.1. RFID Presenter. The RFID Presenter is the physical user interface for the execution of the conference/lecture talk; it

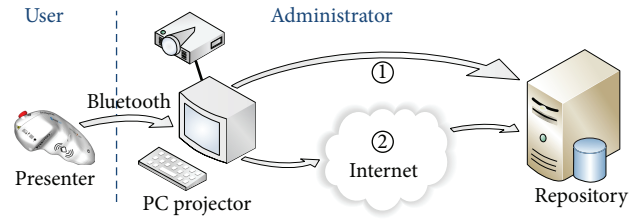

Figure 2: System architecture.

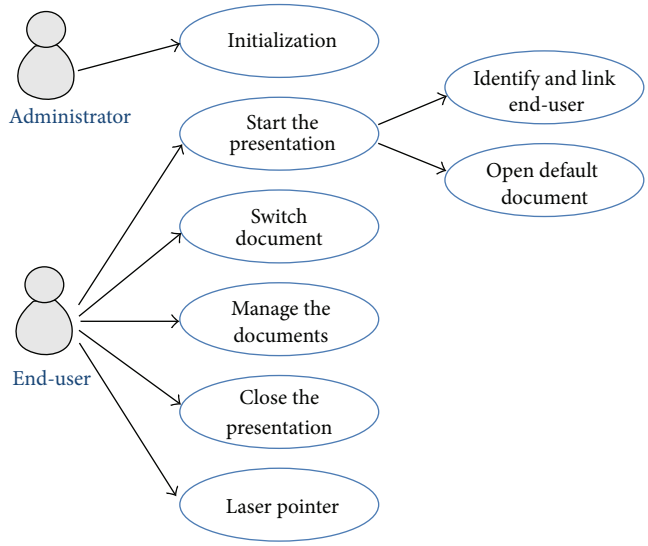

Figure 3: Use cases.

identifies the user ID and transmits all the instructions to the conference manager thorough a wireless link:

(i) identify the user ID with a RFID reader;

(ii) open documents;

(iii) switch between different documents;

(iv) move forward or backward in PowerPoint documents;

(v) play or pause a video file;

(vi) close a presentation.

The aim of the RFID Presenter is the total substitution of the interaction with the personal computer for a conference speaker or a lecturer, and it has to be design accordingly.

3.2. Conference Manager. A personal computer holds the conference manager application that is paired with the associated RFID Presenter. The application is installed and associated once and after that nobody has to interact with it; it runs as a transparent gateway between the RFID Presenter, the project, and the repository.

In the local use case, an administrator has to do the pairing setting and the file association, but in the remote use case the latter can be done by the end-user itself.

3.3. Bluetooth. Selection of wireless communication technology is one of the keys in the system architecture. Two different options have been considered: Wi-Fi and Bluetooth.

Wi-Fi can provide a direct access to the documents in the repository and even to a Wi-Fi Projector. Instead, Wi-Fi transceivers have high energy consumption, it is complicated to set the Wi-Fi settings without external keyboards and screens, and it is necessary high computer capacities for document management.

Bluetooth, however, does not allow a direct access to the documents in the repository and a personal computer is necessary for its connection with the projector, but it has other important advantages like the following:

(i) the ease paring with a PC;

(ii) low price ($10 versus $30);

(iii) the low power performance (30 mA versus 200 mA);

(iv) the low computing requirement;

(v) the high level software libraries.

3.4. Repositories. The document repository can be local or remote. Local documents are saved on the hard disk of the PC, it is the more common use case, and it has been used as the validation scenario.

When documents are saved in a remote repository, all the cloud technologies can be used, like FTP servers, Dropbox, or Google Drive tools. It brings more control for the end-user, more flexibility for last minute changes, and even better diffusion options once talks, conferences, or lectures have been finished.

4. RFID Presenter

This chapter describes the design of the RFID Presenter, the functional and nonfunctional requirement description, hardware and software considerations, and the 3D printing of the mechanical packaging.

The main and novel goal of this project is to integrate the RFID identification to a remote presenter. In any conference, talk or lecture, all speakers can be identified with an identification card, so let us consider that those cards are RFID cards in order to personalize each end-user talk regarding their presentation documents (slides, videos, PDFs, etc.). This is possible integrating a RFID reader to the presenter and transmitting the ID to the CM application.

The system requirements can be described as follows.

(i) The prototype has to be as close as possible to a commercial product: the working group has to make a hard effort in the definition of the requirements to create a prototype that can be compared with other real products.

(ii) The device has to be user-friendly: the presenter is the only input interface between end-user and the projector so the physical design has to be ergonomic but with extended capabilities.

(iii) A presentation can have several documents: the end-user has to be able to switch the document shown to the audience.

(iv) The system has to be able to work continuously during one conference's session: in the worst case, a conference starts in the morning at 8 AM and finishes before the lunch at 2 PM; and in the afternoon it usually spends less time. We specified 12 hours autonomy as the minimum time that it has to run without interruptions.

All of these requirements have been taken into account in the design process. Now they are developed more in depth as the description of the design process.

4.1. Functional Requisites. Analyzing a typical presentation, the main actions that speakers do during a presentation are as follows: to start the presentation with one document, to switch to other documents, to navigate through the document content, and finally to close all the documents. The use of the laser pointer is also very welcome.

On the other hand, the system administrator is the person who has to turn on and initialize the presenter device.

Following the same order of Figure 3, the first function is the *initialization*. This is a function done by the administrator and it pairs the presenter with the PC in the first time; it opens the wireless connection and checks the link between them. In this moment, the system is ready to work.

Start the Presentation. The end-user puts his personal identification card next to the RFID reader. This action will send the ID to the CM. If the identification is correct, the CM loads all the presentation documents assigned to the end-user, and she/he sees only the one she/he chose previously.

Switch Document. One of the added values of the RFID Presenter is the switching capability between different documents. The end-user needs to see all documents in the screen in order to select them according to the talk. To that end, CM has to show a new layer in the projection with extra information that allows seeing the document being selected.

Manage the Documents. This work supports these documents for the validation of the RFID Presenter.

(i) Power Point document: typical presentation document by Microsoft Office. Main actions over this kind of document are move forward and backward.

(ii) PDF document: this document format is a standard between different operative systems so it could be very useful. Actions defined for this document are as follows: go to the next or previous page, move to first or last page, and maybe adjust the document to the width of the display.

(iii) Video file: a video is very useful to show to the audience a demo or a prototype in operating. Play and pause video are basics and controlling the volume would be very interesting if you cannot check the acoustics of the conference room.

Table 1: Defaults functions.

Document	Joystick 5-position				
	Left	Right	Up	Down	Enter
PowerPoint	Go backward	Go forward	[No function]	[No function]	[No function]
PDF document	Go to previous page	Go to next page	Go to first page	Go to last page	Adjust width display
Video file	Move backward	Move forward	Up volume	Down volume	Play/pause
Audio file	Move backward	Move forward	Up volume	Down volume	Play/pause
Flash animation	Key "left"	Key "right"	Key "up"	Key "down"	Key "enter"
Prezi presentation	Go backward	Go forward	Zoom in	Zoom out	[No function]

(iv) Audio file: in this case, we also want to start and pause it; and control the volume of the audio.

(v) Flash animation: in certain areas, a flash animation can be a good way to show experimental results so we include this one with a basic interaction.

(vi) Prezi presentation: one example of novel presentation system so we have integrated this one into conference application. The main actions are move forward, move backward, zoom in, and zoom out.

Close the Presentation. When a speaker finishes his presentation the CM has to include an extra visual layer where speakers can close all the used documents.

Laser Pointer. At any time, the speaker can use a laser pointer to mark any important part of the document shown. This option is really useful to give to the audience a visual reference about the important information.

4.2. Interaction Model. Two viewpoints have been used in the design of the interaction model, a functional and ergonomic viewpoint.

(i) Functional design: the presenter has to execute all the defined functions with the simplest input interaction system.

(ii) Ergonomic design: the presenter has to be comfortable and the interaction has to be as user-friendly as possible.

These two perspectives have to develop together because the user has to sense an immediate value gain with the prototype [6].

The *reading* of the RFID card is done approaching it to the RFID reader of the presenter, and it will be marked with a specific image in order to guarantee a good lecture.

The *switching* and *control* of presentation documents will be done with a digital joystick and five different and clear interactions: turn left, turn right, turn up, turn down, and push joystick when it is in the central position. Joystick will be located at the top of the presenter and can be controller with the thumb finger. In Table 1 all the actions are related with these five joystick interactions.

The switch button indicates the *switch* action, and while it is pushed the joystick sweeps between other documents. If the switch button is released the selected document is reproduced. This button is located on the front of the presenter and can be triggered using the index finder.

Table 2: Interface with the computer.

Function	I/O device	Notify to PC
Initialization	Joystick	Yes
Start the presentation	RFID Reader	Yes
Switch documents	Switch button + Joystick	Yes
Manager the document	Joystick	Yes
Close the presentation	Switch button + Joystick	Yes
Activate laser pointer	Laser button + Laser LED	No

The *closing function* is done with the switch button, including an extra *close session* option as a presentation document. If the end-user selects it all the session is closed.

The *initialization* is done pushing the joystick in the central position when the CM asks for the paring validation.

And finally the *laser pointer*, which is located in the front of the presenter, is controlled with a dedicated button below the switch button.

In summary, the RFID Presenter has one RFID reader, one five-position joystick, two dedicated buttons, and one laser emitter. Table 2 shows the implemented functions with their input/outputs interactions. Note that all functions, but the laser pointer, are transmitted to the CM, as they require to be projected somehow.

The design is completed with an On/Off switch and two LED diodes: one blue that is active when the Bluetooth connection is opened and one green/red that switches when the battery is low.

4.3. 3D Design. The mechanic design of the RFID Presenter must fulfill the two main requirements defined in Section 4.2; it has to be as close as possible to a commercial product and it has to be as user-friendly as possible (Figure 4). Moreover, it must support all the interaction interfaces mentioned before and the intrinsic fabrication limits within the rapid prototyping technology.

The design process has been led by continuous end-user feedbacks over subsequent versions of a rapid prototype that has been developed with a 3D open source printer (300 μm). The aim of these feedbacks has been to prioritize the ergonomic issue while fulfilling the functional and interaction requirements. Three iterations have been done until

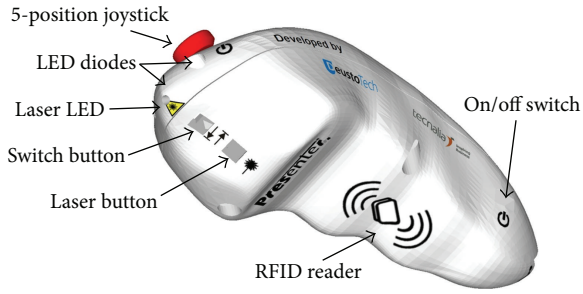

FIGURE 4: Button configuration and 3D design.

the last prototype has been considered acceptable by end-users, which has been printed with an industrial color 3D precision printer (100 μm). Figure 5 shows the evolution from the first design to the final prototype.

4.4. Hardware Architecture. The hardware architecture of the RFID Presenter is shown in Figure 6. It is based on a microcontroller, a power management electronic, I/O peripherals, and a Bluetooth transceiver.

The controller is a PIC 18F2520 chip of Microchip, with 8 bits processor, 32 KB flash memory, 25 IO, I2C and UART hardware communication ports, 3 timers, and so forth.

The battery is a 3.7 V-550 mA/h rechargeable LIPO battery. It can be charged with +5 V, such as a USB port, through MAX1555 integrated circuit; and a simple battery reader, based on a voltage divider, monitors the energy level (the USB port is only used for charge, not for communications). Then, the power is regulated to 3.3 V with a low dropout regulator TPS73133 integrated circuit.

The RFID reader is a SM 125 chip of Sonmicro, which can be read 125 KHz. tags. SM 125 can be controlled over UART port or I2C bus by a controller. In Version 4 of the RFID Presenter we use UART interface.

The joystick is a generic model and data is sent by digital signals to the controller. The *switch button* is an independent peripheral, a pulse switch model that generates one digital signal.

The Bluetooth RF communication is done with an EB301 module of A7 Engineering, and it uses serial communication (UART) between the controller and remote PC.

Finally, the laser pointer is a LM-102-B119 of Wenta Electronic that works independently to the controller and it is activated and deactivated with a pulse switch like switch button.

5. "Conference" Manager (CM)

The conference manager is an easy to use desktop application whose main view is shown in Figure 7. It has three main functions: the interface for the *initialization* process, the communication gateway with the RFID Presenter, and the control use of the documents used in the presentation.

The *initialization* starts with the uploading of all the presentation documents by the end-user. Then the administrator links, on one hand, the identification (ID) of the end-user to the RFID card that will be used in the conference, and on the other hand, the RFID Presenter with the computer connected to the projector. The latter requires the selection of the serial port name, pushing the connect button and confirming over the presenter device. The initialization is finished pushing the *presentation mode* button and setting it in background mode.

The control of the presentation starts as soon as the end-user puts the conference card next to the RFID Presenter. The CM checks the ID in the data base and a successful identification opens the first document, and its associated viewer that the end-user has previously selected.

The activation of the *switch button* launches in the CM the change document menu shown in Figure 8, and the joystick data activates the functions defined in Table 1.

To finalize the presentation, the end-user has to close his session and, for this, he has to reply the change document process but in this case, he has to select the last option *close session* in the menu. In Figure 8 we can see the list of documents and this last option.

In this example the desktop application of Figure 7 shows one option for the *Speaker Management* because this version uses a local repository. When the presentation mode is active, the conference manager runs the process responsible for controlling the user presentation and this process does not know if the documents are in a local or remote repository.

5.1. CM Architecture. The conference manager architecture (shown in Figure 9) is designed for working independently to the local or remote repositories. It has been implemented with Microsoft.NET framework 3.5 with some external libraries. Some SW components will be briefly summarized in the next lines.

Presenter Driver. This component uses a serial port under the Bluetooth protocol to establish the link with the RFID Presenter. When a message arrives to the computer, *Presenter Driver* validates and formats it before notifying the conference manager component.

Repository Manager. The main function of this manager is to isolate the conference manager component for the real repository (local or remote) to guarantee the correct operation of the system with both repository types. In the local repository version, end-user data and document references are saved in a XML file and the documents in a specific folder of the computer.

Viewers. They are launched by the conference manager and they receive the joystick's command. Each kind of document has its own viewer to implement the appropriate interaction. For developing these viewers, we use external libraries and COM components. For example, we use the *Microsoft.Office.Interop.PowerPoint* extension for PPT viewer, *PDFnet* library for PDF viewer, or *Shockwave Flash* COM component for Flash player.

Conference Manager. This component is always waiting for receiving a notification from the *Presenter Driver* with a RFID Presenter message. It executes one or more actions

Figure 5: Version 1 and Version 4 of the prototype.

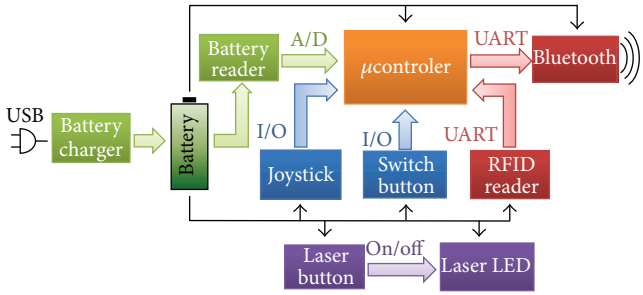

Figure 6: Block diagram.

Figure 7: Conference main form.

Figure 8: Switch document menu.

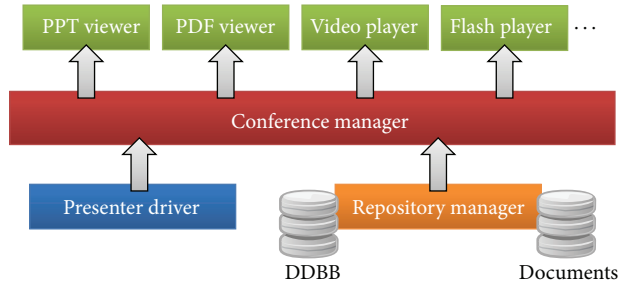

Figure 9: SW components within the conference manager architecture.

over the *viewers* based on the message and the state of the presentation. These actions can be as follows.

(i) Start a new presentation with a new RFID value: get end-user data and documents from the *Repository Manager* and launch the default document viewer.

(ii) Play a joystick command over the present viewer: when the conference manager component receives these kinds of messages, the command will be codified and sent directly to the current viewer. This will identify the joystick's command and execute the desired function.

(iii) Switch document: this action has three phases; the first one is an extra layer with the document list (shown in Figure 8); the second one is the joystick commands for the navigation between them (no acting over the viewers); and the last step is the selection of the new document. In this moment, the conference manager component closes the extra layer and the current viewer and launches a new viewer with the selected document.

(iv) Close the presentation: Finally, the conference manager component closes all viewers and erases the end-user data and the documents from the temporary memory to wait for the next end-user.

In Figure 9, the application data only moves in one direction, bottom-up. This condition can be explained because the inputs of the system are the RFID Presenter and the repository; and the outputs are the viewers.

5.2. Document Viewers. The document viewers and their software design are one of the key parts of this design, and this design is prepared to easily include more document types in the future.

In Figure 10 we can see the simple software architecture for the document viewers. We have defined an interface with only three methods (*Show*, *Hide*, and *ButtonPressed*) that all document viewers have to implement. The conference manager component always works onto this interface and it

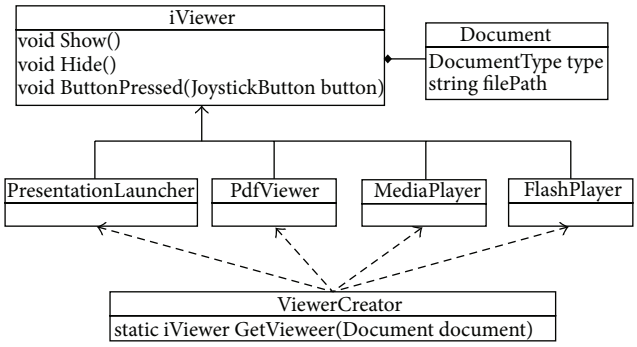

Figure 10: Document viewer's software design (this design is based on factory method pattern but simpler).

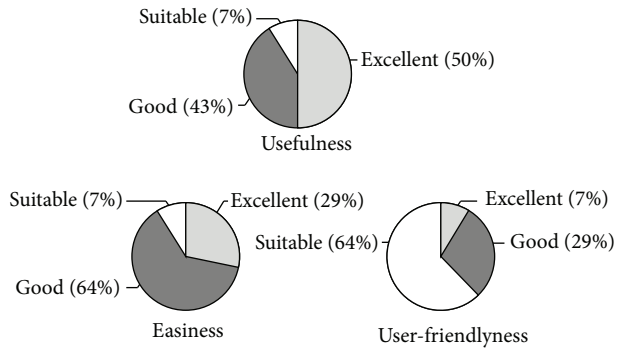

Figure 11: Validation results.

does not have to know what kind of document it is or how it works.

When the conference manager loads a new document, it uses the *ViewerCreator* to get the appropriate viewer and it calls the *Show* method to launch the project screen. If the conference manager component needs to close the viewer, it uses the *Hide* method and if joystick commands are received the conference manager component calls the *ButtonPressed* method.

5.3. Conference Administration. The system can use a local repository and in such case the administrator can work in the computer used in the conference.

But the system can also use a remote repository and the administration can be done in a Web page by the end-users. They can register in the Web page and administrate their own documents and personal information. The conference administrator only has to associate the conference card to the web users.

6. Validation

The validation has been carried out during the entire design process, in order to previously detect those key facts that many times make the product fail. The validation shown here is done to the physical device, the presenter, and we differentiate between technical validation and interaction validation.

6.1. Technical Evaluation. In this kind of testing, we use the typical procedures to validate the device such us in-circuit functional test or a debug port (disabled it for the final version).

Each component in the RFID Presenter was tested independently before being included in the prototype and then, whenever we develop a new PCB design, they were tested again. With this methodology, we solved technical problems very soon and we could develop the latest versions faster.

In the final version, we want to remark an important functional requirement for the validation of the prototype: the consumption of the device is low enough to work for more than 12 hours straight.

RFID reader is the component with higher consumption, 45 mA when reads and 20 mA when it is not active, but the device only does one read for each speaker so we can considered an average consumption of 20 mA.

Bluetooth is the other component with an important consumption. In this case, Bluetooth module consumes 27 mA when it is transferring information but less than 5 mA when the module is idle (more than 95% of the time, the Bluetooth module is in idle mode).

Considering all components, the average consumption of the prototype is 32,8 mA with consumption peaks of 95.6 mA when RFID reader reads a card and sends its code through Bluetooth module.

The functionality and, above all, the new services implemented have been tested based on a test protocol defined at the beginning of develop. It includes six parts with several questions in each part (power management, buttons, RFID reader, Bluetooth connection, switch document option, and laser pointer).

Version 4 of the prototype beats all the test protocol without any faults.

6.2. Interaction Evaluation. In the final interaction evaluation, we prepared a questionnaire with 12 questions and one last free question for comments. Also, two members of the project development wrote down any additional comment that user could make during the proof.

First questions were about objective information as if the user had used a presenter before (only half had used one), the size of the hand measured from the wrist to the end of the middle finder (the sizes were from 16 to 21 centimeters), or the hand they usually use (only one user was left-handed).

The rest of the questions can be grouped in three categories: the usefulness of the system, the easiness to learn and use the system, and the user-friendliness of the system and their interfaces. In Figure 11 we present a summary of the user evaluations for these three main questions.

Test users could evaluate different questions from bad, suitable, good, to excellent.

Based on these results, users considered the RFID Presenter very useful and they are capable of using it very quickly but it could be more comfortable and user-friendly.

7. Future Work

Following with the new services offered to the end-user, in the remote administrative version, he can personalize actions of the RFID Presenter. For example, he can set the actions for go next or previous page in the PDF viewer or even he can have more actions than buttons and select which actions are executed with each button.

In present version, web administration system has implemented the minimum code necessary to use it but it does not include any external repository like Dropbox or Google Drive. These kinds of repositories are very popular and many people use them as backup system or to work in different computers. Also, the system is designed for several conferences but present implementation only can work with one conference.

The shown system only consumes documents from the Cloud but maybe it is possible that generates information for social networks or for the conference itself (how many time each speaker consumes, or who is talking in every moment...).

Other possibility in future developments is its integration into a traditional mouse peripheral. It will be possible with a trackball in place of the joystick and an extra button to select this new mode.

8. Conclusions

Every day, systems and users connected to the Internet upload new information that can be accessible by any day-to-day object through a wireless connection.

Current technologies allow us to develop a great variety of new devices or enlarge the capabilities of existent ones. Rapid prototyping technologies are one of the key factors in developing, analyzing, and validating the products based on the Internet of Things concept. With adding manufacturing processes we can design, print, and test our product ideas, without any electronics inside, in really short time.

The development of a presenter, which has end-user recognition feature and Internet accessibility, lets us implement new and useful services never seen before. Without a proper validation during the development of the prototype, we would not be able to sustain the end-user approval.

The final results demonstrate that end-users appreciate the new capabilities of the product and also can be a competitive advantage for the manufactures.

Conflict of Interests

The authors declare that they have no conflict of interests regarding the publication of this paper.

References

[1] K. Finkenzeller, *RFID Handbook: Fundamentals and Applications in Contactless Smart Cards and Identification*, Jon Willey and Sons, 2003.

[2] E. Welbourne, L. Battle, G. Cole et al., "Building the internet of things using RFID: the RFID ecosystem experience," *IEEE Internet Computing*, vol. 13, no. 3, pp. 48–55, 2009.

[3] A. Gluhak, S. Krco, M. Nati, D. Pfisterer, N. Mitton, and T. Razafindralambo, "A survey on facilities for experimental internet of things research," *IEEE Communications Magazine*, vol. 49, no. 11, pp. 58–67, 2011.

[4] L. Atzori, A. Iera, and G. Morabito, "The Internet of Things: a survey," *Computer Networks*, vol. 54, no. 15, pp. 2787–2805, 2010.

[5] E. S. Martinussen and T. Arnall, "Designing with RFID," in *Proceedings of the 3rd International Conference on Tangible and Embedded Interaction (TEI '09)*, pp. 343–350, February 2009.

[6] M. Kranz, P. Holleis, and A. Schmidt, "Embedded interaction: interacting with the internet of things," *IEEE Internet Computing*, vol. 14, no. 2, pp. 46–53, 2010.

[7] "Withings Scales," http://www.withings.com/en/scales.

[8] H. Jabbar, T. Jeong, J. Hwang, and G. Park, "Viewer identification and authentication in IPTV using RFID technique," *IEEE Transactions on Consumer Electronics*, vol. 54, no. 1, pp. 105–109, 2008.

[9] "Presenter Remote Red Laser Pointer," http://www.kensington.com/kensington/us/us/p/1443/K33374USA/presenter-remote-red-laser-presenter.aspx.

[10] "Presenter Expert Red Laser with Cursor Control," http://www.kensington.com/kensington/us/us/p/1443/K72425AM/presenter-expert-red-laser-with-cursor-control.aspx.

[11] "Logitech Wireless Presenter R400," http://www.logitech.com/en-us/product/wireless-presenter-r400.

[12] "Logitech Professional Presenter R800," http://www.logitech.com/en-us/product/professional-presenter-r800.

[13] "Ring Pointer," http://www.geniusnet.com/wSite/ct?xItem=58132&ctNode=3619&mp=1.

Hindawi Publishing Corporation
International Journal of Antennas and Propagation
Volume 2014, Article ID 187029, 6 pages
http://dx.doi.org/10.1155/2014/187029

Research Article

Enhanced Loop Structure of NFC Antenna for Mobile Handset Applications

Byungje Lee,[1] Byeongkwan Kim,[2] and Sunghyun Yang[3]

[1] *Department of Wireless Communications Engineering, Kwangwoon University, No. 447-1, Wolgye-Dong, Nowon-Gu, Seoul 139-701, Republic of Korea*
[2] *Defence R&D Center, Hanwha Corporation, 52-1 Woisam-Dong, Yuseong-Gu, Daejeon 305-156, Republic of Korea*
[3] *Department of Electronic Engineering, Kwangwoon University, No. 447-1, Wolgye-Dong, Nowon-Gu, Seoul 139-701, Republic of Korea*

Correspondence should be addressed to Byungje Lee; bj_lee@kw.ac.kr

Received 27 November 2013; Accepted 20 February 2014; Published 8 April 2014

Academic Editor: Yuan Yao

A new structure of an NFC loop antenna for mobile handset applications is proposed. The proposed antenna consists of conventional loop elements and a parasitic loop embedded capacitor to enhance its performance. Although the sintered ferrite sheets with higher relative permeability ($\mu_r \approx 200$) have been used to reduce the performance deterioration due to the eddy current on the battery pack of a mobile handset, their costs are high, and they are considerably breakable. In this paper, with the proposed structure, we effectively enhance the performance of an NFC loop antenna by employing the ferrite-polymer composite with lower relative permeability ($\mu_r \approx 55$).

1. Introduction

A near-field communication (NFC) system has attracted much attention as a short-range wireless communication technology at 13.56 MHz which allows devices to communicate through inductive coupling and provides users with the card mode service and the reader/writer (R/W) mode service. The demand for a mobile NFC service has been increased due to its high security without a complex pairing process [1–4]. Currently, the NFC antenna technology faces several challenges such as reducing the thickness, high manufacturing costs, and performance degradation when it is embedded on the metallic components such as the PCB ground or the battery pack of mobile devices. To prevent performance degradation of an NFC antenna due to an eddy current [5] on the metallic components near the NFC antenna, a ferrite sheet is generally inserted between the NFC antenna and the metallic components. In most cases, NFC antennas are embedded in the battery pack of a mobile phone, so that a sintered ferrite sheet with high relative permeability has been attached between the NFC antenna and the metal case of a phone battery to avoid an eddy current. Also, a thickness of a ferrite sheet is usually limited in industry because an NFC antenna must be designed within a very small volume. Therefore, a very thin (80 μm) sintered ferrite sheet has been used with high relative permeability ($\mu_r \approx 200$) to simply avoid performance degradation of an NFC antenna due to an eddy current. However, since the sintered ferrite has higher manufacturing cost and is considerably breakable, ferrite-polymer composites are interesting as an alternative in industry. A ferrite-polymer composite is flexible and durable, and its manufacturing cost is reasonable. But, due to lower relative permeability ($\mu_r \approx 55$) than that of the sintered ferrite, it is difficult to effectively reduce an eddy current and achieve good performance from a conventional structure of an NFC loop antenna with a thin (80 μm) ferrite-polymer composite, so that a detection range and a load modulation level become deteriorated. So far, studies on enhancing the performance of an NFC antenna with a ferrite-polymer composite have not been investigated yet. Therefore, enhancement of the performance of an NFC antenna with

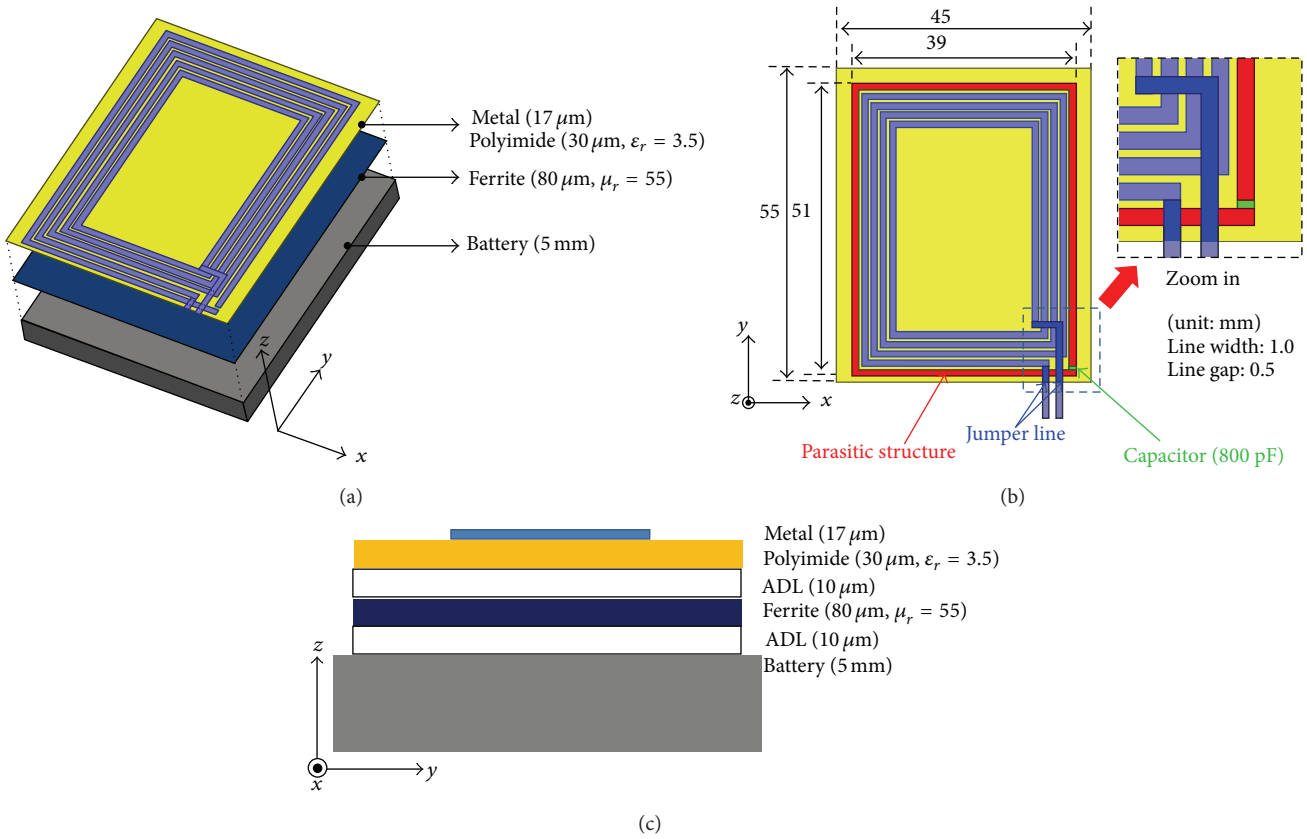

Figure 1: Geometry of the proposed NFC loop antenna; (a) overall view, (b) top view printed on FPCB, and (c) side view.

a ferrite-polymer composite challenges and warrants further study.

In this paper, a novel structure of an NFC loop antenna is proposed for mobile handset applications by improving the performance of an NFC loop antenna when a ferrite-polymer composite is attached between the embedded NFC loop antenna and the phone battery. The proposed loop antenna has a parasitic loop structure with a capacitor in order to tune the parasitic loop to be operated at 13.56 MHz. The current direction on the resonated parasitic loop is the same as those of nearby loop antenna elements. This additional current from a parasitic loop induces more intensive H-field in the near-field region, so that a thin ferrite-polymer composite sheet can be used for the proposed loop antenna, in spite of its lower relative permeability. Therefore, in the Euro pay, MasterCard and Visa (EMV) test for the card mode and in the detection range test for the reader/writer (R/W) mode, the proposed loop antenna gives better performance than that of a conventional NFC loop antenna when both are attached on the same ferrite-polymer composite sheet.

2. Antenna Structure and Analysis

Figure 1(a) shows the overall view of the proposed NFC loop antenna structure. It is printed on the polyimide (ε_r = 3.5 and thickness = 30 μm) FPCB (flexible printed circuit board) whose size is 45 × 55 mm^2 as shown in Figure 1(b), and it is mounted on the battery pack (50 × 60 × 5 mm^3) of a mobile phone. The ferrite-polymer composite sheet (μ_r = 55, tan δ_m = 0.07, and thickness = 80 μm) is attached by using an adhesive layer (ADL, thickness = 10 μm) as shown in Figure 1(c). The line width of each loop is 1 mm, and the gap distance between loops is 0.5 mm. The parasitic loop is printed at outermost location. A capacitor (880 pF) is embedded in order to tune this parasitic loop to be operated at 13.56 MHz.

Figure 2 shows the simulated H-field intensity (RMS value) along with a normal direction (z-direction) on the center of a conventional loop antenna without a parasitic loop element for different relative permeability of a ferrite sheet (thickness = 80 μm) when a conventional 4-turn loop antenna is assembled as the same layout shown in Figure 1(c) and connected with a matching circuit toward an NFC chip (Z_{in} = 80 Ω) [6]. It is noticed that the relative permeability value of the ferrite sheet mainly affects the intensity of the H-field. Also, the lower value of relative permeability may disrupt the generation of the H-field intensity from the loop antenna in the near-field region. Thus, a conventional loop antenna by using a ferrite-polymer composite sheet of lower permeability (μ_r = 55) may not achieve good performance of a NFC loop antenna.

Figure 3 shows the simulated H-field intensity along with a normal direction (z-axis) on the center of a conventional

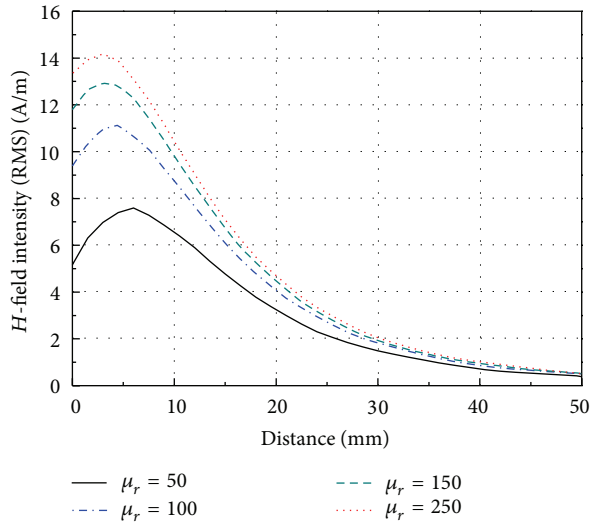

FIGURE 2: Simulated H-field intensity along with a normal direction (z-axis) on the center of the 4-turn loop antenna by varying relative permeability of a ferrite sheet (thickness = 80 μm).

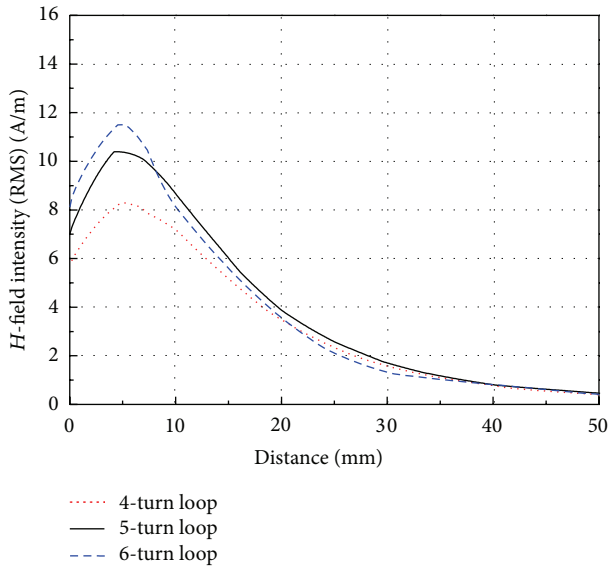

FIGURE 3: Simulated H-field intensity along with a normal direction (z-axis) on the center of the loop antenna with varying number of the loop turns.

loop antenna with varying number of the loop turns when the ferrite-polymer composite sheet (μ_r = 55 and thickness = 80 μm) is employed. Even though the number of loop turns increases, the H-field intensity does not be significantly enhanced. This is due to the rapid increment of an electrical resistance, which is a meaningful loss mechanism especially in the near-field loop antenna, as the number of loop turns increases [7, 8]. Thus, in general, the number of loop turns for an NFC antenna is restricted by 4 or 5 because the electrical resistance of a conventional loop antenna wound from the

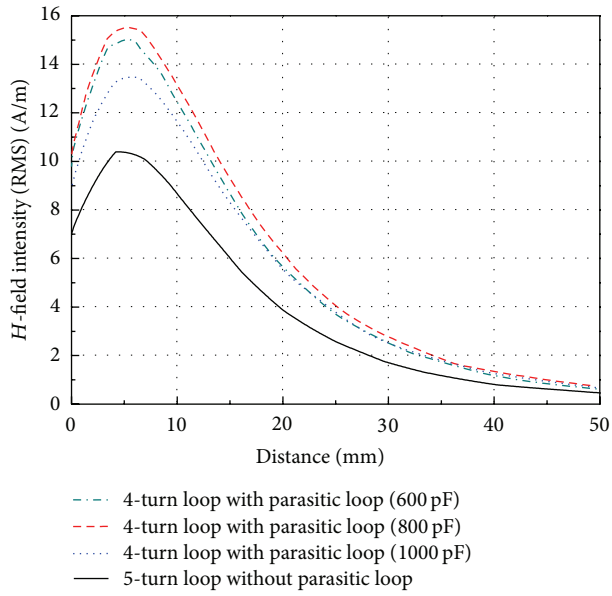

FIGURE 4: H-field intensity along with a normal direction (z-axis) on the center of the loop antenna with varying capacitance of a capacitor embedded in the parasitic loop.

outermost line into the innermost line is exponentially increased due to proximity effect among the closely located loop elements as the number of loop turns increases.

To improve the H-field intensity when the lower relative permeability of a ferrite material is used, a novel structure of an NFC loop antenna is increasingly demanded. The proposed loop antenna shown in Figure 1 has an additional parasitic loop structure embedded with a capacitor. When this parasitic loop structure is coupled by the nearby loop antenna and resonated at the operating frequency (13.56 MHz), the H-field intensity of the proposed loop antenna is significantly improved. Figure 4 shows the H-field intensity with varying capacitance of a capacitor embedded in the parasitic loop. It is noticed that the proposed antenna (4-turn loop with a parasitic loop embedded capacitor) gives more intensive H-field than that of a conventional 5-turn loop antenna only.

Figure 5 shows that the current on the resonated parasitic loop has the same direction as those on the nearby 4-turn loop antenna. This additional current helps to induce more intensive H-field in the near-field region. Thus, although it has lower relative permeability (μ_r = 55), the thin (80 μm) ferrite-polymer composite sheet with this proposed structure of an NFC loop antenna can be applied to reduce performance degradation of an NFC antenna due to an eddy current. As mentioned, it is more flexible and durable, and has much lower manufacturing cost than a sintered ferrite sheet ($\mu_r \approx 200$). Figure 6 presents the H-field distribution of the proposed loop antenna with the parasitic loop embedded capacitor (800 pF) in the near-field region. The proposed antenna generates the H-field toward the positive z-axis direction, but it prevents generating the H-field toward the negative z-axis direction.

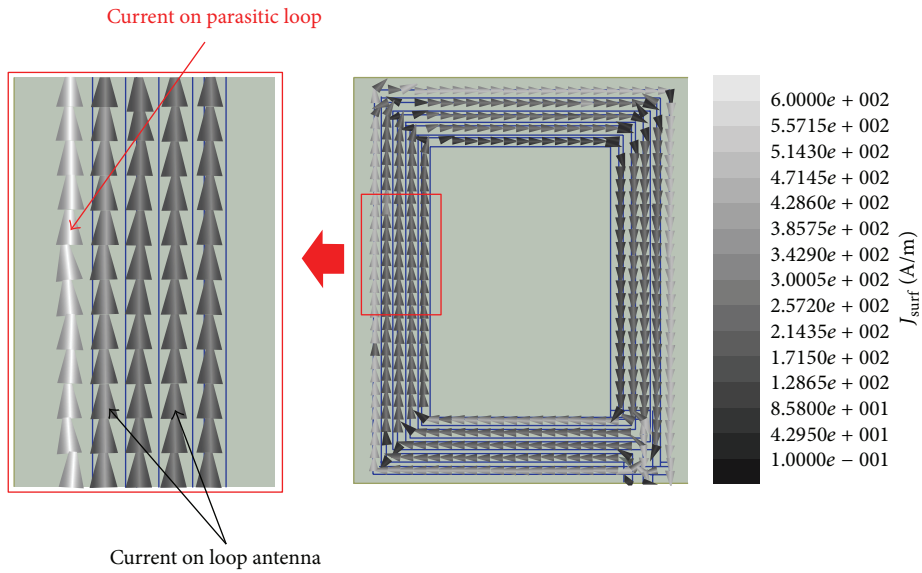

Figure 5: Current direction on the proposed loop antenna with the parasitic loop embedded capacitor (800 pF).

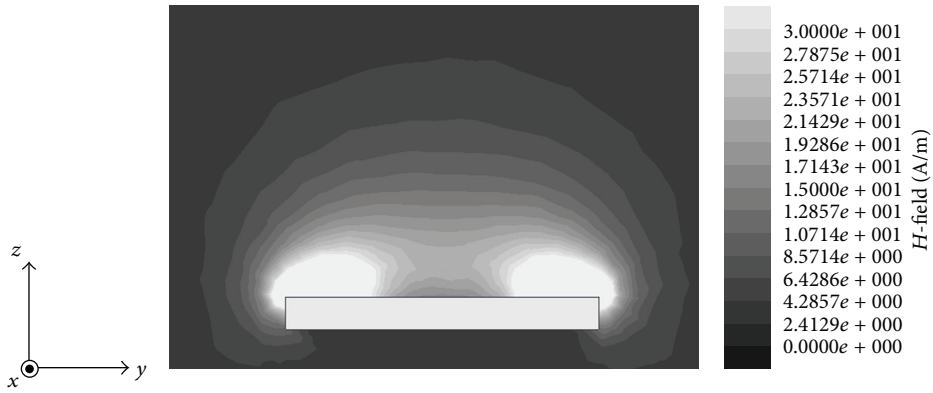

(a)

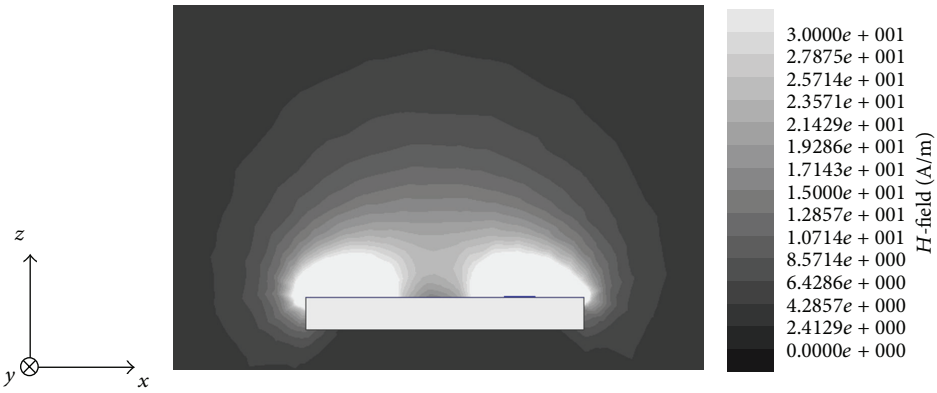

(b)

Figure 6: Near-field (H-field) distribution of the proposed loop antenna with the parasitic loop embedded capacitor (800 pF); (a) yz-plane and (b) zx-plane.

Table 1: Measured inductance and resistance of the proposed antenna.

	Inductance, L_a [nH]	Resistance, R_a [Ω]
Conventional 5-turn loop only	1970	13
4-turn loop with a parasitic loop	1350	7

Table 2: Measured results in the card mode and in the R/W mode tests.

	Card mode Load modulation Level [mV_{pp}] Min. spec. at (r, ϕ, z)				R/W mode Detection range [cm]
	8.8 (0, 0, 0)	***7.2*** (0, 0, 1)	***4.0*** (0, 0, 2)	***2.4*** (0, 0, 3)	
Conventional 5-turn loop only	27	12	4.4	1.6	46
4-turn loop with a parasitic loop	50	25	11	4.3	56

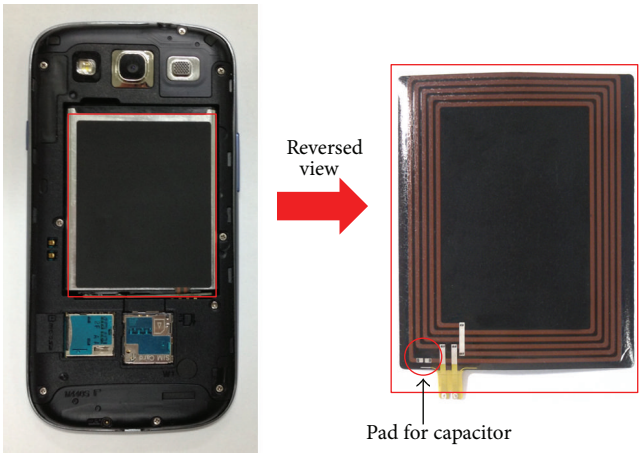

Figure 7: Prototype NFC antenna mounted on a mobile handset.

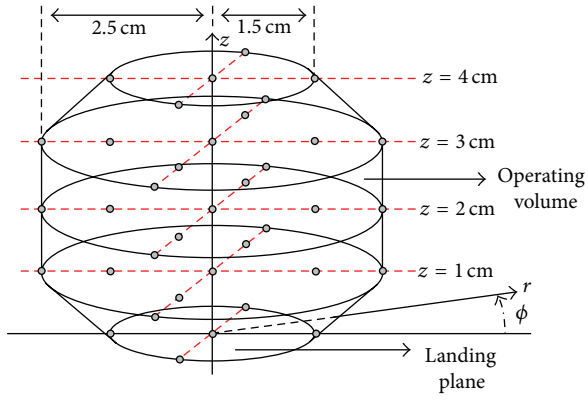

Figure 8: Operating volume for the EMV test.

3. Measured Result

To verify the performance of the proposed NFC loop antenna, the prototype antenna is mounted on the battery pack of a commercial mobile handset embedded NFC chip (PN544, NXP Semiconductor corp.) [5], as shown in Figure 7. When the proposed antenna embedded on the phone battery is mounted on a mobile handset, its inductance and resistance are measured first as shown in Table 1. With these measured values, the matching circuit between the NFC chip and the antenna is designed [6]. After that, the card mode and the R/W mode tests are conducted. The card mode test is accomplished by the EMV test which measures a load modulation level (V_{pp}) within a specific operating volume (r, ϕ, z) as shown in Figure 8. The specification of the EMV test applied is a global standard based on the ISO14443 for the contactless card payment [7, 8]. In addition, the R/W mode test is conducted by measuring the detection range responding to a reference tag (Mifare 1 k). Table 2 shows the measured detection ranges (R/W mode test) and some of the measured load modulation levels (card mode test). When a mobile handset is in the R/W mode, the detection range of the proposed antenna is 56 mm. In the card mode, all of the measured load modulation levels within the specific operating volume (r, ϕ, z) meet the criteria values of an NFC system when the reader supplies the power of 600 mW.

4. Conclusion

A new structure of a compact NFC loop antenna is proposed for mobile handset applications by adding the parasitic loop on the outer side of a conventional loop antenna in order to improve its performance. The proposed antenna is designed with the ferrite-polymer composite sheet. Although this sheet has a low relative permeability ($\mu_r \approx 55$), it is more durable and has lower cost than the sintered ferrite sheet ($\mu_r \approx 200$). With the same size, the performance of the proposed NFC loop antenna in a load modulation level for the card mode test and in a detection range for the R/W mode test is better than that of a conventional NFC antenna.

Conflict of Interests

The authors declare that there is no conflict of interests regarding the publication of this paper.

Acknowledgments

This work (Grant no. C0015229) was supported by Business for Cooperative R&D between Industry, Academy, and Research Institute funded by Korea Small and Medium Business Administration in 2012, the National R&D Program through the National Research Foundation of Korea (NRF) funded by the Ministry of Science, ICT and Future Planning (no. 2013M1A7A1A02043817), and a research grant from Kwangwoon University in 2014.

References

[1] J. Fischer, "NFC in cell phones: the new paradigm for an interactive world," *IEEE Communications Magazine*, vol. 47, no. 6, pp. 22–28, 2009.

[2] R. Want, "Near field communication," *IEEE Pervasive Computing*, vol. 10, no. 3, pp. 4–7, 2011.

[3] P. E. Ross, "Phone-y money," *IEEE Spectrum*, vol. 49, no. 6, pp. 60–63, 2012.

[4] NFC Forum, http://nfc-forum.org/.

[5] K. Finkenzeller, *RFID Handbook: Radio-Frequency Identification Fundamentals and Applications*, John Wiley & Sons, London, UK, 2003.

[6] NXP Semiconductors, "AN 190810: PN544 C2 antenna design guide," Application Note, Rev. 1.0, April 2010.

[7] EMVco, "EMV contactless specification for payment systems: Book D," EMV Contactless Communication Protocol Specification, Rev. 2.2, June 2012.

[8] B. Lee, B. Kim, F. J. Harackiewicz, B. Mun, and H. Lee, "NFC antenna design for low-permeability ferromagnetic material," *IEEE Antennas and Wireless Propagation Letters*, vol. 13, pp. 59–62, 2014.

Hindawi Publishing Corporation
International Journal of Antennas and Propagation
Volume 2014, Article ID 149051, 5 pages
http://dx.doi.org/10.1155/2014/149051

Research Article

Study on the Optically Transparent Near-Field and Far-Field RFID Reader Antenna

Yuan Yao, Junsheng Yu, and Xiaodong Chen

Beijing Key Laboratory of Work Safety Intelligent Monitoring, School of Electronic Engineering, Beijing University of Posts and Telecommunications, No. 10 Xitucheng Road, Beijing, China

Correspondence should be addressed to Yuan Yao; yaoy@bupt.edu.cn

Received 18 November 2013; Accepted 8 February 2014; Published 13 March 2014

Academic Editor: Chaowei Wang

A study on the optically transparent RFID reader antenna which can operate in both near-field and far-field is proposed in this paper. The antenna with a dimension of 45 mm × 45 mm is fabricated using Indium tin oxide film and can operate from 915 to 935 MHz covering the China UHF RFID band. The strong and uniform magnetic field is excited by magnetic dipole source. Both simulation and measurement results are shown to illustrate the performance of the proposed antenna. The measured reading distances are up to 40 mm and 100 mm for near-field and far-field applications, respectively.

1. Introduction

Recently, UHF RFID systems are getting more and more attention in a number of practical applications, due to automatic identification for efficiently tracking and managing objects. Based on types of objects and applications, inductively coupled near-field working mode is used to transfer information between reader and tag. Near-field reading can be useful for objects having metals and liquids in their vicinity, because normal far-field tags' performance is affected by the presence of these objects [1, 2]. Far-field communication is widely used due to its long read range. Due to promising performance at item-level tagging (ITL) of small, expensive, and sensitive objects and different applications such as pharmaceutical logistics and biosensing applications, it is considered as a possible solution for ITL in pharmaceutical and retailing industry.

To design a near-field and far-field UHF RFID antenna, some structures have been presented. Shrestha et al. use a segmented loop and a patch, respectively, to achieve near-field and far-field operations, but they have too large size of 184 mm × 174 mm [3]. Borja et al.'s antenna has a dimension of 72.3 mm × 72.3 mm [4].

UHF RFID systems present several opportunities, for instance, in clothing stores. One such case would be the possibility to automatically read the tag associated with a piece of clothing being tried on in front of a mirror. However, the conventional reader antennas made of metals damage the sensory experience of the clients. Thus, an RFID reader antenna which can ensure invisibility of the antenna is expected. This feature is attractive for aesthetical reasons and to avoid that clients feel uncomfortable with unusual devices in the fitting room. The antenna cannot be hidden behind the mirror because this is not electromagnetically transparent. Therefore, we propose in this paper to print an optically transparent antenna on the glass surface of the mirror.

There are currently several possible materials to create transparent antennas, like spray-on conductive substances [5] or metallic conductive films. However, most of these materials do not present the best optical transparency for the mirror application. Indium tin oxide (ITO) films seem to be the most viable solution so far, for they present the best compromise between optical transparency and electrical conductivity. Even though the associated ohmic losses reduce the performance of the antenna, there are ways, such as some particular deposition techniques [6], to improve conductivity.

In this paper, an optically transparent UHF RFID reader antenna is proposed with simple and compact configuration for both near-field and far-field operations. The impedance bandwidth is suitable for China standard (920–925 MHz), and it can provide the strong and uniform magnetic field in an adequate interrogation zone. Both simulation and

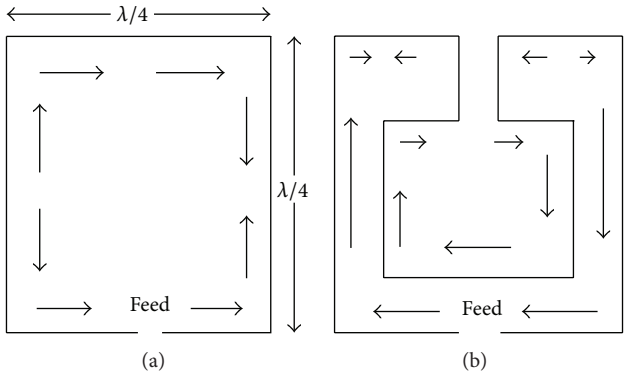

FIGURE 1: Current distributions of (a) one-wavelength-perimeter loop and (b) folded-dipole loop.

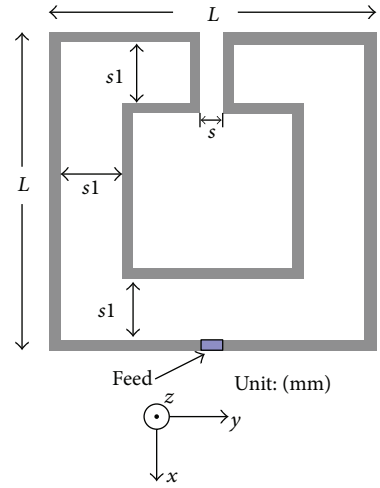

FIGURE 2: Prototype of the folded-dipole loop antenna.

measurements results are provided to illustrate the good performance of the designed antenna.

2. Antenna Design

Loop antennas are commonly used for inductively coupled near-field RFID systems. At UHF band, the optimal size of the loop antenna is electrically large or comparable to the wavelength. The amplitude and phase distribution of the current, in the case, is not uniform, and it reverses at every half-wavelength, which results in a weak and nonuniform magnetic field at the center of the loop [7], as shown in Figure 1(a). Some ideas were proposed to solve the problem of current reverse. A segmented loop antenna can avoid in-phase of current [8]. Dual-dipoles also can achieve a uniform magnetic field in near-field region for pure near-field operation [9].

A novel folded-dipole loop antenna was proposed as shown in Figure 1(b). This antenna can achieve a uniform magnetic field easily and has a good far-field gain. The folded-dipole is fabricated using ITO film. The electrical properties of ITO films are specified through the sheet resistance and coating thickness. In this design, an ITO film with sheet resistance equal to 7 Ω/sq and coating thickness equal to 250 nm is selected for the antenna. The ITO film is printed on the polyethylene terephthalate with thickness of 0.1 mm and permittivity of 2.25. Detailed dimensions are shown in Figure 2, s = 3 mm, $s1$ = 8.5 mm, the antenna size is L (45 mm) × L (45 mm), and line width is 1 mm.

3. Results and Discussion

Simulations and optimizations were performed using Ansoft High Frequency Structure Simulator (HFSS) software, which uses the finite element method (FEM).

Figure 3 shows the fabricated antenna after parameter optimization. The measured S_{11} agrees with the simulated one with a slight deviation to the right side by 1 MHz as shown in Figure 4. The measured bandwidth ranges from 916 to 936 MHz, which covers the China UHF RFID band.

FIGURE 3: Photograph of the fabricated antenna.

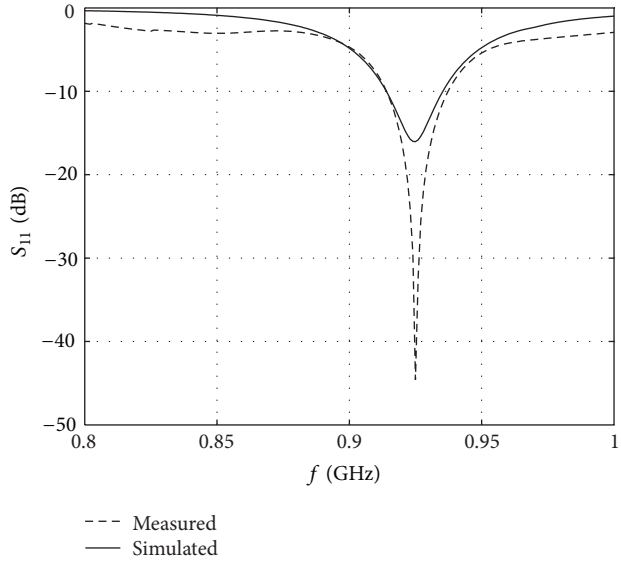

FIGURE 4: Simulated and measured S_{11} of the antenna.

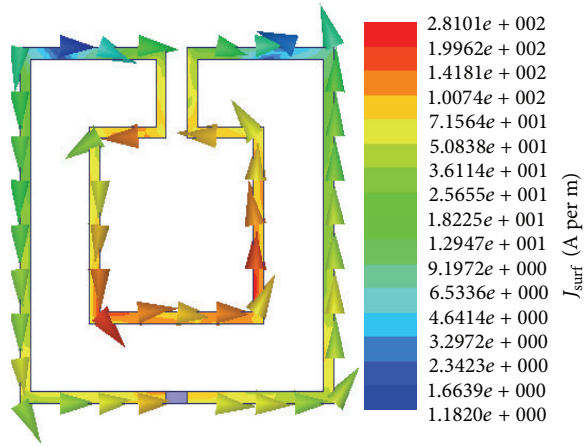

Figure 5: Simulated current distribution on the antenna.

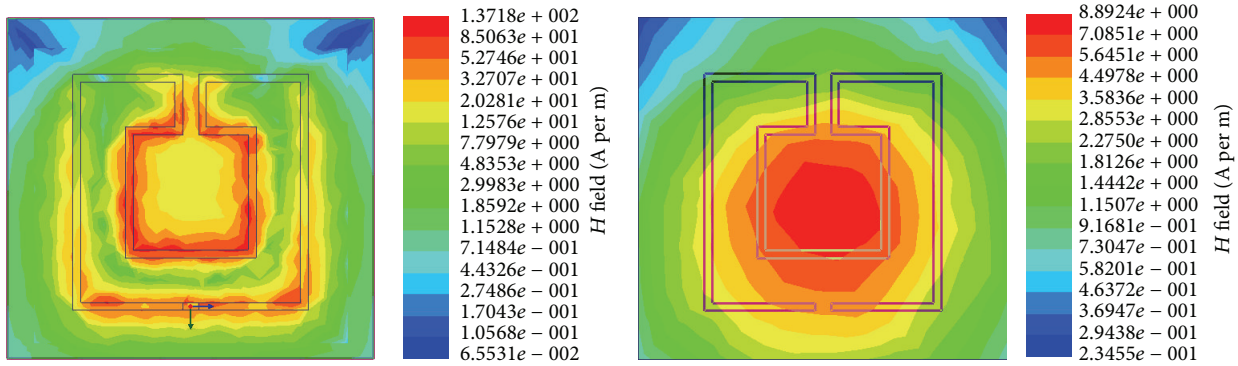

(a) (b)

Figure 6: Magnetic field distribution Hz at (a) $z = 0$ mm and (b) $z = 10$ mm.

The simulated current distribution along this folded-dipole loop is shown in Figure 5. We can see that the current reverses at the outer loop, however, which is unidirectional along the inner loop. Figure 6 shows the resulting z-component of the magnetic field on an xy-plane above the antenna at $z = 0$ and $z = 10$ mm. We can see that the field distribution is uniform in the center region.

Based on the fabricated antenna, we measure the read range and width by using the Impinj UHF button. The test scene is presented in Figures 7(a) and 7(b) and shows the prototype of the Impinj UHF near-field tag whose diameter is around 1 cm. Under the transmission power level of 15 dBm, the measured reading distance is 40 mm. When the tag is attached to a water-item container, the reading range is still the same. Additionally, a far-field tag is also measured, and reading range is around 100 mm due to the good far-field gain of the reader antenna. When the far-field tag is attached to the bottle of water, the reading range is reduced to 4.5 mm.

Figure 8 shows the measured reading range at different distances between the reader antenna and tag. We use the square lattice; its size is 1 cm × 1 cm.

The simulated and measured radiation patterns of the proposed antenna are, respectively, shown in Figure 9 which makes the antenna suitable for far-field application. It can be seen that the gain of the antenna is relatively low compared with this kind of antenna made of metals, because the conventional metal antenna can achieve the gain of 0 dBi under the same structure. But the reading range can achieve 1 m when we use a far-field UHF RFID tag and the transmission power of the reader is 30 dBm. So even though the gain of the proposed antenna is low because of the ohm loss of the ITO film, the capability of reading far-field tag is good enough.

4. Conclusion

In this paper, a novel UHF reader antenna was proposed for near-field and far-field simultaneous operations. A magnetic dipole was folded to produce a uniform magnetic field distribution at UHF. This RFID reader antenna is designed for the China UHF RFID band. With the Impinj UHF button near-field tag, the maximum read range obtained was 40 mm under 15 dBm transmission power. The near-field reading performance was not degraded when the tag was attached to a water container. The far-field read range, with a commercial far-field tag, was approximately 100 mm. This novel RFID

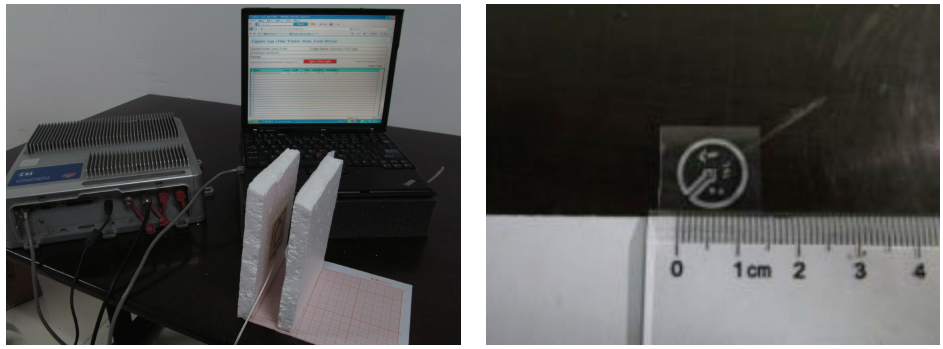

(a) (b)

Figure 7: Antenna measurement. (a) Test scene of read range measurement. (b) Impinj UHF button near-field tag.

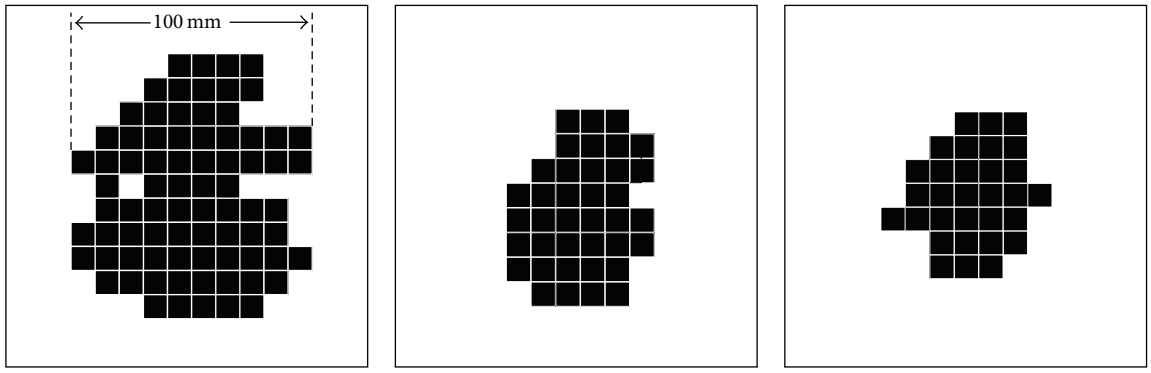

(a) (b) (c)

Figure 8: Measured read width at xy-plane. (a) $z = 10$ mm, (b) $z = 20$ mm, and (c) $z = 40$ mm.

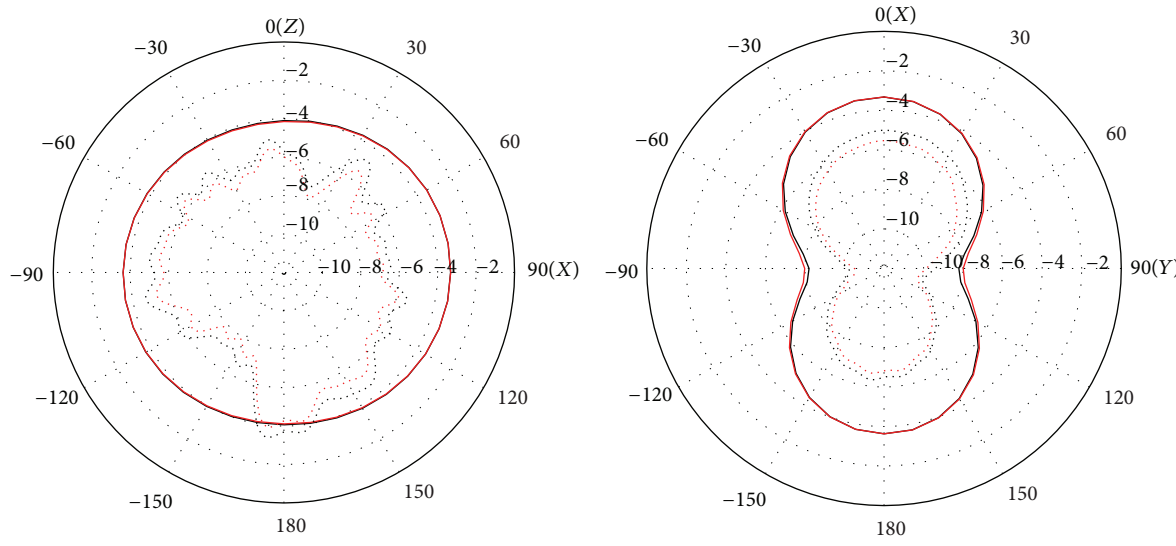

(a) (b)

Figure 9: Simulated and measured far-field radiation patterns at (a) xz-plane and (b) xy-plane.

reader antenna can be applied for near-field and far-field operations.

Conflict of Interests

The authors declare that there is no conflict of interests regarding the publication of this paper.

Acknowledgments

This work is supported by the National Natural Science Foundation of China under Grant no. 61201026, Beijing Natural Science Foundation (4133091), and Beijing Higher Education Young Elite Teacher Project (Grant no. YETP0438).

References

[1] D. M. Dobkin and S. M. Weigand, "Environmental effects on RFID tag antennas," in *Proceedings of the IEEE MTT-S International Microwave Symposium*, pp. 135–138, June 2005.

[2] X. Qing, Z. N. Chen, and C. K. Goh, "Platform effect on RFID tag antennas and co-design considerations," in *Proceedings of the IEEE Microwave Conferenc*, pp. 1–4, December 2008.

[3] B. Shrestha, A. Elsherbeni, and L. Ukkonen, "UHF RFID reader antenna for near-field and far-field operations," *IEEE Antennas and Wireless Propagation Letters*, vol. 10, pp. 1274–1277, 2011.

[4] A. L. Borja, A. Belenguer, J. Cascon, and J. R. Kelly, "A reconfigurable passive UHF reader loop antenna for near-field and far-field RFID applications," *IEEE Antennas and Wireless Propagation Letters*, vol. 11, pp. 580–583, 2012.

[5] F. Colombel, X. Castel, M. Himdi, G. Legeay, S. Vigneron, and E. Motta Cruz, "Ultrathin metal layer, ITO film and ITO/Cu/ITO multilayer towards transparent antenna," *IET Science, Measurement and Technology*, vol. 3, no. 3, pp. 229–234, 2009.

[6] C. C. Serra, C. R. Medeiros, J. R. Costa, and C. A. Fernandes, "Mirror-integrated transparent antenna for RFID application," *IEEE Antennas and Wireless Propagation Letters*, vol. 10, pp. 776–779, 2011.

[7] A. L. Popov, O. G. Vendik, and N. A. Zubova, "Magnetic field intensity in near field zone of loop antenna for RFID systems," *Technical Physics Letters*, vol. 36, no. 10, pp. 882–884, 2010.

[8] X. Qing, C. K. Goh, and Z. N. Chen, "Segmented loop antenna for UHF near-field RFID applications," *Electronics Letters*, vol. 45, no. 17, pp. 872–873, 2009.

[9] X. Li and Z. Yang, "Dual-printed-dipoles reader antenna for UHF near-field RFID applications," *IEEE Antennas and Wireless Propagation Letters*, vol. 10, pp. 239–242, 2011.

Hindawi Publishing Corporation
International Journal of Antennas and Propagation
Volume 2014, Article ID 897041, 8 pages
http://dx.doi.org/10.1155/2014/897041

Research Article

Power Transmission of UHF Passive Embedded RFID in Tires

Shengbo Hu,[1,2] Bing Si,[3] Heng Shu,[1,2] and Jinrong Mo[1,2]

[1] *Institute of Intelligent Information, Guizhou Normal University, Guiyang 550001, China*
[2] *Department of Guizhou Education, Center for RFID and WSN Engineering, Guiyang 550001, China*
[3] *Institute of New Technology, Guizhou Academy of Sciences, Guiyang 550001, China*

Correspondence should be addressed to Shengbo Hu; hsb@nssc.ac.cn

Received 5 August 2013; Revised 28 December 2013; Accepted 30 December 2013; Published 17 February 2014

Academic Editor: Yuan Yao

UHF passive RFID tags embedded in tires have a deep impact on tire life cycle management and tire monitoring. In this work, we present the power transmission of UHF passive embedded RFID in tires. In UHF passive embedded RFID systems in tires, the bidirectional radio link between reader and tags goes through air and tires. The total path loss contains reflection loss at tire-air boundaries and attenuation loss in the tires. The power transmission is based on the permittivity of tires and tire-air boundary conditions. We give an OCP method for measuring the permittivity of tires. By analyzing the radio link for UHF passive RFID, we establish a model of wave propagation of UHF embedded RFID in tires and make numerical analyses. Numerical analyses show that the error of the OCP methods for measuring the permittivity of tires is small, the parallel polarization and normal incidence of wave are chosen for improving the performance of the UHF embedded RFID in tires, and distance is chosen to keep power transmission function from locating valley.

1. Introduction

Acting as sensors, passive RFID tags can avoid sensor nodes bulky and battery powered. For that reason, UHF passive tags embedded in tires have been used widely for tire life cycle management in the USA and the European Union [1, 2]. To meet the Automotive Industry Action Group's B-11 standard for North American, Michelin began offering automakers the option of purchasing tires with embedded tags [3]. Besides, the combinations of UHF passive tags embedded in tire and tire pressure monitoring are paid attention highly to improve the reliability of tire and tire control systems [4].

However, range has been one of the hardest challenges in UHF passive RFID embedded in tires, because the rubber makes it harder to read the tag. When Michelin took off-the-shelf, UHF passive tags and embedded them in tires, the read distance dropped to less than three inches [3]. The main difference between the common RFID and RFID embedded in tires is communication medium, which attenuates RF power from the reader in RFID embedded in tires. To improve the range and reliability of RFID embedded in tires, it is of great concern to study power transmission of wave propagation for UHF passive embedded RFID in tires, because the tags do not contain any battery and rely on the electromagnetic field for both power and communication. In this paper, we present the power transmission of wave propagation for UHF passive embedded RFID in tires and lay out the foundations for reliable communication in this environment.

In UHF passive RFID systems, a bidirectional radio link is established between reader and tags, which can be classified a forward link from the reader to tags and a backward link from the tags to reader [5]. Depending on the characteristics of reader and tags, the propagation channel properties like path loss and fading, the power transmission coefficient and the channel transmissions are investigated in [5–7]. In UHF passive embedded RFID systems in tires, the bidirectional radio link between reader and tags goes through air and tires. The total path loss contains several factors: reflection loss due to reflected power at tire-air boundaries, attenuation loss in the tires, and spreading loss which is simply due to the radiation properties of antenna. Each of these factors can be analyzed using the permittivity of tires and tire-air boundary conditions.

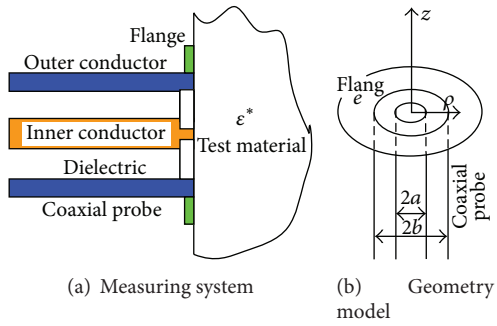

Figure 1: Measuring reflection coefficients with open ended coaxial probe.

So, this paper focuses on wave propagation for UHF passive embedded RFID in tires based on the permittivity of tires and tire-air boundary conditions. Hence, Section 2 presents how to measure the permittivity of tires. Section 3 describes the radio link for UHF RFID systems. Section 4 gives a propagation model of UHF passive embedded RFID systems in car tires. Section 5 describes numerical calculation and discussion. Section 6 concludes this paper.

2. Measuring the Permittivity of Tires

2.1. Measuring the Permittivity. Several techniques have been developed for measuring the permittivity [8–10]. However, some, such as resonant cavity or wave-guide transmission line cells, require test hardware machining and destructive processing. And open ended coaxial probe (OCP) technique is currently one of the most popular techniques for measuring the permittivity. OCP technique can perform nondestructive, broadband (RF and microwave bands), and high temperature measurement. Its well-developed theory makes it possible to obtain sufficiently accurate results.

A schematic for a coaxial open ended probe is shown in Figure 1. To reduce significantly measuring error, the material being tested is placed in close contact with the probe's flat end. The reflection coefficient, measured with a vector network analyzer (VNA), is used as inverse calculation of the permittivity of the material.

An equivalent circuit of admittance model for a coaxial open ended probe is shown in Figure 2. In Figure 2, Y_c is the probe characteristic admittance, and $Y(\omega, \varepsilon^*)$ is the load admittance, including the inner admittance $Y_i(\omega) = j\omega C_i$ of the capacitance C_i between outer conductor and inner conductor and the outer admittance $Y_o(\omega, \varepsilon^*)$, obtained by solving the following equation [11]:

$$Y_o(\omega, \varepsilon^*) = j\frac{2\omega\varepsilon_0\varepsilon^*}{[\ln(b/a)]^2}\iint_a^b\int_0^\pi \cos\varphi\frac{e^{-jkr}}{r}d\varphi d\rho' d\rho, \quad (1)$$

where $k = \omega\sqrt{\mu\varepsilon'}$, μ is the permeability, ω is the operating frequency, (ρ, ρ', φ) are cylindrical coordinates, $r = [\rho^2 + \rho'^2 - 2\rho\rho'\cos\varphi]^{1/2}$, and a and b are, respectively, the interior and the external radius of the probe. And (1) can be the series expansion form of (2):

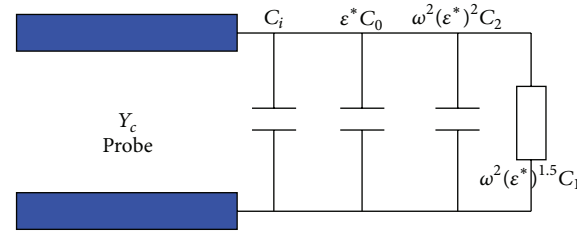

Figure 2: The equivalent circuit of admittance model for a coaxial open ended probe.

$$Y_o(\omega, \varepsilon^*) = \sum_{n=0}^{\infty}(-1)(-j\omega)^{n+1}C_n\varepsilon^{*(n+2)/2}, \quad (2)$$

where

$$C_n = \frac{2(\mu_0\varepsilon_0)^{(n+2)/2}}{n!\mu_0[\ln(b/a)]^2}\iint_a^b\int_0^\pi r^{n-1}\cos\varphi d\varphi d\rho' d\rho. \quad (3)$$

Equation (3) shows that C_n is constant. For convenience, (2) can be truncated to 3 terms with the C_0, C_1, and C_2. So, $Y(\omega, \varepsilon^*)$ can be given as below:

$$Y(\omega, \varepsilon^*) = j\omega C_i + j\omega\varepsilon^* C_0 + \omega^2(\varepsilon^*)^{1.5}C_1 + j\omega^3(\varepsilon^*)^2 C_2, \quad (4)$$

where $\varepsilon^* C_0$ is the fringing capacitance of the probe, $\omega^2(\varepsilon^*)^2 C_2$ is the fringing capacitance generated from a test material, and $\omega^2(\varepsilon^*)^{1.5}C_1$ is the equivalent conductance radiated from the probe.

The load admittance $Y(\omega, \varepsilon^*)$ can be obtained from the EM wave reflection coefficient $\Gamma(\omega, \varepsilon^*)$ using the following relation:

$$Y(\omega, \varepsilon^*) = Y_c\frac{1 - \Gamma(\omega, \varepsilon^*)}{1 + \Gamma(\omega, \varepsilon^*)}. \quad (5)$$

Hence, measuring the permittivity can be performed using the following steps.

Step 1. Using VNA, we measure the four different reflection coefficients Γ_1, Γ_2, Γ_3, and Γ_4 associated with the four different frequencies using a standard material with the known permittivity. Using (4) and (5), the four unknown parameters C_i, C_0, C_1, and C_2 can be solved.

Step 2. Using VNA, we measure the reflection coefficients Γ associated with some frequencies using the test material. Using (4) and (5), the permittivity of the test material can be calculated by a suitable iterative method.

2.2. Measurement Setup for Tires. The tire sidewall and the position of the RFID tag embedded in tire are displayed in Figure 3. The tag is embedded parallel to the outer steel mesh

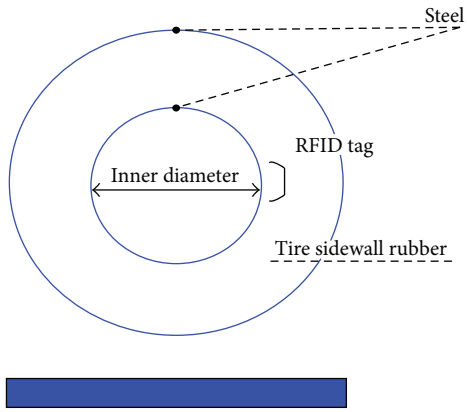

Figure 3: The RFID tag embedded in tires.

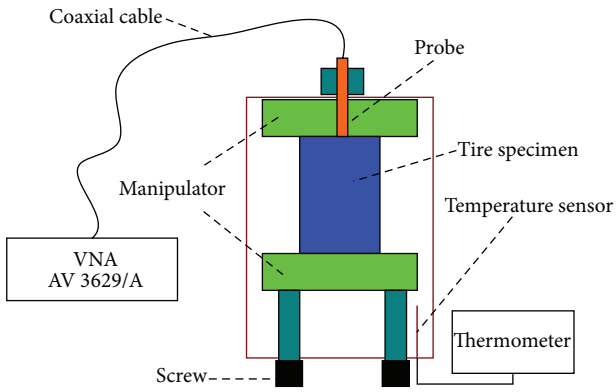

Figure 4: The OCP measurement system.

at a distance that depends on the tire size and ranges from 4 to 8 cm above the inner steel mesh [1].

To reduce significantly measuring error using OCP technique, the tire sidewall specimen has to meet the following conditions.

(i) The surface of the tire sidewall specimen has to be flat. A piece of the tire sidewall is cut out, and the cross section is polished to obtain a flat surface.

(ii) The specimen has to have semi-infinite thickness so that the penetration of the field must be much smaller than the specimen's thickness.

(iii) There must not be air gaps between probe and the tire sidewall specimen.

Figure 4 illustrates an OCP measurement system. The system consists of a VNA, a thermometer, a coaxial probe, and a manipulator with screw for fixing the tire sidewall specimen. Tightening the screw, the probe is pressed against the specimen until no more variation of the measurement results is observed.

2.3. Simulation Verifying Using HFSS. Simulation verifying using HFSS to verify the measurement accuracy using OCP technique, an OCP model using HFSS (high frequency structure simulator) is set up to compare. Given the measured permittivity of tire specimen using the measuring methods presented in Section 2.1, the reflection coefficient is solved using the OCP model. And the simulation and measurement reflection coefficients are compared.

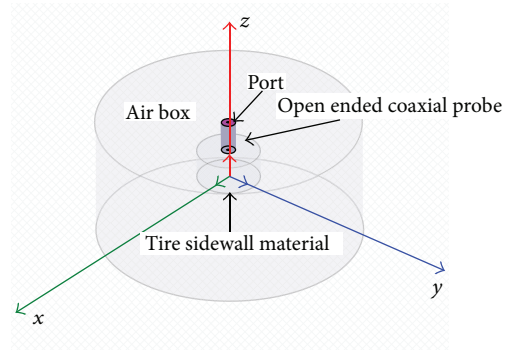

Figure 5: OCP model based on HFSS.

The OCP model based on HFSS is shown in Figure 5. In Figure 5, the inner and outer conductors of the probe are made of gilded brass, and the space between the inner and outer conductor is filled in Teflon dielectric material. The tire specimen is modeled as a cylinder. To avoid perfectly conducting boundaries around the tire sidewall material, an air box is implemented that surrounds the whole simulation setup.

3. Radio Link for UHF Passive RFID

In passive UHF RFID systems, a bidirectional radio link is established between reader and tags, including a forward link from the reader to tags and a backward link from the tags to reader. What radio link for UHF passive RFID differs from conventional radio is that the backward link resembles radar link. Besides, the RFID tag's antenna absorbs waves as a function of its load match and reemits waves as a function of its load mismatch.

3.1. Power Absorbing Coefficient. RFID tag consists of an antenna and chip. The impedance matching of tag antenna and chip strongly influences the RF power transmission and the communication performance between reader and tags. Because of IC technological limit, the impedance of a chip cannot be chosen arbitrarily [12]. So, the chip's input impedance is designed to switch between two values, between the conjugate impedance called as absorbing impedance Z_{chip1} and other impedance called as reflecting impedance Z_{chip2}. The quality of the impedance match can be defined by the power absorbing coefficient τ, which is the power accepted by the chip and the available power P_{tag} at the antenna port [5, 12]:

$$\tau = \frac{4\,\text{Re}\left[Z_{\text{ant}}\right]\text{Re}\left[Z_{\text{chip1}}\right]}{\text{Re}\left[Z_{\text{ant}} + Z_{\text{chip1}}\right]^2 + \text{Im}\left[Z_{\text{ant}} + Z_{\text{chip1}}\right]^2}, \quad (6)$$

where Z_{ant} is the tag antenna's input impedance and $0 \le \tau \le 1$. When $\tau = 1$, all available power is absorbed by the chip. And when $\tau = 0$, no available power is absorbed by the chip. So, the range of frequency that τ reaches a demand value is defined as the bandwidth of the tag antenna. This shows that a best designed tag antenna is very important to improve the performance of UHF passive RFID.

3.2. Power Transmission Coefficient. In a passive RFID, the power absorbed by the chip in forward link can be expressed as

$$P_{\text{chip}} = \tau P_{\text{tag}} = \tau \left|S_{21}\right|^2 P_{\text{TX.reader}}, \tag{7}$$

where $P_{\text{TX.reader}}$ is the transmitted power from reader and P_{chip} must be higher than the tag's sensitivity for the tag's normal work. And $|S_{21}|^2$ is the power transmitted coefficient in the forward link, depending on the antenna power transmission of reader and tag (e.g., antenna gain) and the propagation channel properties like path loss and fading [5].

The power received by the reader from the tag can be expressed as in the backward link:

$$P_{\text{RX.reader}} = \left|S_{12}\right|^2 \eta P_{\text{tag}} = \left|S_{12}\right|^2 \eta \left|S_{21}\right|^2 P_{\text{TX.reader}}, \tag{8}$$

where η is the modulation efficiency, which is defined as the ratio of the power scattered by the tag and the power available at the tag antenna output. $|S_{12}|^2$ is the power transmitted coefficient in the backward link. As real propagation environment is symmetrical, $|S_{12}|^2 = |S_{21}|^2$.

4. Model of Power Transmission of UHF Passive RFID Embedded in Tires

4.1. Harmonic Waves. For time-harmonic fields, when the medium presents a conductivity σ and permeability μ, at the operating frequency ω, a permittivity ε^*, the wave equation can be written as a time-independent wave equation towards $+z$ direction:

$$\nabla^2 E - \gamma^2 E = 0, \tag{9}$$

$$\nabla^2 H - \gamma^2 H = 0, \tag{10}$$

$$-\gamma^2 = k^2 \left(1 - j \tan\delta\right) = \omega^2 \mu \varepsilon^*, \tag{11}$$

where $\varepsilon^* = \varepsilon'(1 - j\tan\delta)$ and $k = \omega\sqrt{\mu\varepsilon'}$ is the wave number corresponding to an unbounded lossless medium with a real dielectric constant ε'.

For uniform plane waves, $\nabla^2 = \partial^2/\partial^2 z$, so (9) and (10) have solutions of the form $Ee^{\gamma z}$ and $He^{\gamma z}$, and the instantaneous values for the fields are given as follows:

$$\begin{aligned} \vec{E} &= \text{Re}\left\{Ee^{-\alpha z}e^{j(\omega t - \beta z)}\right\}, \\ \vec{H} &= \text{Re}\left\{He^{-\alpha z}e^{j(\omega t - \beta z)}\right\}, \end{aligned} \tag{12}$$

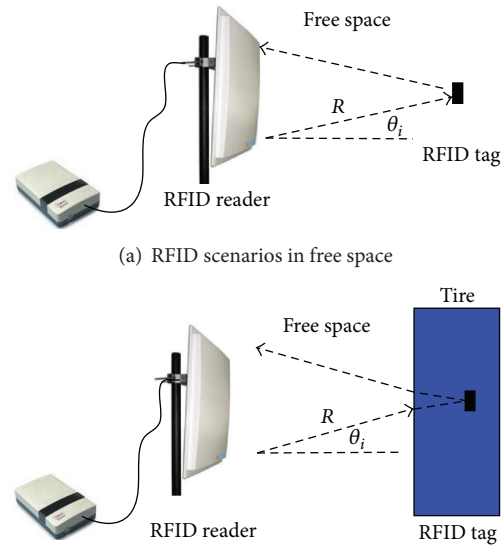

(a) RFID scenarios in free space

(b) RFID scenarios embedded in tire

Figure 6: RFID scenarios.

where the attenuation constant α and the phase constant β can be expressed respectively as follows [13]:

$$\begin{aligned} \alpha &= \omega\left(\frac{\mu\varepsilon'}{2}\right)^{1/2}\left[\left(1 + \tan^2\delta\right)^{1/2} - 1\right]^{1/2}, \\ \beta &= \omega\left(\frac{\mu\varepsilon'}{2}\right)^{1/2}\left[\left(1 + \tan^2\delta\right)^{1/2} + 1\right]^{1/2}. \end{aligned} \tag{13}$$

So, the electric strength decreases with distance z are given as:

$$E = E_0 e^{-\alpha z}\cos\beta z. \tag{14}$$

Substituting (14) into power equation, we have

$$P = P_0 \left|\cos 2\beta z\right| e^{-2\alpha z}. \tag{15}$$

4.2. Power Transmission for RFID Embedded in Tires. The RFID scenarios in space and embedded in tires are shown in Figure 6. In Figure 6, the incident angle of waves is θ_i.

In the free space, the absorbing power by the RFID tag is given as

$$\begin{aligned} P_{\text{chip}} &= \tau P_{\text{tag}} = \tau \left|S_{21}\right|^2 P_{\text{TX.reader}} \\ &= \tau\left(\frac{\lambda}{4\pi R}\right)^2 G_T P_{\text{TX.reader}}, \end{aligned} \tag{16}$$

where λ is the free space wavelength, R is the distance from RFID reader, and G_T is the gain of the tag's antenna.

In the scenarios embedded in tires, (16) can be modified as

$$P_{\text{chip}} = \tau P_{\text{tag}} = \tau \left|S_{21}\right|^2 P_{\text{TX.reader}} = \tau \left(\frac{\lambda}{4\pi R_1}\right)^2 \left|T_c\right|^2 G_T \left|\cos 2\beta l\right| e^{-2\alpha l} P_{\text{TX.reader}} \quad (17)$$
$$= \tau \left(\frac{\lambda}{4\pi R_1}\right)^2 G_t T\left(f, \theta_i, l\right) P_{\text{TX.reader}},$$

where R_1 is the distance between tires and the reader, T_c is electric field transmission coefficient at boundary of tires and free space, and $T(f, \theta_i, l) = |T_c|^2 |\cos 2\beta l| e^{-2\alpha l}$ is power transmission function, depending on θ_i and the distance l in tires.

When a plane EM wave incident at an oblique angle on tires interface, there are two cases to be considered: incident electric field has polarization parallel to the plane of incidence, and incident electric field has polarization that is perpendicular to the plane of incidence. So, from the boundary conditions, that is, continuity of tangential electric and magnetic fields at the car tire interface, and using the Snell's laws of reflection and refraction, the T_c can be derived as follows.

Case 1. Parallel polarization:

$$T_c = \frac{2\eta_1 \cos\theta_i}{\eta_1 \cos\theta_t + \eta_0 \cos\theta_i}. \quad (18)$$

Case 2. Perpendicular polarization:

$$T_c = \frac{2\eta_1 \cos\theta_i}{\eta_1 \cos\theta_i + \eta_0 \cos\theta_t}. \quad (19)$$

5. Numerical Analyses

5.1. Measuring the Permittivity of Tires. A standard tire (CPC2205/55 R16 91V) with the known permittivity (the permittivity is $\varepsilon' = 3.5$ and $\tan\delta = 0.03$ at frequency 866 MHz) is used to determine the parameters C_i, C_0, C_1, and C_2. Using the measuring methods presented in Section 2.1, C_i, C_0, C_1, and C_2 are 0.00113 pF, 2.324 × 10–14 pF, 1.518 × 10–42 pF, and 1.6345 × 10–50 pF, respectively.

The measuring results for reflection coefficients in a Smith chart are shown in Figure 7, using a test car tire (GL 274A, made in Guizhou Tire Co., LTD., China) with a vector network analyzer (AV 3629/A) between 100 MHz and 5 GHz at room temperature. Using (4) and (5), the permittivity of the test car tire can be determined to be $\varepsilon' = 3.78$ and $\tan\delta = 0.038$.

Measuring and simulation results can be compared using the methods presented in Section 2.3. In the OCP model, the inner and outer radiuses of the probe are 0.65 mm and 2.35 mm, respectively. The thickness of Teflon with a relative permittivity of ε' and $\tan\delta = 0.001$ is 1.35 mm. The test tire is modeled as a cylinder with a radius of 10 mm and a height of 10 mm. The absolute error of the real part of simulation and measuring coefficients and the absolute error of the imaginary part of these versus frequency are shown in Figure 8. And the absolute error of the simulation and measuring coefficients is shown in Figure 9. Figures 8 and 9 show that there is small deviation (<0.004) between simulation and measurement. So, it shows that the numerical simulation has good agreement with physical experiment, and the methods measuring the permittivity of tires are feasible.

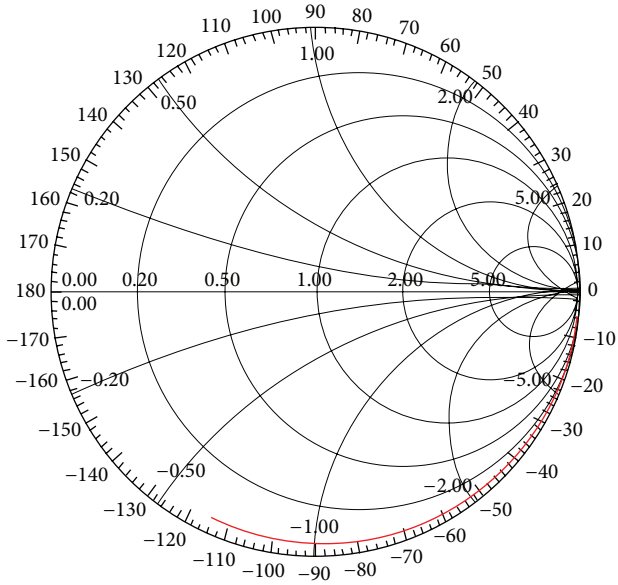

Figure 7: Measured reflection coefficients of a test car tire.

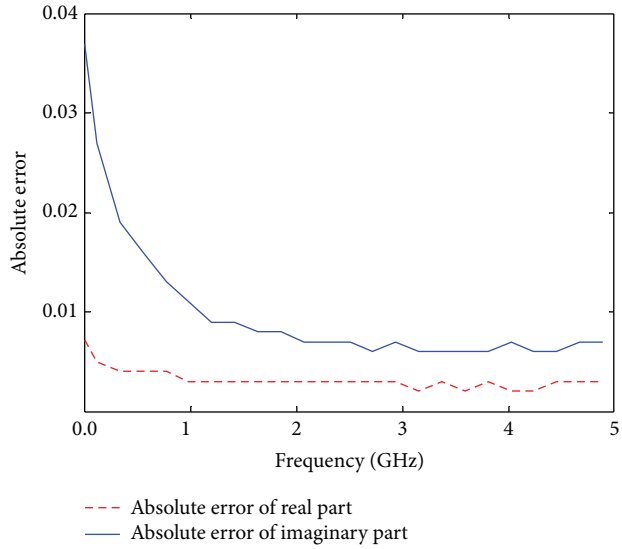

Figure 8: Absolute error values of real part and imaginary part.

5.2. Effects of Incident Angle θ_i on T_c. The permittivity of the test tire is $\varepsilon' = 3.78$ and $\tan\delta = 0.038$ at frequency 866 MHz from Section 5.1. The incident angle θ_i is 0°~90°. A magnitude of T_c for the parallel and perpendicular polarization is shown in Figure 10.

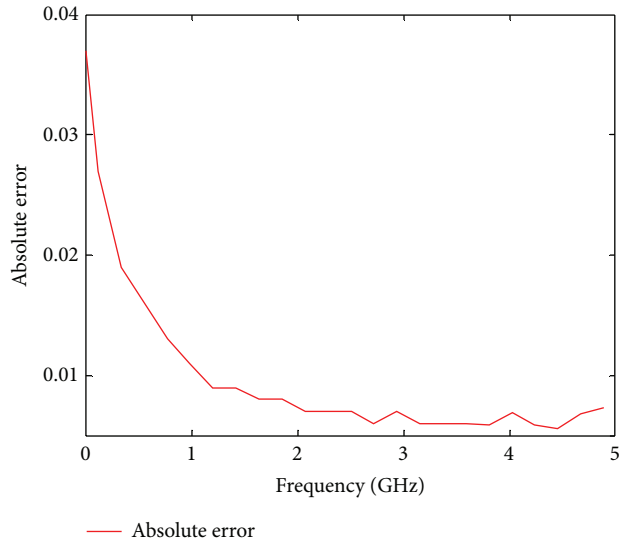

Figure 9: Absolute error values.

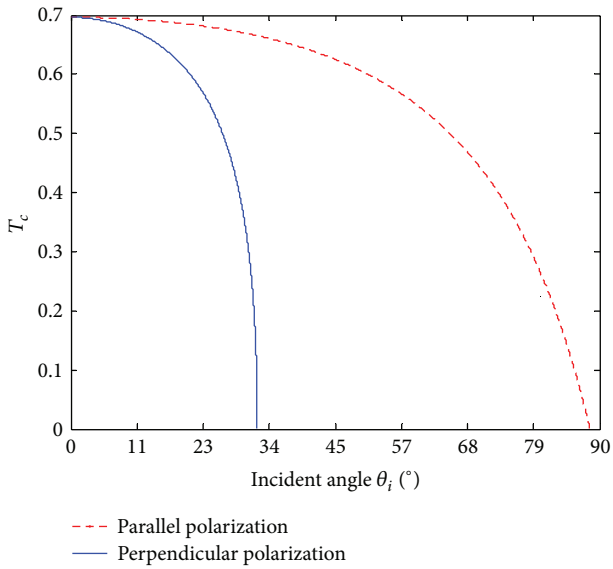

Figure 10: Effects of θ_i on T_c.

In Figure 10, T_c for the parallel and perpendicular polarization decreases with increasing incident angle θ_i. T_c for the perpendicular polarization decreases faster than T_c for the parallel polarization. This conclusion can be obtained from the experiment in Figure 11. The experiment setup contains a reader XC-RF807 and two liner polarization antennae XC-AF26 (one is a horizontal polarization antenna and the other one is vertical polarization). The carrier frequency of the reader is 866 MHz, and the power o is 30 dBmW. The gain of the antenna is greater than 12 dBi, and the frequency range is from 840 MHz to 868 MHz. The distance between GL274A tire and reader is 1 m, and the depth of the tag embed in the tire is 9 mm. Figure 12 shows the relation between the identification rate and angle of incidence.

Figure 11: Experiment setup.

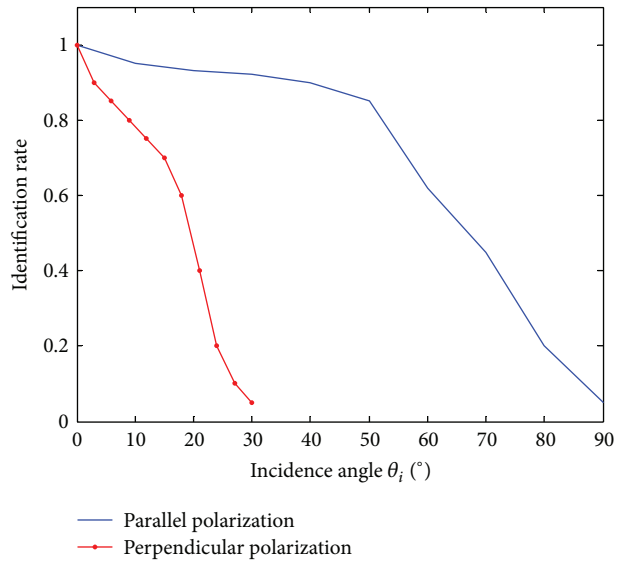

Figure 12: Relations between angle of incidence θ_i and the identification rate.

So, the parallel polarization and normal incidence are chosen for improving the performance of UHF RFID embedded in tires.

5.3. Effects of Distance l on $T(f, \theta_i, l)$. For convenience, The incident angle θ_i is 0°, and the permittivity of the test tire is $\varepsilon' = 3.78$ and $\tan\delta = 0.038$ at frequency 866 MHz f. A magnitude of $T(f, \theta_i, l)$ for the distance l is shown in Figure 13.

In Figure 13, $T(f, \theta_i, l)$ decreases periodically with increasing the distance l in tires. This conclusion can be obtained from the experiment in Figure 11. In this experiment, 8 GAL274A tires are used from Guizhou tire limited company in China. When the tires are vulcanizing, the depths of the tag embedded in the tire are 0.0 mm (tag is pasted on the surface of the tire), 3.0 mm, 6.0 mm, 9.0 mm, 12 mm, 15 mm, 18 mm, 21 mm, and 24 mm, respectively (because of the limitation of the thickness of the tire, the biggest embedded depth is 24 mm). Figure 14 shows the relation between the recognition rate and the embedded depth l. It means the recognition rate of tire embedded RFID

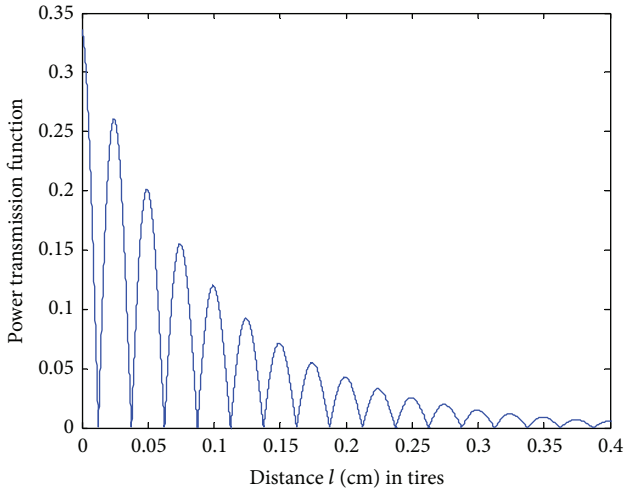

Figure 13: Effects of l on $T(f, \theta_i, l)$.

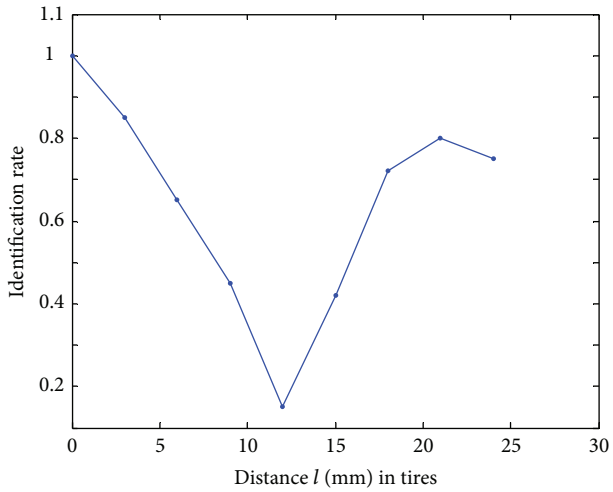

Figure 14: Relations l and identification rate.

system declines along with l also fluctuates along with l. This means the power transmission of tire embedded RFID system declines along with l also fluctuates along with l.

So, the distance l is chosen to keep $T(f, \theta_i, l)$ from locating valley.

6. Conclusions

From now on, UHF RFID tags embedded in tires have a deep impact on tire life cycle management and tire monitoring. So, we present the power transmission of wave propagation for UHF embedded RFID in tires.

In UHF passive embedded RFID systems in tires, the bidirectional radio link between reader and tags goes through air and tires. The total path loss contains reflection loss at tire-air boundaries. So, we give the OCP method for measuring the permittivity of tires. By analyzing the radio link for UHF passive RFID, we establish a model of wave propagation of UHF embedded RFID in tires and make numerical analyses. Finally, we make the conclusion as follows.

(i) The error of the OCP methods for measuring the permittivity of tires is small. And the methods can be used in measuring the permittivity of tires for designing the UHF embedded RFID in tires.

(ii) It is necessary to optimize and design the antenna of tag for the impedance matching of tag antenna and chip. This can improve the performance of the UHF embedded RFID in tires.

(iii) The parallel polarization and normal incidence are chosen for improving the performance of the UHF embedded RFID in tires. Finally, the distance l is chosen to keep $T(f, \theta_i, l)$ from locating valley.

Conflict of Interests

The authors declare that they have no financial and personal relationships with other people or organizations that can inappropriately influence their work; there is no professional or other personal interests of any nature or kind in any product, service, and/or company that could be construed as influencing the position presented in this paper.

Acknowledgments

The authors wish to thank the editor and reviewers for their valuable comments, corrections, and suggestions, which led to an improved version of the original paper. This research is a project partially supported by the Guizhou Natural Science Foundation (Grant no. 2012[38]), the National Natural Science Foundation of China (Grant no. 61362004), and Guizhou Science and Technology Innovation Group for RFID & WSN.

References

[1] S. Basat, K. Lim, I. Kim, M. M. Tentzeris, and J. Laskar, "Design and development of a miniaturized embedded UHF RFID tag for automotive tire applications," in *Proceedings of the 55th Electronic Components and Technology Conference (ECTC '05)*, pp. 867–870, Lake Buena Vista, Fla, USA, June 2005.

[2] RFID 24-7, USA, "Michelin rolls out RFID-enabled tires for London Olympic," 1 pages, 2012, http://www.rfid24-7.com/article/michelin-rolls-out-rfid-enabled-tires-for-london-olympics/.

[3] RFID Journal, USA, "Michelin embeds RFID tags in tires," 2 pages, 2012, http://www.rfidjournal.com/article/view/269/1/1.

[4] RFID Journal, USA, "RFID chip to monitor tire pressure," 2 pages, 2012, http://www.rfidjournal.com/article/view/93/1/1.

[5] J. D. Griffin and G. D. Durgin, "Complete link budgets for backscatter-radio and RFID systems," *IEEE Antennas and Propagation Magazine*, vol. 51, no. 2, pp. 11–25, 2009.

[6] P. V. Nikitin and K. V. S. Rao, "Antennas and propagation in UHF RFID systems," in *Proceedings of the IEEE International Conference on RFID (IEEE RFID '08)*, pp. 277–288, Las Vegas, Nev, USA, April 2008.

[7] P. V. Nikitin and K. V. S. Rao, "Theory and measurement of backscattering from RFID tags," *IEEE Antennas and Propagation Magazine*, vol. 48, no. 6, pp. 212–218, 2006.

[8] V. Komarov, S. Wang, and J. Tang, "Permittivity and measurement," in *The Wiley Encyclopedia of RF and Microwave Engineering*, vol. 4, pp. 3693–3711, 2005.

[9] C. C. Courtney, "Time-domain measurement of the electromagnetic properties of materials," *IEEE Transactions on Microwave Theory and Techniques*, vol. 46, no. 5, pp. 517–522, 1998.

[10] S. Jing, D. Ding, and Q. Jing, "Measurement of electromagnetic properties of materials using transmission/reflection method in coaxial line," in *Proceedings of the 3rd Asia Pacific Conference on Environmental Electromagnetics*, pp. 129–135, Hangzhou, China, 2003.

[11] D. K. Misra, "A quasi-static analysis of open-ended coaxial lines," *IEEE Transactions on Microwave Theory and Techniques*, vol. 35, no. 10, pp. 925–928, 1988.

[12] J. Grosinger and A. L. Scholtz, "Antennas and wave propagation in novel wireless sensing applications based on passive UHF RFID," *Elektrotechnik und Informationstechnik*, vol. 128, no. 11-12, pp. 408–414, 2011.

[13] A. V. Hippel, *Dielectrics and Waves*, John Wiley & Sons, New York, NY, USA, 1954.

Hindawi Publishing Corporation
International Journal of Antennas and Propagation
Volume 2013, Article ID 264671, 6 pages
http://dx.doi.org/10.1155/2013/264671

Research Article

RFID Application of Smart Grid for Asset Management

Xiwei Wang,[1] Qi Dang,[1] Jinglin Guo,[1] and Hongbin Ge[2]

[1] *Beijing China Power Information Technology Co., Ltd., State Grid Electric Power Research Institute, Haidian District, Beijing 100192, China*
[2] *Beijing University of Posts and Telecommunications, Haidian District, Beijing 100876, China*

Correspondence should be addressed to Qi Dang; dangqi@sgepri.sgcc.com.cn

Received 26 August 2013; Accepted 8 October 2013

Academic Editor: Yao Yuan

RFID technology research has resolved practical application issues of the power industry such as assets management, working environment control, and vehicle networking. Also it provides technical reserves for the convergence of ERP and CPS. With the development of RFID and location-based services technology, RFID is converging with a variety of sensing, communication, and information technologies. Indoor positioning applications are under rapid development. Micromanagement environment of the assets is a useful practice for the RFID and positioning. In this paper, the model for RFID applications has been analyzed in the microenvironment management of the data center and electric vehicle batteries, and the optimization scheme of enterprise asset management is also proposed.

1. Introduction

With the innovation of technology and applications, RFID requires a combination with other technologies and concepts of innovative design to meet the application requirements in different aspects of the management and production. In this paper, the applications and design for the intensive assets management are proposed, which are from the concrete practice of the enterprise asset management of data center equipment and electric vehicle battery: State Grid Corporation data center construction and electric vehicles network construction & operation.

1.1. Overview of Application for Life Cycle Asset Management. IT Asset Management based on RFID is a priority for the asset life-cycle management framework. State Grid Corporation of China has launched the construction of the centralized disaster recovery center, the important aspect of which is condition monitoring for environments and equipment in large data center. In the construction of electric vehicle charging service network, battery asset management is an important foundation for electricity service implementation.

The ultra-large-scale data centers require real-time sensing device status in the room and cabinet, focusing on internal regional environmental management, including internal dynamic management of the device in the room, internal static management of the device in the cabinet, and collaborative management of the staff. The battery device management is divided into the storage environment and external operating environment. Each battery data of the battery management system in a warehouse environment can be collected in real time. Real-time status of the battery in car, obtained by means of the vehicle terminal in the running environment, ensures regulatory convergence in the open and warehousing environments.

It improves application performance based on data provided by the business system as well as combining fine control of RFID technology. The application is important for changing the operating approach, enhancing management level, improving basis of operating efficiency, improving asset quality, extending equipment life, and optimizing network asset costs.

2. Proposed RFID Application Model Based on Cyber-Physical Systems Architecture

Real Time Location Systems are a kind of positioning method based on radio signal, using active RFID technology. Other indoor positioning technologies include passive RFID,

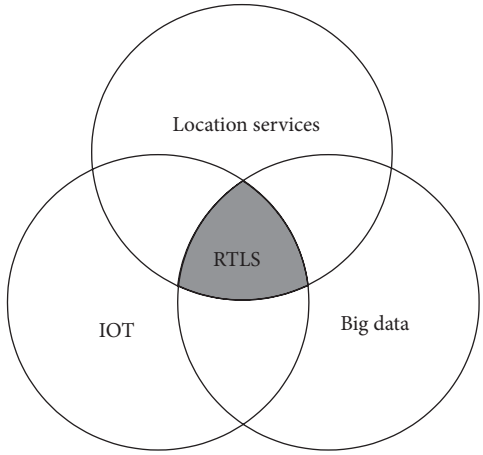

Figure 1: RFID-based real-time location system.

Wi-Fi and UWB. The pioneering research of social network [1], complex network [2–5], big data [6–11], and cyber-physical systems (CPS) [12–16] is emerging, which change the understanding of large-scale systems as in Figure 1 shows. CPS is the integration of computing and physical systems, which is the next generation of intelligent system to integrate computing, communication, and control.

In practice, techniques combination and application innovations can realize the effective management of assets physical state. Technique combinations include RTLS, RFID, and sensor technology. Application innovations guide the scheme for application through the research on RFID application model based on CPS architecture including acquisition, transmission, analysis, and decision making.

2.1. Proposed System Structure Model. The large enterprises' various RFID applications demand is the main factor; thus the RFID Application Model is proposed as Figure 2 shows. The model is divided into perception, transmission, calculation, control, and the supporting unit to form a complete closed-loop system, wherein the calculating unit includes a variety of real-time processing engine. This model meets the design requirements of the corporate assets applications and open environment applications.

Considering the huge amounts of data, the system needs to be configured flexible computing unit, capable of handling multidimensional data associated with the local real-time processing, timing, and behavior change information, including the location and spatial information and flow data, as well as the internal state and personnel state behavior. In short, the design model needs to meet the design requirements of the system in the context of the development of the Internet of Things and big data.

Considering the location status, time and other factors, the function $C(P, H, x, y, t)$ of the application model is established, as shown in the formula (1). Through the associated analysis of the position, status, and other data within the predetermined time, the preset rules for real-time behavioral analysis engine are obtained as the initial conditions of the model function. Subsequently, using the function and initial conditions, the completeness of the information recorded is formed:

$$C(P, H, x, y, t) = P(x, y, t) + \Delta P(t) + H(x, y, t) + \Delta S(t). \quad (1)$$

In the function, $P(t)$ represents the device location and $H(t)$ represents staff position; $\Delta P(t)$ represents a relative position; $\Delta S(t)$ represents a change of state; (x, y, t) represents the two-dimensional position coordinates and time.

2.2. Analysis for the Comparative Model. Based on IoT application model, Big Data technology helps us for deep relationship. The important difference compared to the previous design is that the results and forecast information is quickly obtained through the phenomena associated with the data analysis, and there is no need to spend too much time to get the answer for the problem causal association. Traditional demand models tend to seek causal association, looking for trends, cycles, and other factors in order to create the function. For example, the user application requirements are described through the method of a random time series, as shown in the following formula

$$Y(t) = f(t) + p(t) + X(t). \quad (2)$$

In the formula (2), t represents time and $f(t)$, $p(t)$ are nonrandom items. $f(t)$, the trend term, reflects the trend of the model $Y(t)$ which is changed by linear or exponential function; $p(t)$, the periodic term, reflects the cyclical change of $Y(t)$, such as year, month, day, or hour periodically; $X(t)$ is a random term, which reflects the impact of various random factors on $Y(t)$. $X(t)$ can be assumed to be a normal stationary random process. The $f(t)$ and $p(t)$ is generally not constant, and therefore $Y(t)$ is a nonstationary random process. Based on the above principles, nonrandom items $f(t)$ and $p(t)$ can be obtained through the acquisition system, and the statistics can be obtained through mathematical methods. Based on the type of user behavior, random item $X(t)$ can be accurately adjusted and standardized, and therefore $Y(t)$ has the higher accuracy, thereby forming a quasi-demand real-time model.

In the formula (1), although each item is random one, through the analysis of random mass data, certain patterns of behavior can be extracted as the analysis basis of the real-time behavior. Massive data analysis does not mean the way of the traditional mathematical statistics for obtaining samples, which emphasizes that the complete data is required as the basis for application, and it does not mean that the analysis of $X(t)$ from the formula (2) copied to $f(t)$ and $p(t)$ can get the result of the formula (1). There is a fundamental change, and the data is a whole complete collection.

The design procedures of the real-time behavior analysis engine come from the early accumulation and effective analysis of data. This model requires a certain modeling time $T0$ before the quasi-real-time system processing and will finally be able to get the key prediction model. The worth considering factors are as follows: (1) pay attention to the relative relationship, combined with the characteristics of RFID technology; (2) collect contact data as the basis for modeling future behavior.

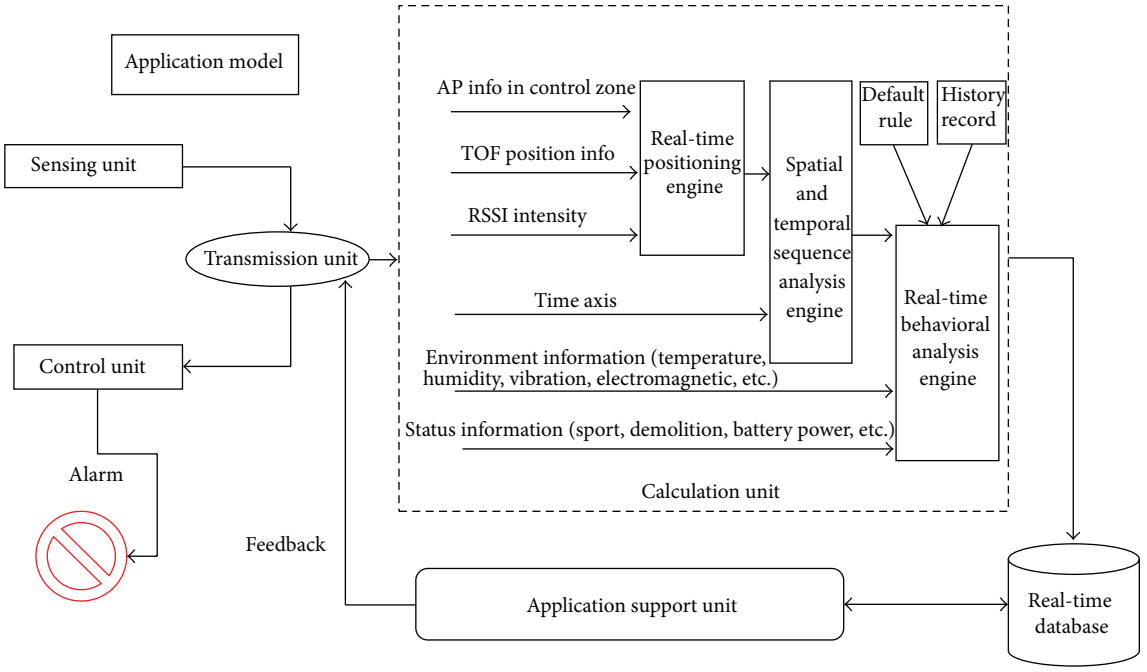

Figure 2: System structure model.

2.3. Consistency Analysis of Large-Scale Enterprise RFID Applications. In addition to the reliability and effectiveness of the system, consistency is a major consideration. The reference architecture depicts the overall application, wherein each unit division also has contact with each other. Each unit can be implemented to make a product, or can be used as a collection of several products, or part of a product. Despite the fact that the manufactured products have reached some kind of consistency request or meet the reliability under certain scenarios, the actual system need pay attention at the system level due to the change of scene, the integration of a variety of technologies, and products. Using the unified model and a simple combination of technologies can easily ensure application consistency, reliability, and validity.

3. RFID Application Analysis and Solutions

3.1. Problems and Demands for Data Asset Management. The data assets precise management requirements include: coordination and management of personnel and equipment based on traditional RFID asset management applications, management for differentiated IT assets and dynamic environment equipment, access to the status and location identification, solving communication interference in small closed environment, the use of a simple and reliable means of communication to reduce the procurement, and low costs of installation and maintenance.

3.2. Key Design for Data Asset Management. Integration of real-time positioning technology, multifrequency communication technology, sensor technology, assets, and personnel indoor mobile positioning is proposed to use. The dual-band communication technology realizes the static positioning and situational awareness of local environmental assets. Integration of sensors, real-time location technology realizes equipment, personnel, mobile monitoring, and indoor navigation as shown in Figure 3.

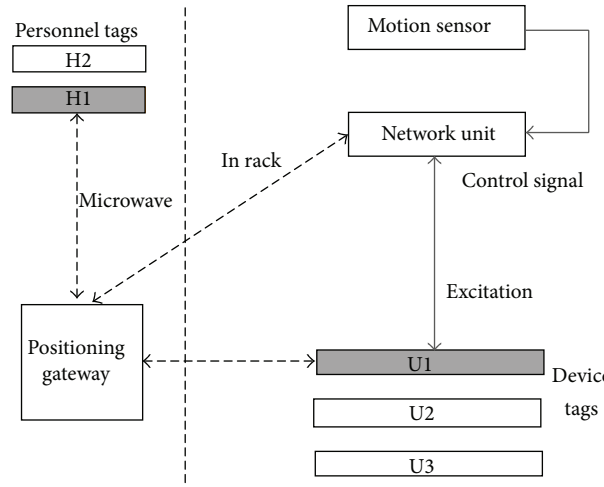

Figure 3: Design on RFID sensor application in real time positioning.

Important components include the following: (1) motion sensor unit: integrated displacement and motion sensor, to complete the door opening and closing judgment and to activate the low-frequency two-way communication of low-frequency transceiver unit with cabinet asset locator tab; (2) low-frequency transceiver unit: completing cabinet positioning communications and moving the collected information to the network unit and also can be part of network unit; (3) network unit: integrated microwave band

RFID communication module, with low frequency control module, sound and light alarm module; providing dynamic positioning with 2.4 G microwave signal transmission, controlling the low-frequency transceiver unit with bidirectional communication; making the alarm and real-time feedback to remind the manager of job exceptions occurred in asset management; (4) positioning tag: integrated the active RFID positioning module with the low-frequency communication module to complete the 2.4 GHz microwave band RFID positioning and low frequency positioning in rack; integrated motion/temperature/humidity sensor, sensing the movement status of the device and the cabinet temperature and humidity environment; (5) personnel tags: integrated active RFID positioning module to complete the 2.4 GHz microwave band RFID location; integrated motion sensors for perception of staff state; (6) positioning gateway: realizing communication with network unit and the RFID tag, being as intelligent front-end unit of the asset monitoring application, running embedded systems, achieving the transmission of location data to background systems and databases.

The switch displacement sensor and low-frequency transceiver unit are installed inside the cabinet. Opening and closing movements trigger the interaction between positioning of labels and the cabinet gateway outside. According to the changes of the environment and equipment state, it is divided into three states: the cabinet opening with the device in stationary state, the device in moving state, and the cabinet closed with the device in stationary state. When the cabinet is turned on and the device is stationary, the cabinet network unit starts communication with the positioning gateway, just updating records and collecting gateway control commands. Under the motion state of the device, the RFID positioning function activated by the tag motion sensor is realizing positioning management in meter level accuracy, using a rack network unit as an auxiliary landmark. As cabinets closed with the device in still, the lower frequency signal transmission is fulfilled by low-frequency transceiver unit and tags then to be unified for communication by network unit and positioning gateway. Networking unit and positioning labels with temperature and humidity sensors constitute environment perception network inside cabinets, and the different cabinet network units form the upper senior-aware network with each other.

In the function (1), the device location $P(t)$ with relative position $\Delta P(t)$ and personal position $H(t)$ is realized by Tag and Low-frequency transceiver unit; the state information of the mobile sensing unit acts as $\Delta S(t)$. Positioning gateway has a computing unit functions.

The position information and the environment perception are mainly realized by hardware, that is, positioning gateway, sensor tag, and low-frequency transceiver unit. While the perception of the state, such as temperature and humidity, is achieved by the integration of special sensors. The design uses active RFID positioning technology and the integration of sensors of various types to achieve equipment location and status perception, which is cost-effective application of the cabinets unit and positioning sensor tag.

The simple design of the sensor could judge the state of the equipment and staff behavior. The data analysis and threshold setting from the use of location data meet the design requirements of the application model well.

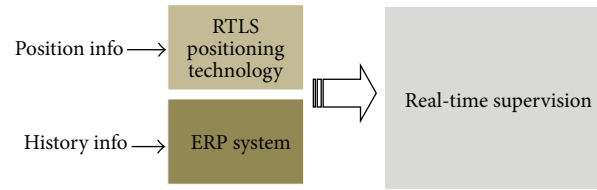

Figure 4: Vehicles battery supervision using RTLS and ERP.

3.3. Problems and Demands for Open Environment Battery Asset Management. The battery storage management can refer to similar data asset management scheme described above. The main difference in warehouse management is the battery maintenance of large amounts of exchange data, roughly in the tens to hundreds of megabytes. The data transmission is the major demand in storage place densely stacked. Only a small amount of data is returned to the operator in the course, on account of the use of CAN and trip computer in conjunction with the mobile communication network, with the amount of data far less than the static data exchange and collection frequency being limited.

3.4. Critical Designs for Open Environment Batteries Asset Management Scheme. Battery storage management has different demands from data asset management, focusing on data delivery to the exclusion of networking, positioning, and collaborative technology. It uses active RFID to complete the Wi-Fi channel open and closed to achieve data transmission. Figure 4 shows vehicles battery supervision need the combination of RTLS and ERP.

RFID is not only identification achieved but also an excitation switch to realize the specified battery WIFI channel established. In the actual process, tens to hundreds of battery management communication can be accomplished only with several IP addresses. Using RFID as the management of the address and the communication channel solves the single battery status data exchange problem, which is a small proportion of the cost for valuable equipment.

In the operating environment, the battery status information collected by the battery management system will be transmitted to the remote by CAN, ECU and on-board computer shown as Figure 5. Environmental status of the battery in the car can be achieved using low-frequency communication. Associated together with cars, $P(t)$ is realized by GPS or GSM, and $\Delta S(t)$ is obtained by RFID sensor.

3.5. Summaries for Battery Assets Management Practice

(1) WIFI excitations realize detections of the battery in the shelf.

(2) DTU monitoring with GPRS dealing with the battery data transmission.

(3) Battery status collected by BMS is transmitted by the CAN bus to the vehicle terminal.

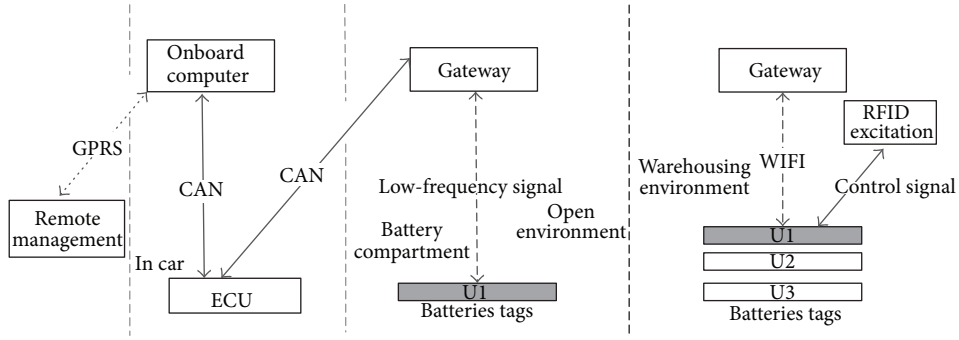

Figure 5: Design on RFID sensor application for battery assets.

4. Analysis for Application Practice

At present, the existing typical implementations include (1) passive UHF RFID application, using cabinet near field antenna design and installation location information, realizing equipment inventory and real-time location, is the case with patented product for data center; (2) active RFID and rack infrared integrated application: the solution can be viewed as the integrated application of active RFID and sensor technology. Real-time location-based applications of the microenvironment of the data center do not depend on a single positioning technology advanced but select and define the product by the actual needs.

(1) Passive RFID Design Defects. According to the comparison between design and model, the relative positional $P(t)$ is primarily obtained on the discrete-time $T1$, $T2$, and $T3$, and so forth. Since adjacent time difference is not the same, along with the lack of temporal association and relationship of state and behavior, the design does not fully comply with the model. In addition, passive RFID location-based applications need to deploy a large number of antenna and reader, and the number of antenna elements cannot be changed, although it is possible to reduce the reader number by port splitters.

(2) Active RFID Scheme Design Features. Based on the above, relative position $\Delta P(t)$ is additionally used with discrete-time changed into real-time and position increases precisely. Despite the timing relationship, the lack of the status and behavioral variables do not fully comply with the model, but the application has been relatively close.

According to application data characteristics of the electric vehicles services platform, operation data can be divided into basic data, information file data, processing data, periodic data, documents data, and statistics query data. Currently, big data with real-time sensor data is the new application. The new practical experiment data would be collected and presented to justify the practice of these proposed models.

5. Advantage of Applications from the Model

The change in location, timing, and behavior is as the information input. The relative position and area position from active RFID form the basis of the space-time cube geospatial data. Staff position change improves the interactivity, using multidimensional and massive data modeling as the formation of real-time applications. The effectiveness and consistency is improved compared to traditional RFID systems. In practical applications, the selection of passive RFID, active RFID, and RFID with sensors tends to the third which has obvious application value due to the fact that the prior two are the actual product, and the last is applied to the actual project.

5.1. Changes for IT Assets Management Application. Real-time positioning sensors can take into account dynamic, static, and cabinet-level position identification. The integrated innovation in application mode based on behavioral analysis can be achieved. For example, classified usage rules of tags created, the function in each tag dynamic changes. Classification model is established based on the usage frequency of the tags, and taking advantage of middleware for the classification management function in Figure 6, the different units of tag can dynamic wake up and close. The specific design includes priority for critical equipment to use active tags; combined with sensor, increasing the equipment motion recognition; the combination of video and active tags to increase staff identification and behavior monitoring; real-time collaborative management of the operation of the device and persons. In addition, the policy is applied mainly for the classification of the cabinet-level identification. Just the cabinet level monitoring with simplified static positioning accuracy and mobile positioning can record formation of $C(P, H, x, y, t)$ to form an effective monitoring.

5.2. Benefit of Vehicle Battery Application. The importance of electric vehicle batteries is obvious, the potential value of which is the life cycle management, and it is extremely important for operator to obtain comprehensive data as commercial design using RFID hardware infrastructure at different stages. From the perspective of standard and industrial development, we still require the reliable design to meet electric vehicles battery needs of production, leasing and operations. However, for State Grid battery management, it is already an important attempt.

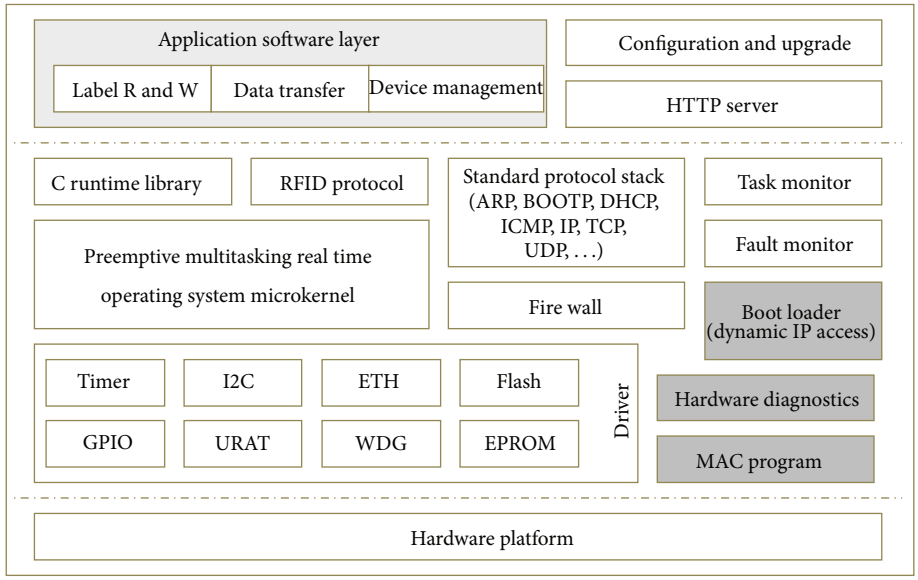

Figure 6: Front-end software infrastructure of RFID applications.

Electric vehicle asset management and IT assets both take advantage of RFID technology to enhance the reliability, security, and trace ability of asset. The difference between data center application and battery management is that the former is applied to closed environment and the latter is applied in complex open environment.

6. Conclusions

In the current social environment and development opportunities, taking advantage of RFID and other technologies, as well as the practical demand-driven, the new application ecological system is being formed; some of which are local for enterprises management and the others are open applications that are beneficial to social services, to promote RFID continuous development.

Conflict of Interests

The authors declare that there is no conflict of interests regarding the publication of this paper.

References

[1] S. Milgram, "The small world problem," *Psychology Today*, vol. 2, no. 1, pp. 60–67, 1967.

[2] R. Cohen and S. Havlin, "Scale-free networks are ultrasmall," *Physical Review Letters*, vol. 90, no. 5, Article ID 058701, 4 pages, 2003.

[3] R. Albert, H. Jeong, and A. Barabási, "Error and attack tolerance of complex networks," *Nature*, vol. 406, no. 6794, pp. 378–382, 2000.

[4] D. J. Watts and S. H. Strogatz, "Collective dynamics of "small-world" networks," *Nature*, vol. 393, no. 6684, pp. 440–442, 1998.

[5] J. M. Kleinberg, "Navigation in a small world," *Nature*, vol. 406, no. 6798, p. 845, 2000.

[6] A. J. G. Hey, *The Fourth Paradigm: Data-Intensive Scientific Discovery*, 2009.

[7] D. Howe, M. Costanzo, P. Fey et al., "Big data: the future of biocuration," *Nature*, vol. 455, no. 7209, pp. 47–50, 2008.

[8] J. Dean and S. Ghemawat, "MapReduce: simplified data processing on large clusters," *Communications of the ACM*, vol. 51, no. 1, pp. 107–113, 2008.

[9] C. Anderson, "The end of theory: the data deluge makes the scientific method obsolete," Wired, 2008.

[10] S. Ghemawat, H. Gobioff, and S. T. Leung, "The Google file system," *ACM SIGOPS Operating Systems Review*, vol. 37, no. 5, pp. 29–43, 2003.

[11] L. Guojie and C. Xueqi, "Research status and scientific thinking of big data," *Strategy and Policy Decision Research*, vol. 6, pp. 647–657, 2012.

[12] E. A. Lee, "Cyber physical systems: design challenges," in *Proceedings of the 11th IEEE Symposium on Object-Oriented Real-Time Distributed Computing (ISORC '08)*, pp. 363–369, Orlando, Fla, USA, May 2008.

[13] Y. Tan, M. C. Vuran, and S. Goddard, "Spatio-temporal event model for cyber-physical systems," in *Proceedings of the 29th IEEE International Conference on Distributed Computing Systems Workshops (ICDCSW '09)*, pp. 44–50, 2009.

[14] J. E. Kim and D. Mosse, "Generic framework for design, modeling and simulation of cyber physical systems," *ACM SIGBED Review*, vol. 5, no. 1, pp. 1–2, 2008.

[15] R. R. Rajkumar, I. Lee, L. Sha, and J. Stankovic, "Cyber-physical systems: the next computing revolution," in *Proceedings of the 47th Design Automation Conference (DAC '10)*, pp. 731–736, ACM, June 2010.

[16] H. Ahmadi, T. F. Abdelzaher, and I. Gupta, "Congestion control for spatio-temporal data in cyber-physical systems," in *Proceedings of the 1st ACM/IEEE International Conference on Cyber-Physical Systems (ICCPS '10)*, pp. 89–98, ACM, April 2010.

Hindawi Publishing Corporation
International Journal of Antennas and Propagation
Volume 2013, Article ID 242840, 10 pages
http://dx.doi.org/10.1155/2013/242840

Research Article

Modelling and Design of HF RFID Passive Transponders with Additional Energy Harvester

Piotr Jankowski-Mihułowicz, Włodzimierz Kalita, Mariusz Skoczylas, and Mariusz Węglarski

Department of Electronic and Communications Systems, Rzeszów University of Technology, W. Pola 2, 35-959 Rzeszów, Poland

Correspondence should be addressed to Piotr Jankowski-Mihułowicz; pjanko@prz.edu.pl

Received 22 May 2013; Accepted 12 August 2013

Academic Editor: Yuan Yao

The huge progress in electronics technology and RFID technique gives the opportunity to implement additional features in transponders. It should be noted that either passive or semipassive transponders are supplied with energy that is derived from the electromagnetic field generated by the read/write device and its antenna. This power source is used to conduct radio-communication process and excess energy could be used to power the extra electronic circuits, but the problem is to determine the additional power load impact on the RFID system proper operation and size of interrogation zone. The ability to power the supplementary electronic blocks applied in the HF passive transponders is discussed in detail this paper. The simulation model and test samples with a harvester that recovers energy from the electromagnetic field of read/write device and its antenna have been developed in order to conduct investigations. The harvested energy has been utilized to supply a microprocessor acquisition block for LTCC pressure sensor developed in research previously described by authors.

1. Introduction

The (radio frequency identification) RFID technique is generally used in the processes of object identification. The permanent cost reduction of a single transponder and standardizations of operating conditions for all involved devices affect the broad implementation of these solutions in security and access control systems, industrial logistics (material supply or goods shipment), identification of measurement samples or valuable materials (in various areas of science, technology, or medicine), and forth [1–5]. Further improvements are feasible in many cases thanks to great achievements in modern electronics and significant progress in new technology of hybrid microelectronic circuits [6–8]. For example, it gives the opportunity to implement additional features in transponders. The extra functional blocks are usually powered by a built—in supply source—disposable battery. Unfortunately, since the batteries are used, the costs of applications with such transponders are very high and system maintenance is inconvenient with respect to totally passive solutions. However, it should be noted that either passive or semipassive transponders are supplied with energy that is derived from the electromagnetic field generated by the read/write device (RWD). This power source is used to conduct a radio-communication process and excess energy can be used to power the extra electronic circuits. But the problem is to determine the additional power load impact on the RFID system proper operation and size of interrogation zone (IZ).

The necessity to integrate a pressure sensor made in (low temperature cofired ceramic) LTCC technology [9] with a passive transponders consisted not only of a chip and antenna but also of a radio-frequency (RF) energy harvesting circuit (Figure 1) has been the key impulse to conduct the presented research.

The considerations also include interrogation zone (IZ) determination problems. The IZ is a space around the RWD where communication and energy conditions are met [6, 10, 11]. Its shape and size is determined by the possibility of performing two tasks: providing transponders with the correct power supply and, as a result, establishing conditions for data radio communication with the RWD. It is the main parameter

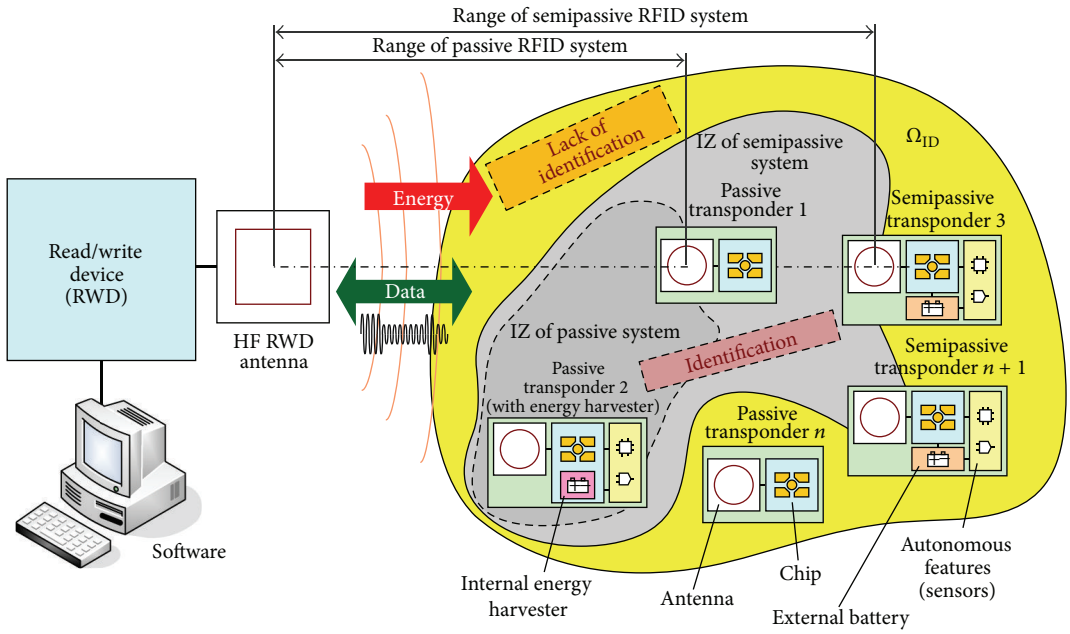

Figure 1: Block diagram of passive and semipassive RFID system.

because it comprehensively covers the matter of energy and communication activity of all RFID system parts. Since the interrogation zone is determined for the whole application (not for a single device), a knowledge base about essential properties of RFID equipment is necessary. But unfortunately, producers very often do not specify some essential electrical and structural parameters for their products. Because of this, the calculation of basic parameters describing interrogation zone (e.g., the maximal distance/range between transponder and the RWD antenna centre) is impossible. At the present stage of knowledge, it is the main reason why the practical implementation of anticollision identification is restrained especially in automated systems operating in dynamic conditions. In this situation, inefficient and time-consuming trial and error methods are commonly used during system configurations. It does not provide reliable information on the operation and efficiency of the automated identification processes. The problems of RFID application predictability become even more important in the context of placing the physical quantity sensors in battery-less passive transponders.

The problem is further complicated in anticollision systems. The main characteristic of the single identification is the possibility to recognize only one object labelled with a radio transponder that has to be alone in the interrogation zone. In the case of the anticollision system, algorithms of multiaccess to radio channel are used and the communication process is carried out simultaneously with several transponders [10]. This makes it possible to automatically distinguish many objects appearing in the IZ at the same time. In both identification systems, it is assumed that labelled objects are present in the operating zone Ω_{ID} (Figure 1), but there is no certainty that they will be recognized. The situation is even more complicated when the dynamic processes (with variable location and/or orientation of object in space) will be analyzed instead of the stationary one (with fixed location and orientation of objects in space) [12].

In RFID systems, the transponders are supplied with energy deriving from the electromagnetic field generated by the RWD. This supply source is always used to conduct a radio-communication process. But in transponders with sensors (sensors with RFID interface), it is necessary to provide energy for powering additional functional blocks.

The semipassive transponders (Figure 1) have a built-in extra source (e.g., lithium battery) which can be exchangeable or not [10]. A part of additional energy can be utilized to enlarge the size of interrogation zone but most of it is used for powering blocks of additional autonomous functions, such as measurement of physical quantities (humidity [13–15], temperature [16–19], light intensity [18], pressure [20], acceleration [21], gas [22], etc.), and writing gathered data in a built-in memory. These extra functions are carried out without the participation of RWDs. Because of battery, these types of transponders are more expensive (with respect to totally passive solutions) and have limited durability and there is necessity to replace worn out batteries. According to practice rules of RFID system usage, there is necessity to mechanically protect the batteries against thefts or to utilize disposable solutions (such transponders have to be replaced when the battery is exhausted or spoiled). However, it should be emphasized that the RWD has to be still active for properly conducting radio communication process, because the extra battery system can never be used for activating the transmitting circuit. It means that the antenna of transponder does not emit the electromagnetic field as it is in the case of conventional short range devices (SRD) [23, 24].

Disadvantages of the above mentioned power supply, development in the branch of new materials, and availability

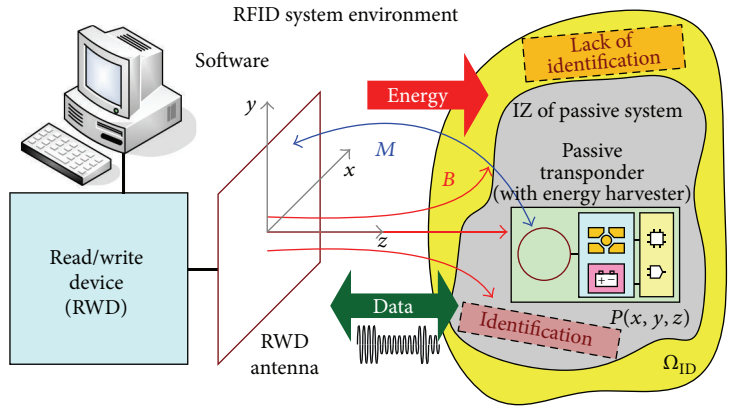

Figure 2: Passive RFID system with inductive coupling and energy harvesting mechanism.

of low power integrated circuits as well as trends towards utilizing alternative energy that can be harvested from the operating environment of RFID systems are the reasons why many current investigations are focused on the integration of sensors with passive transponders [25–29]. The research results are useful in many applications of contactless automatic identification (medicine [30] and healthcare [31, 32], building industry [33], and supply chains [34]), although it is impossible to save measurement data in memory of such a hybrid construction without activation of RWD devices.

On the base of elaborated 3D IZ model, authors present (Section 2) the aspects connected with recovering excess energy which is supplied by an RWD device and with its utilization to power a pressure sensor with a passive RFID chip. Using the model and a passive chip with energy harvester, they propose the construction of sensor with RFID interface (Section 3) that is designed to work in the HF band of inductively coupled RFID systems (operating frequency f_0 = 13.56 MHz), according to the communication protocol ISO/IEC 15693 [35]. Analyzing conducted tests and derived results (Section 4), readers can see that synthesis model of 3D interrogation zone can be used for predicting spatial placements of sensors in different kinds of RFID system applications [36].

2. Model of Passive Transponder with Energy Harvester

RFID systems working in the HF band utilize the typical operating frequency f_0 = 13.56 MHz. Because the wavelength λ is about 22 m, the RWD and transponder antennas are made in the form of small loop in relation to λ. The inhomogeneous magnetic field generated into the RWD antenna vicinity is the medium for both transferring energy and wireless data exchange. The most common mean of data transmission is the load modulation with amplitude-shift keying. The load modulation with subcarrier is used because of the necessity for transferring energy to the passive transponders. These mechanisms are implemented in protocols normalized by ISO/IEC 15693, 14443, 18000-3, and others.

The inductively coupled RFID HF systems operate in the zone for which an inhomogeneous magnetic field (characterised by the induction B or magnetic field strength H) and strong coupling (characterised by the mutual inductance M) between antennas of the communication set occur (Figure 2).

The efficiency estimation of energy transmission from RWD to passive transponder is complicated for this kind of medium, especially in the proposed solution with autonomous features (e.g., module for measuring physical quantities). Since the extra module disturbs the proper operation of transponder, the careful study of its impact on main parameters is compulsory. This problem is explained in details on the elaborated model of a passive transponder with the active build-in block for harvesting energy from the RFID system environment (Figure 3).

The presented model is valid for all antenna arrangements existing in proximity [37] or long range [38] RWD devices. It is suitable for the transponder located in a $P(x, y, z)$ point of the Cartesian coordinate system (Figure 2). It includes all elements of real solution: loop antenna, chip with extra energy harvester, and in addition microprocessor for controlling autonomous features. The microprocessor system tasks are to gather data from sensors (e.g., by using A/C converter) and write it to a chip internal memory by using a communication interface (e.g., I^2C bus). It is powered by the harvester and it is active only when the transponder is in the interrogation zone and the energy conditions are satisfied.

The antenna loop is a parallel circuit in which L_T is the self-inductance and R_T represents the resistance of wire used for creating the winding and it also characterizes ohmic losses. The electric capacity C_{TS} is the resultant of all capacitances between the coils and it results from a uniform distribution of wire electrical parameters along the entire length of winding. The equivalent of loop antenna has been also included in the general scheme in order to facilitate a subsequent experimental verification (R_{TS} and L_{TS} denote the serial resistance and the inductance of series antenna circuit). The source U_{RT} represents voltage inducing in the antenna loop when the transponder is in the magnetic field of read/write device. It is expressed by (1) where pulsation $\omega = 2\pi f_0$ and I_R means the current in the winding as

$$U_{RT} = j\omega \cdot M \cdot I_R. \quad (1)$$

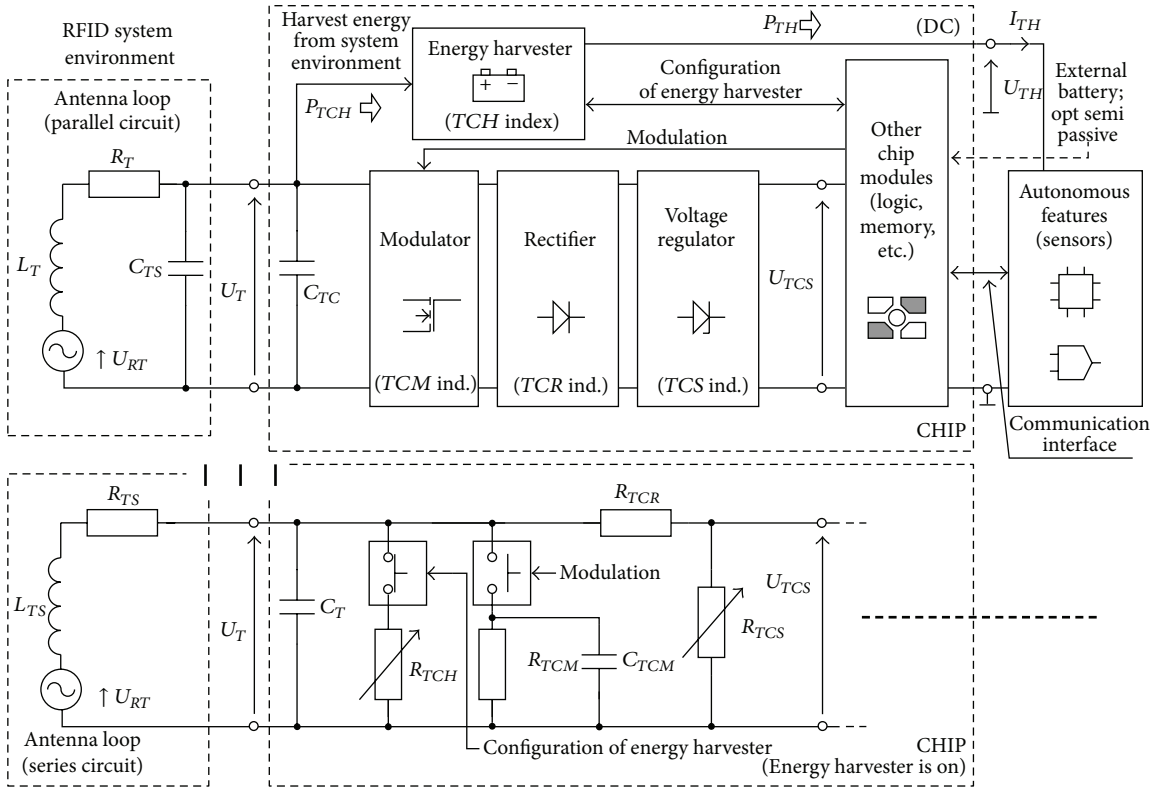

Figure 3: Model and electric equivalent of passive RFID transponder with energy harvester.

The maximum value of voltage U_T on loop antenna terminals is obtained for the parallel resonance between the inductance L_T and the capacitance C_T of active chip. The capacitance C_T is expressed by (2) where C_{TC} means the self-capacity of chip (an energy storage cell for powering radio communication processes), C_{TCR} is the resultant of rectifier and voltage regulator capacitances, and C_{TCH} describes the electric capacity of energy harvester as

$$C_T = C_{TC} + C_{TCR} + C_{TCH} \cong C_{TC}. \quad (2)$$

The synthesis of rectifier and voltage regulator is made separately [39, 40]. Although the rectification takes place in a half-wave or full-wave rectifier [41], it is controlled by the voltage regulator [39]. In the case of passive transponders working in the HF band, both of the circuits are commonly realized on fast switching diodes in MOS technology [42]. It should be mentioned that the proposed model will be also valid for all blocks manufactured on a flexible substrate in a printed electronic technology which is possible thanks to the tremendous progress in the nanomaterial science [43, 44].

The rectifier and voltage regulator are characterized by the capacitances included in the C_T quantity and by the resistances R_{TCR} and R_{TCS}. These elements of transponder equivalent affect electric circuit parameters which are seen at the loop antenna terminals. The R_{TCR} is a generalized parameter of voltage rectifier circuit obtained on the base of diode graphical model (static characteristic). Its value mainly depends on a circuit design and elements included in a specified construction of chip from a given manufacturer. Since the piecewise linear approximation of diode characteristic is generally used in electronic circuit analyses, the linear nature can be assumed for this value. The second quantity R_{TCS} represents the internal structure of voltage regulator. Although this block is used for powering the internal structure of transponders, it can be assumed that the stabilized voltage U_{TCS} is constant. This approximation is justified due to negligibly small current drawn and limited impact of this phenomenon on circuit parameters seen at the loop antenna terminals.

The variable resistance R_{TCH} represents the harvester internal structure. If minimum losses are assumed in this block (the power P_{TCH} at the input is almost equal to the power P_{TH} supplied to the autonomous feature module), the resistance value can be determined from (3) in which U_{TRMS} means RMS voltage U_T and U_{TH}, I_{TH}, respectively, dc current and voltage on the power output of energy harvesting block as

$$R_{TCH} = \frac{U_{TRMS}^2}{P_{TCH}} \cong \frac{U_{TH}}{I_{TH}}. \quad (3)$$

Since the harvester derives energy from the electromagnetic field of read/write device and therefore affects the interrogation zone, the possibility of its functional property configuration is usually available by manufacturers. Depending on a chip design, it is possible to reduce or control the output values of voltage U_{TH} and/or maximum current I_{TH} [45, 46]. These properties describe appropriate operation boundaries

of energy recovery block and ability to power the autonomous function modules together with connected sensors.

The modulator capacitance C_{TCM} and resistance R_{TCM} are also included in the model (Figure 3). The proper transponder operation does not depend on these parameters in the considered range. It is due to the fact that radio-communication processes are conducted according to adequate protocols (for the HF band: ISO/IEC 15693, 14443, 18000-3, and others) and the load modulation with subcarrier is used for transmitting data in the transponder-RWD direction.

Taking into account the underlying assumptions, it is possible to determine the voltage value induced at the loop antenna terminals under the load of modelled chip input circuits (4). Then, the voltage drops in the unloaded divider R_{TCR} and R_{TCS} are described by (5) as

$$U_T = j\omega \cdot M \cdot I_R \times \left(1 + \left(\left(1/R_{TCH}\right) + \left(1/\left(R_{TCR} + R_{TCS}\right)\right) + j\omega C_T\right) \times \left(j\omega L_{TS} + R_{TS}\right)\right)^{-1}, \tag{4}$$

$$U_T = U_{TCS} \cdot \left(1 + \frac{R_{TCR}}{R_{TCS}}\right). \tag{5}$$

Because the U_{TCS} part is constant for $U_T > U_{TCS}$, the variable resistance R_{TCS} of voltage regulator is given by (6)

$$R_{TCS} = \left|U_{TCS}\left(R_{TCH}\left(\omega^2 L_{TS} C_T R_{TCR} - R_{TCR} - j\omega L_{TS} - j\omega C_T R_{TS} R_{TCR} - R_{TS}\right) - R_{TS} R_{TCR} - j\omega L_{TS} R_{TCR}\right) \times \left(U_{TCS}\left(R_{TCH}\left(1 + j\omega C_T R_{TS} - \omega^2 L_{TS} C_{TS}\right) + R_{TS} + j\omega L_{TS}\right) - j\omega M I_R R_{TCH}\right)^{-1}\right|. \tag{6}$$

The minimum value of U_T ($U_{T\min}$) voltage is the base for determining the interrogation zone. The $U_{T\min}$ value is the characteristic parameter of chip construction. It clearly impacts on (7) (where $\mu_0 = 4\pi \cdot 10^{-7}$ H/m) and on its base it is possible to determine the minimum value of magnetic field strength $H_{\min}$ as

$$H_{\min} = \frac{\left|U_{T\min}\right|}{\mu_0} \cdot \left|\left[1 + \left(\left(1/R_{TCH}\right) + \left(1/\left(R_{TCR} + R_{TCS}\right)\right) + j\omega C_T\right) \cdot \left(j\omega L_{TS} + R_{TS}\right)\right]\left(j\omega \cdot N_T \cdot S_T\right)^{-1}\right|. \tag{7}$$

The field strength $H_{\min}$ is the elementary parameter that defines the IZ. It is differentiated on the base of value $U_{T\min}$ for the given direction of data transmission and the kind of operations (read/write) proceeded in the internal transponder's memory. The operation of transponderwith the active harvester is also described by (7). If the $1/R_{TCH}$ factor is omitted then the $H_{\min}$ parameter is valid for the typical passive transponder.

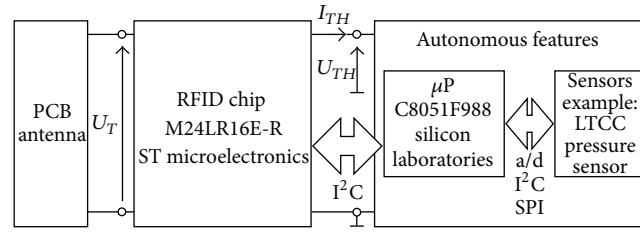

Figure 4: Block diagram of the elaborated transponder.

3. Implementation of Passive Chip with Energy Harvester

The special laboratory stand has been made for experimental verification of the calculated value $H_{\min}$. The stand allows to measure the maximum distance between the RWD and transponder antennas for which the correct operation of RFID system is ensured.

The batteryless system has been made in order to exemplify the possibility of passive chip integration with the previously presented pressure sensor [9]. The special circuit for recovering energy from the RFID system environment is the built-in chip (Figure 4). The presented solution is dedicated for transponders that work in inductively coupled RFID systems in the HF band ($f_0 = 13.56$ MHz) and operate according to the communication protocol ISO/IEC 15693 [35].

The chip M24LR16E-R STMicroelectronics [45] is an integral part of transponder. It is equipped with a 16 kb EEPROM with a password protection. The memory organisation depends on the access mode: 2048 B in I^2C mode and 512 blocks of 32 b in RF mode. The access is possible by a dual interface: wireless RFID and serial wire link I^2C. The energy harvesting block can operate in four configurable ranges of current sink—the maximum value of $I_{TH\max}$ (Figure 3) is equal to 6 mA, 3 mA, 1 mA, or 300 μA. The internal tuning capacitance ($C_T = 27.5$ pF for 1 V_{pp}) is included at the loop antenna terminals.

The square antenna has been synthesised in order to carry out the experimental verification. The winding diagram of loop antenna (Figure 5(a)) has been developed in the HyperLynx 3D EM 15.21 package (Mentor Graphics). The test antenna has been realized practically on a PCB substrate by using a CNC plotter LPKF ProtoMat S100 (Figure 5(b)).

The project has been prepared for the typical two-sided FR-4 laminate (thickness: 1.55 mm, permittivity: 4.85, dielectric losses: 0.025 for $f = 10$ MHz, thickness of copper: 17.5 μm) and for the assumed parameters of applied chip ($C_T = 27.5$ pF, $f_0 = 13.56$ MHz). The loop parameters of model calculated in the HyperLynx 3D EM package have been confirmed experimentally by measuring the test

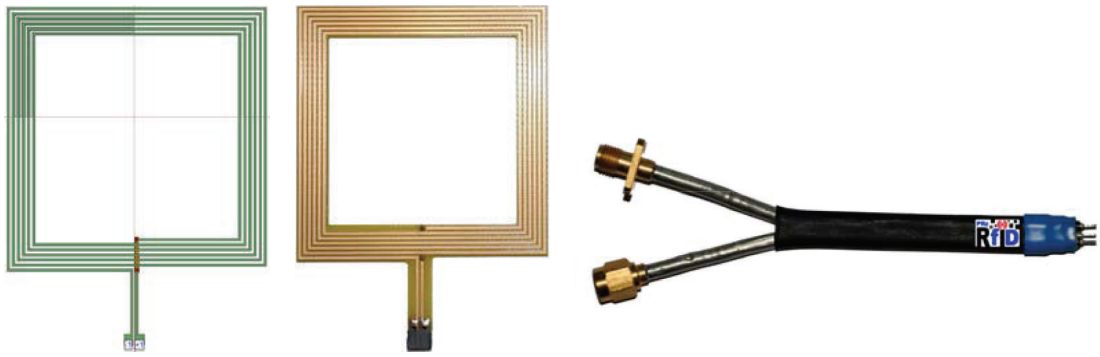

Figure 5: Transponder antenna: (a) HyperLynx 3D EM winding model, (b) test antenna, and (c) differential probe.

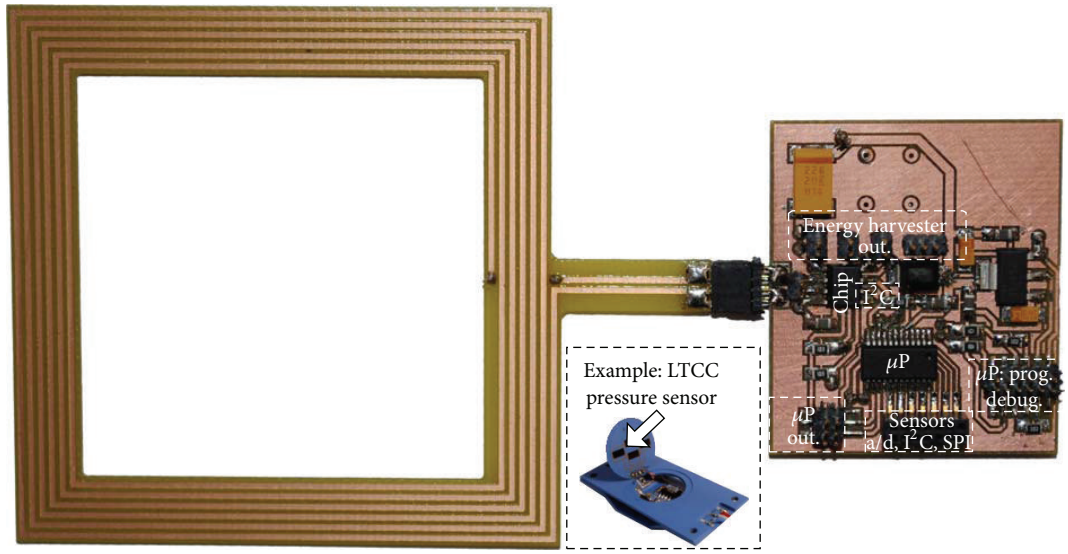

Figure 6: Practical realization of the transponder with harvester of additional energy.

antenna using a two-port network analyzer (Agilent PNA-X N5242A) and the differential probe (Figure 5(c)) which has been prepared especially for connecting equipment without any disturbances.

The antenna impedance Z_T has been calculated from (8) on the basis of measured S-parameters [47] (for $Z_0 = 50\,\Omega$) as

$$Z_T = j\omega L_{TS} + R_{TS} = 2Z_0 \frac{\left(1 - S_{11}^2 + S_{21}^2 - 2S_{12}\right)}{\left(1 - S_{11}\right)^2 - S_{21}^2}. \quad (8)$$

The convergence of measured and calculated data confirms the accuracy of realized project (Table 1). The parallel resonance with the C_T capacitance at f_0 frequency is achievable for obtained parameters. It means that this test antenna construction allows to effectively transfer energy from the RWD to the chip and additionally to power the extra feature blocks.

The expanded sensor block is built on the C8051F988 microprocessor (Figure 6). This (integrated circuit) IC is the industry's lowest power microcontroller of 8051 family (MCU). It consumes as little as 10 nA in a sleep mode (with full memory retention) and 150 μA/MHz in an active mode, which saves power when the application runs. It is capable of operating down to 1.8 V. It also offers the industry's fastest wake-up and analog settling time. It is equipped with all functions needed in the project: 10-bit AD converter for connecting the LTCC sensor, I^{2}C interface for transferring data to the RFID chip, and 2 built-in supply monitors (brown-out detector) for the sleep and active modes.

Table 1: Calculated and measured parameters of the transponder antenna.

Parameter	HyperLynx calculation results	Measurement results
LTS	5.08 μH	5.10 μH
RTS	8.59 Ω	8.68 Ω

4. Tests and Results

Designed elements of HF long range RFID systems with inductive coupling (working frequency: $f_0 = 13.56$ MHz)

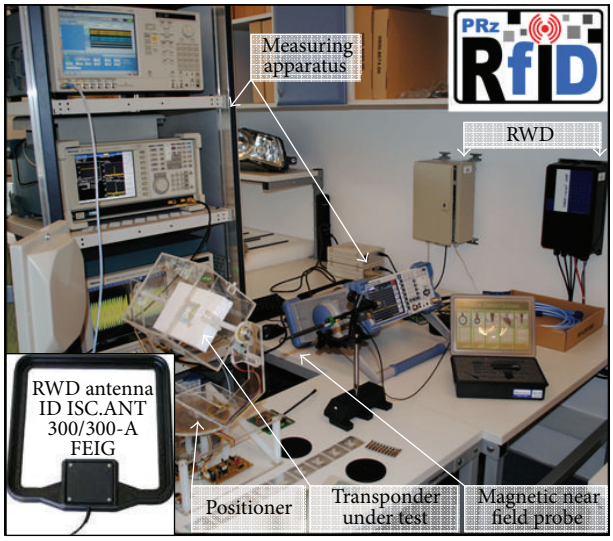

Figure 7: Test stand in the RFID laboratory in the Department of Electronic and Communications Systems.

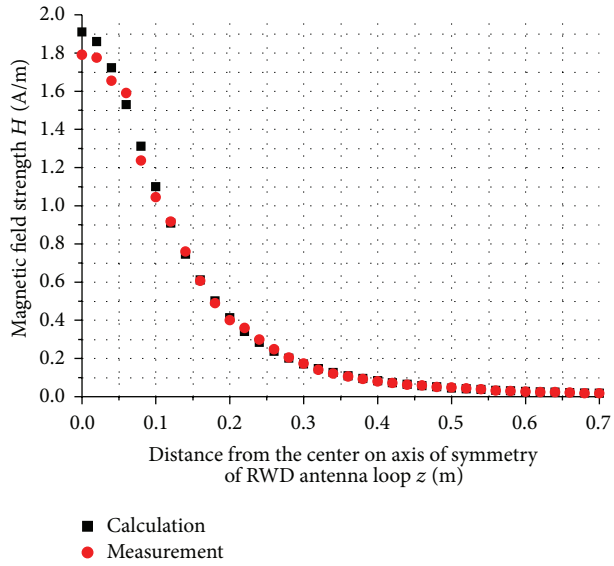

Figure 8: Magnetic field strength in test stand.

have been used to carry out final tests of the elaborated method useful for determining the minimum value of magnetic field strength $H_{\min}$ (read range). All measurements of the experiment have been performed in the specialized RFID laboratory. The special test stand has been prepared for this reason (Figure 7). The parameters used in the equivalent calculations have corresponded to the parameters of devices available in the laboratory. The laboratory equipment has made it possible to conduct all kinds of experimental research in the range of inductively coupled RFID system activity, in both the energy and communication aspects.

The square RWD antenna (side length $a = 0.3$ m, number of loop turns $N_R = 1$) has been installed in the test stand. The antenna was supplied by the RWD ID ISC.LR200 FEIG (output power 1 W, current in the winding $I_R = 0.45$ A). The calculation and measurement results of magnetic field strength in the symmetry axis of RWD antenna are presented in Figure 8.

The calculation has been made for the antenna model that had been considered in [38] in details. The calculated results have been compared with the measurements obtained in the laboratory stand using spectrum analyzer R&S FSL18, oscilloscope Tektronix DPO71254B, magnetic near-field probe HZ-14, and also P7504, CT1.

On the base of calculated and measured result convergence, the correctness of magnetic field strength determination in the elaborated test stand has been confirmed. The possibility of energy harvesting on different kinds of its value level has been also estimated. It has been necessary in order to establish appropriate conditions for powering the autonomous functions of the designed transponder. The measurement results of chip harvester efficiency are presented in Table 2. The measurements have been made by a Tektronix DMM4020 digital multimeter. The power consumption variations have been obtained by using elaborated load simulator

Table 2: Measurements of power efficiency for energy harvesting block.

RFID chip configuration (maximum current I_{TH})	I_{TH}	U_{TH}	P_{TH}
mA	mA	V	mW
3	0.30	3.28	1.0
	0.50	3.20	1.6
	0.70	3.13	2.2
	0.90	3.05	2.7
	1.00	3.02	3.0
	1.20	2.95	3.5
	1.40	2.89	4.0
	1.60	2.83	4.5
	1.80	2.77	5.0
	2.00	2.72	5.4
	3.00	2.51	7.5
6	4.00	2.30	9.2
	5.00	2.11	10.6

(it changed the power levels according to predicted activities of microprocessor control system).

The main application parameters of test transponders have been determined on the base of above mentioned calculations and measurements (Table 3).

The calculations have been performed for transponder model described by (6) and (7). The mathcad environment has been used for preparing calculation program tools. The data in Table 3 represents three modes of designed transponder: (1) energy harvester OFF, (2) energy harvester ON and $P_{TH} = 1$ mW, and (3) energy harvester ON and $P_{TH} = 4$ mW. The power P_{TH} has been measured by an oscilloscope Tektronix DPO71254B with probes P7504 CT1 (index [a] in Table 3).

Table 3: Calculated and measured parameters of the developed transponder.

Transponder state	Status of energy harvester	P_{TH}	Parameter	Calculating results	Measuring results
1	OFF	[a]0 mW	z_{ID}	—	[b]0.6 m
			$H_{\min}$	[c]0.028 A/m [d]0.027 A/m	[e]0.027 A/m
2	ON	[a]1 mW	z_{ID}	—	[b]0.35 m
			$H_{\min}$	[c]0.120 A/m [d]0.121 A/m	[e]0.123 A/m
3	ON	[a]4 mW	z_{ID}	—	[b]0.19 m
			$H_{\min}$	[c]0.461 A/m [d]0.454 A/m	[e]0.462 A/m

[a]Measurement: oscilloscope Tektronix DPO71254B, probes P7504, CT1.
[b]UID measurement: inventory command (0x01) ISO/IEC 15693 (FEIG ID ISOStart 2011 version 08.03.01).
[c]Calculation: equation (7) for RWD-transponder model (square RWD antenna model [38]; transponder antenna loop: HyperLynx 3D EM model; chip: product specification data).
[d]Calculation: RWD antenna model on the base of measured z_{ID}.
[e]Measurement: spectrum analyzer R&S FSL18, magnetic near-field probe HZ-14.

The real communication process has been carried out between the RWD device and the prepared test samples of analyzed transponder and the transmission correctness has been controlled by the spectrum analyzer Tektronix RSA 3408B. The parameter z_{ID} has been determined as the basic quantity of the interrogation zone and it denotes the maximum operating distance (read range) of transponder located in the symmetry axis of RWD antenna loop. The index[b] in Table 3 means the measurement of unique identifier (UID) in the test stand for inventory command (0x01) ISO/IEC 15693 (FEIG ID ISOStart 2011 version 08.03.01).

Calculations of the $H_{\min}$ have been made by two methods. The index[c] in Table 3 means that the calculations result from (7) for the RWD-transponder model (square RWD antenna model [38]; transponder antenna loop: HyperLynx 3D EM model; chip: product specification data). The index[d] in Table 3 means that the calculations result from RWD antenna model derived on the base of measured z_{ID}. The minimum value of magnetic field strength $H_{\min}$ (index[e] in Table 3) has been measured by means of the spectrum analyzer R&S FSL18 and magnetic near-field probe HZ-14.

The result convergence confirms the accuracy and correctness of developed simulation equivalent to real passive transponder with harvesting module.

5. Conclusion

The basic application parameters presented in Table 3 have been calculated for the passive transponder electric circuit equivalent and also the same quantities have been measured for the test electronic circuit. The verification of the developed model is confirmed on the base of the obtained result convergence. The developed methodology for testing passive and semipassive transponders with harvester that derives energy from RFID system environment is the key approach to determine the tree-dimensional interrogation zone (e.g., by using Monte Carlo method [36]) for both single and anticollision RFID systems. It provides reliable information on the operation and efficiency of automated identification processes and it allows RFID system designers to eliminate inefficient and time-consuming trial and error methods.

Acknowledgments

This work was supported in part by the Polish National Science Centre (NCN) under Grant no. 4711/B/T02/2011/40 (in the scope of RFID sensor) and the Polish National Centre for Research and Development (NCBR) under Grant no. PBS1/A3/3/2012 (in the scope of energy harvesting in RFID transponders). This work was developed by using equipment purchased in the Operational Program Development of Eastern Poland 2007–2013 of the Priority Axis I Modern Economics of Activity I.3 Supporting Innovation under Grant no. POPW.01.03.00-18-012/09-00 and the Program of Development of Podkarpacie Province of The European Regional Development Fund under Grant no. UDA-RPPK.01.03.00-18-003/10-00.

References

[1] D. Brown, "Part II: applications," in *RFID Implementation*, pp. 133–222, McGraw-Hill, New York, NY, USA, 2007.

[2] E. C. Jones and C. A. Chung, "Part 2: integrating RFID into logistics," in *RFID in Logistics: A Practical introduction*, CRC Press, New York, NY, USA, 2008.

[3] K. Weigelt, M. Hambsch, G. Karacs, T. Zillger, and A. C. Hübler, "Labeling the world: tagging mass products with printing processes," *IEEE Pervasive Computing*, vol. 9, no. 2, pp. 59–63, 2010.

[4] S. Cheng, K. Tom, L. Thomas, and M. Pecht, "A wireless sensor system for prognostics and health management," *IEEE Sensors Journal*, vol. 10, no. 4, pp. 856–862, 2010.

[5] V. P. Plessky and L. M. Reindl, "Review on SAW RFID tags," *IEEE Transactions on Ultrasonics, Ferroelectrics, and Frequency Control*, vol. 57, no. 3, pp. 654–668, 2010.

[6] R. Bridelall and A. Hande, "Novel RFID technologies: energy harvesting for self-powered autonomous RFID systems," in *RFID Systems: Research Trends and Challenges*, M. Bolić, D.

Simplot-Ryl, and I. Stojmenović, Eds., pp. 473–495, Wiley, New York, NY, USA, 2010.

[7] V. Pillai, H. Heinrich, D. Dieska, P. V. Nikitin, R. Martinez, and K. V. S. Rao, "An ultra-low-power long range battery/passive RFID tag for UHF and microwave bands with a current consumption of 700 nA at 1.5 V," *IEEE Transactions on Circuits and Systems I*, vol. 54, no. 7, pp. 1500–1512, 2007.

[8] N. D. Phan, I. J. Jang, and J. W. Lee, "A 2-Kb one-time programmable memory for UHF passive RFID tag IC in a standard 0. 18 μm CMOS process," *IEEE Transactions on Circuits and Systems I*, no. 99, pp. 1–13, 2012.

[9] S. Slosarczyk, I. Vehec, W. Kalita, R. Bauer, and W. Sabat, "3D-tvarovany modul s integrovanym senzorom tlaku," *The AAPS Journal*, pp. 228–230, 2007.

[10] K. Finkenzeller, "Differentiation features of RFID systems," in *RFID Handbook: Fundamentals and Applications in Contactless Smart Cards, Radio Frequency Identification and Near-Field Communication*, pp. 11–28, Wiley, New York, NY, USA, 3rd edition, 2010.

[11] P. Jankowski-Mihułowicz and W. Kalita, "Interrogation zone—a basic application parameter of RFID systems," *Electronics*, no. 8, pp. 67–72, 2010.

[12] P. Jankowski-Mihułowicz, W. Kalita, and B. Pawlowicz, "Problem of dynamic change of tags location in anticollision RFID systems," *Microelectronics Reliability*, vol. 48, no. 6, pp. 911–918, 2008.

[13] C. W. Lee, S. J. Lee, M. Kim, Y. Kyung, and K. Eom, "Capacitive humidity sensor tag smart refrigerator system using the capacitive to voltage converter (CVC)," in *International Journal of Science and Advanced Technology*, pp. 15–26, 2011.

[14] E. Abad, B. Mazzolai, A. Juarros et al., "Fabrication process for a flexible tag microlab," in *Smart Sensors, Actuators, and MEMS III*, vol. 6589 of *Proceedings of SPIE*, p. 5890, Gran Canaria, Spain, May 2007.

[15] A. Oprea, N. Bârsan, U. Weimar, M. Bauersfeld, D. Ebling, and J. Wöllenstein, "Capacitive humidity sensors on flexible RFID labels," *Sensors and Actuators B*, vol. 132, no. 2, pp. 404–410, 2008.

[16] T. Volk, D. Jansen, H. Speletz, B. Fleiner, D. Bau, A. Kreker et al., "Active RFID sensor with integrated file system for logistic applications," in *Proceedings of the European Workshop on Smart Objects: Systems, Technologies and Applications*, pp. 1–7, June 2010.

[17] S. Kim, J. Cho, H. Kim, H. Kim, H. Kang, and S. Hong, "An EPC Gen 2 compatible passive/semi-active UHF RFID transponder with embedded FeRAM and temperature sensor," in *Proceedings of the IEEE Asian Solid-State Circuits Conference (A-SSCC '07)*, pp. 135–138, November 2007.

[18] D. Cartasegna, A. Cito, F. Conso, A. Donida, M. Grassi, L. Malvasi et al., "Smart RFID label for monitoring the preservation conditions of food," in *Sensors and Microsystems*, vol. 54 of *Lecture Notes in Electrical Engineering*, pp. 381–385, Springer, Berlin, Germany, 2010.

[19] A. Oprea, J. Courbat, N. Bârsan, D. Briand, N. F. de Rooij, and U. Weimar, "Temperature, humidity and gas sensors integrated on plastic foil for low power applications," *Sensors and Actuators B*, vol. 140, no. 1, pp. 227–232, 2009.

[20] L. Yang, A. Rida, T. Wu, S. Basat, and M. M. Tentzeris, "Integration of sensors and inkjet-printed RFID tags on paper-based substrates for UHF cognitive intelligence applications," in *Proceedings of the IEEE Antennas and Propagation Society International Symposium (AP-S '07)*, vol. 1–12, pp. 1193–1186, June 2007.

[21] A. Tani, M. Ugaji, and Y. Yamabe, "A building structural-performance monitoring system using RFID tag with sensors," in *Proceedings of the International Conference on Computing in Civil Building Engineering*, p. 441, 2010.

[22] E. Abad, S. Zampolli, S. Marco et al., "Flexible tag microlab development: gas sensors integration in RFID flexible tags for food logistic," *Sensors and Actuators B*, vol. 127, no. 1, pp. 2–7, 2007.

[23] ERC, *Recommendation 70-03 Relating to the Use of Short Range Devices (SRD)*, Version of 22 August, ERC, New York, NY, USA, 2011.

[24] S. Mandal and R. Sarpeshkar, "Low-power CMOS rectifier design for RFID applications," *IEEE Transactions on Circuits and Systems I*, vol. 54, no. 6, pp. 1177–1188, 2007.

[25] Y. Jia, M. Heiß, Q. Fu, and N. A. Gay, "A prototype RFID humidity sensor for built environment monitoring," in *Proceedings of the 2008 International Workshop on Education Technology and Training and 2008 International Workshop on Geoscience and Remote Sensing*, vol. 2, pp. 496–499, December 2008.

[26] J. Virtanen, L. Ukkonen, T. Björninen, A. Z. Elsherbeni, and L. Sydänheimo, "Inkjet-printed humidity sensor for passive UHF RFID systems," *IEEE Transactions on Instrumentation and Measurement*, vol. 60, no. 8, pp. 2768–2777, 2011.

[27] A. Vazt, H. Solart, I. Rebollot, I. Gutierrezt, and R. Berenguert, "Long range, low power UHF RFID analog front-end suitable for battery less wireless sensors," in *Proceedings of the IEEE MTT-S International Microwave Symposium Digest (MTT '10)*, pp. 836–839, May 2010.

[28] I. Fernandez, A. Asensio, I. Gutierrez, J. Garcia, I. Rebollo, and J. de No, "Study of the communication distance of a MEMS pressure sensor Integrated in a RFID passive tag," *Advances in Electrical and Computer Engineering.*, vol. 12, no. 1, pp. 15–18, 2012.

[29] Z. Zou, D. S. Mendoza, P. Wang et al., "A low-power and flexible energy detection IR-UWB receiver for RFID and wireless sensor networks," *IEEE Transactions on Circuits and Systems I*, vol. 58, no. 7, pp. 1470–1482, 2011.

[30] M. Ghovanloo and S. Atluri, "An integrated full-wave CMOS rectifier with built-in back telemetry for RFID and implantable biomedical applications," *IEEE Transactions on Circuits and Systems I*, vol. 55, no. 10, pp. 3328–3334, 2008.

[31] E. Y. Chow, A. L. Chlebowski, S. Chakraborty, W. J. Chappell, and P. P. Irazoqui, "Fully wireless implantable cardiovascular pressure monitor integrated with a medical stent," *IEEE Transactions on Biomedical Engineering*, vol. 57, no. 6, pp. 1487–1496, 2010.

[32] Y. Shih, T. Shen, and B. P. Otis, "A 2.3 μW wireless intraocular pressure/temperature monitor," *IEEE Journal of Solid-State Circuits*, vol. 46, no. 11, pp. 2592–2601, 2011.

[33] M. van Ackeren and M. Bollerott, *Humidity and Temperature Transponder*, Fraunhofer Institute for Microelectronic Circuits and Systems, Duisburg, Germany, 2010.

[34] EU-Commision, Information and Society-and-Media, *Internet of Things in 2020—Roadmap For the Future*, INFSO D. 4 Networked Enterprise & RFID, INFSO G. 2 Micro & Nanosystems, Working Group RFID of The ETP EPoSS, 2008.

[35] ISO, "Identification cards—contactless integrated circuit(s) cards—vicinity cards—part 3: anticollision and transmission protocol," ISO/IEC 15693-3:2001, ISO, 2001.

[36] P. Jankowski-Mihułowicz and M. Węglarski, "Determination of 3-dimentional interrogation zone in anti-collision RFID systems with inductive coupling by using Monte Carlo method," *Acta Physica Polonica A*, vol. 121, no. 4, pp. 936–940, 2012.

[37] P. Jankowski-Mihułowicz and M. Węglarski, "Synthesis of read/write device antenna for HF proximity range RFID systems with inductive coupling," *Przeglad Elektrotechniczny*, vol. 88, no. 3, pp. 70–73, 2012.

[38] P. Jankowski-Mihułowicz, "Synthesis of read/write device antenna for HF long range RFID systems with inductive coupling," *Electronics*, no. 8, pp. 73–77, 2010.

[39] M. H. Choi, B. D. Yang, N. S. Kim, Y. S. Kim, S. J. Lee, and K. Y. Na, "A 13. 56 MHz radio frequency identification transponder analog front end using a dynamically enabled digital phase locked loop," *Transactions on Electrical and Electronic Materials*, vol. 11, no. 1, pp. 20–23, 2010.

[40] S. Meillère, H. Barthélemy, and M. Martin, "13. 56 MHz CMOS transceiver for RFID applications," *Analog Integrated Circuits and Signal Processing*, vol. 49, no. 3, pp. 249–256, 2006.

[41] Y. Lam, W. Ki, and C. Tsui, "Integrated low-loss CMOS active rectifier for wirelessly powered devices," *IEEE Transactions on Circuits and Systems II*, vol. 53, no. 12, pp. 1378–1382, 2006.

[42] J. Lee, D. H. T. Vo, Q. Huynh, and S. H. Hong, "A fully integrated HF-band passive RFID tag IC using 0.18-μm CMOS technology for low-cost security applications," *IEEE Transactions on Industrial Electronics*, vol. 58, no. 6, pp. 2531–2540, 2011.

[43] K. Myny, S. Steudel, P. Vicca et al., "Plastic circuits and tags for 13.56 MHz radio-frequency communication," *Solid-State Electronics*, vol. 53, no. 12, pp. 1220–1226, 2009.

[44] M. Jung, J. Kim, J. Noh et al., "All-Printed and roll-to-roll-printable 13.56-MHz-operated 1-bit RF tag on plastic foils," *IEEE Transactions on Electron Devices*, vol. 57, no. 3, pp. 571–580, 2010.

[45] ST-Microelectronics, "M24LR16E-R product specification," Document ID 018932, December 2011.

[46] IDS-Microchip-AG, "IDS-SL13A smart label chip with sensor for unique idenfication monitoring and data logging," IDS-SL13A_SD-05. document, December 2008.

[47] X. Qing, C. K. Goh, and Z. N. Chen, "Impedance characterization of rfid tag antennas and application in tag co-design," *IEEE Transactions on Microwave Theory and Techniques*, vol. 57, no. 5, pp. 1268–1274, 2009.

Hindawi Publishing Corporation
International Journal of Antennas and Propagation
Volume 2013, Article ID 982813, 6 pages
http://dx.doi.org/10.1155/2013/982813

Research Article

Compact and Circular Polarized RFID Antenna for Portable Terminal Applications

Yuan Yao, Youbo Zhang, Junsheng Yu, and Xiaodong Chen

School of Electronic Engineering, Beijing University of Posts and Telecommunications, Beijing 100876, China

Correspondence should be addressed to Yuan Yao; yaoy@bupt.edu.cn

Received 23 June 2013; Accepted 29 July 2013

Academic Editor: Chaowei Wang

A novel compact and circular polarized antenna is proposed which can be easily fabricated and embedded into RFID readers. Circular polarization characteristic of the proposed antenna is achieved by introducing a crossed branch. The modified meandering line structure gives the antenna compactness characteristic. A prototype is fabricated and measured. The results show that this circular polarized antenna with compact dimension can cover the Chinese RFID operating band from 920 MHz to 925 MHz, which make's the antenna suitable for handheld terminal application of RFID readers.

1. Introduction

In recent years, UHF RFID systems have moved from obscurity into mainstream applications due to some of their attractive features such as good reading ranges, high date rates, and potentially low cost [1–3]. An RFID system consists of reader, reader antenna, and tags. Since the tag antennas are linearly polarized, a circularly polarized RFID reader antenna is preferred to detect the random orientated tags [4–7]. In some applications, handheld or portable readers are required. And also RFID readers are now integrating with other portable terminal devices such as mobile phone. In these applications, the RFID reader antennas should be compact and easily integrated.

Monopole antennas [8–10] have been widely used in wireless communications with compact characteristic, good radiation patterns, simple structure, and easy integration with other devices, especially the meandering line structure, but they are usually used for linear polarization. Relatively very few designs are available in the open literature for achieving CP radiation using meandering line monopole structure.

In this paper, an antenna with compact and circular polarized characteristics for RFID reader application is proposed. The antenna covers the required bandwidths of RFID in China from 920 MHz to 925 MHz. Monopole antenna with meandering line structure is designed to achieve compact characteristic, and cross loaded branches are used to achieve circular polarization. One distinguishing feature of the proposed antenna is that meandering line monopole antennas, which have been widely used in terminals and usually used for linear polarization, can achieve circular polarization radiation. Details of the antenna design are presented, and simulated and measured results are given to demonstrate the performance of the proposed antenna.

2. Antenna Design

Figure 1 shows the geometry of the proposed antenna. The antenna is mounted on FR4 substrate with permittivity of 4.4 and dielectric loss tangent of 0.02 and thickness of 1.6 mm. Since the antenna is used in handset device, a palm-size test bench of 120 mm (L) $*$ 60 mm (W) $*$ 1.6 mm (h) is included to emulate the handset circuit board. A small antenna chip with the size of 50 mm $*$ 6 mm $*$ 1.6 mm is fabricated perpendicularly on the corner of the slab. In fact, most of the space is occupied by the test bench, so the space occupied by the antenna is relatively small.

The antenna is mainly composed of a rectangular ground with a rectangular clearance at the corner where the antenna chip is fabricated, a meander line, a feed line, a short line, and

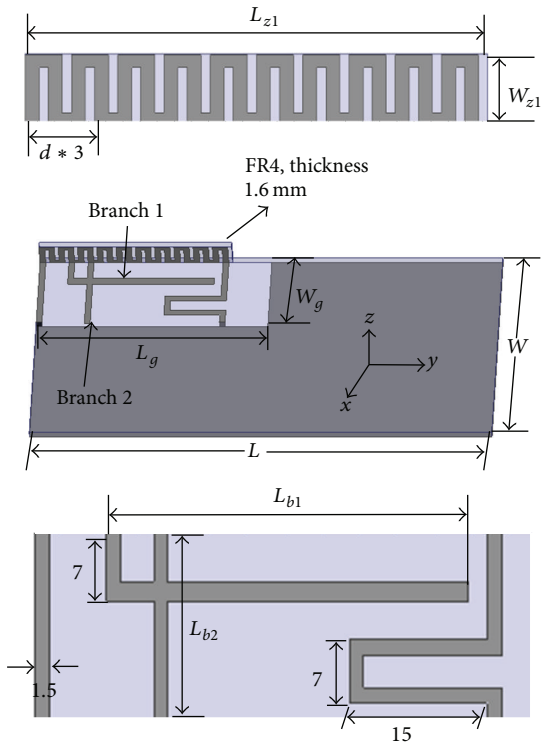

Figure 1: The geometry of the proposed antenna.

Table 1: Antenna dimensions.

Parameter	L	W	L_g	W_g	L_{z1}
Value (mm)	120	67	60	22	50
Parameter	W_{z1}	L_{b1}	L_{b2}	d	
Value (mm)	6	35	18	2.5	

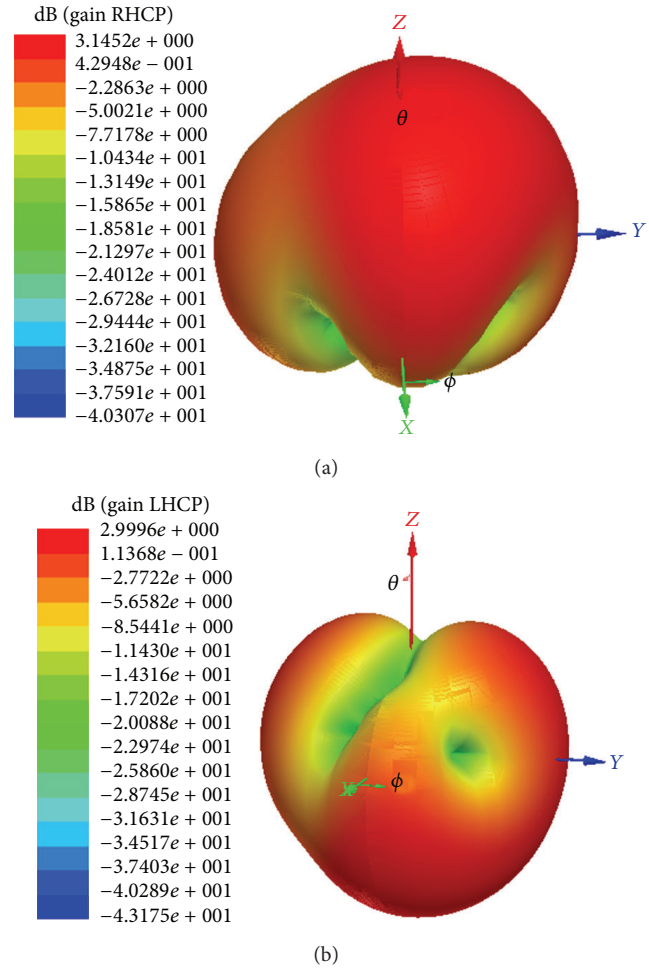

Figure 2: 3D radiation patterns of the proposed antenna. (a) RHCP pattern. (b) LHCP pattern.

a crossed branch. The meander line is printed on the small antenna chip, perpendicular to the test bench. The ground plane is printed on the back side of the slab while the feed line, crossed branch, and the short line are printed on the front side of the slab. The meander line and the crossed branch are fed by the feed line. In the fabricated prototype, a 50 Ohm coaxial line is used to connect the antenna prototype and the test instrument.

Simulator Ansoft HFSS is used to simulate and optimize the proposed antenna design. Through numerous simulations, we can find that the impedance matching and AR bandwidth are primarily dependent on the meandering line structure and the cross shaped branch, separately. The crossed branch is a paramount factor and needs serious consideration in the AR of the designed frequency band. By carefully selecting the parameter of the cross, a broadband circular polarization is obtained. The finally chosen dimensions of the proposed antenna are illustrated in Table 1.

Figure 2 shows the radiation patterns of the proposed antenna at 920 MHz. From the results, we can see that the antenna has circular polarization characteristic. At one side, the antenna has left handed circular polarization (LHCP),

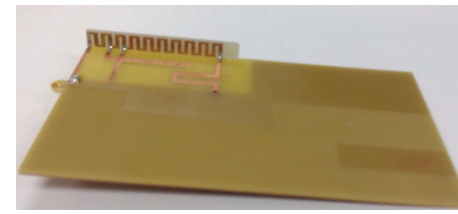

Figure 3: Photograph of the fabricated antenna.

and at the other side, the antenna has right-handed circular polarization (RHCP). It means that no matter the tags' orientation and position, the RFID reader antenna can identify them.

3. Simulation and Measurement Results

In order to verify the proposed antenna design, a prototype is fabricated as shown in Figure 3. All the measured results are carried out in anechoic chamber using VNA and other

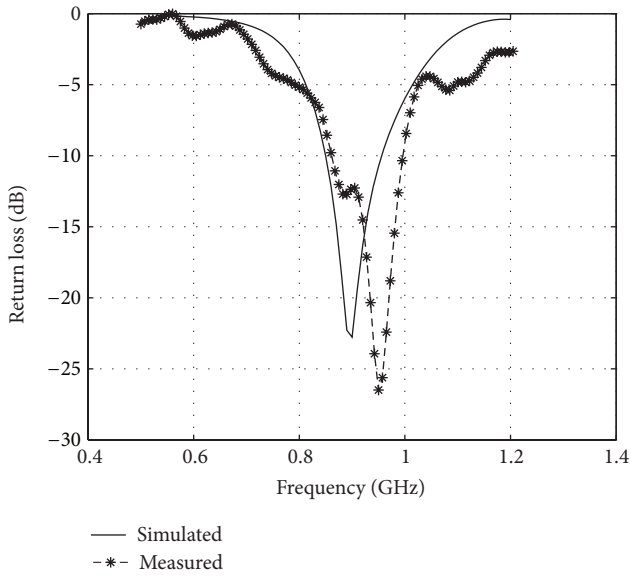

Figure 4: Simulated and measured S11 of the proposed antenna.

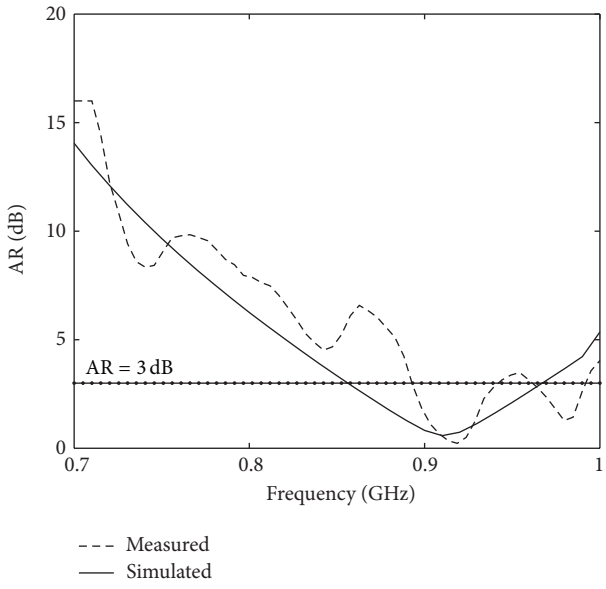

Figure 5: Simulated and measured axial ratio.

microwave test instruments. The simulated and measured reflection coefficients of the proposed antenna are shown in Figure 4. As can be seen, the proposed antenna has broadband impedance matching characteristic from 850 MHz to 950 MHz defined by S11 < −10 dB, which covers most of the current RFID frequency bands.

Figure 5 shows the measured axial ratio in the broadside direction ($\theta = 0^{\circ}$). As can be seen, an AR bandwidth of around 50 MHz from 890 MHz to 940 MHz for AR ≤ 3 dB is shown, which means that the antenna achieves good circular polarization characteristic.

The simulated and measured RHCP radiation patterns of the antenna in X-Z plane and Y-Z plane at two different frequencies 920 MHz and 925 MHz are compared in Figure 6. The RHCP gain maximum, which is about 1.5 dBi, is found about 10 degree's away from $+Z$ direction, and the beam width defined by > −3 dBi is about 120 degree's at 920 MHz. The measured peak RHCP gain at 925 MHz is about 2.0 dBi, and the beam width is about 100 degree's, narrower than the lower frequency which is caused by the higher peak gain. As can be seen, the antenna achieves good CP radiation patterns.

4. Parameter Study

For the purpose of optimized performance, parametric studies of the dimensions of the antenna structure are carried out. In this antenna design, the length of the crossed branches will have a big impact on the antenna performance, including the return loss and the axial ratio. In order to investigate the effects of the length of the crossed branch, we carried out a parameter study via HFSS. Figure 7 shows the simulated results of various branch 1 lengths L_{b1}. From Figure 7(a), we can see that when L_{b1} changes from 34 mm to 37 mm, the frequency of S11 < −10 dB goes down. The circular polarization characteristic will be also affected by the dimension of branch 1. As shown in Figure 7(b), when L_{b1} is changed from 34 mm to 37 mm the axial ratio turns worse. Taking into consideration both the return loss and axial ratio performance, we chose $L_{b1} = 35$ mm as the optimized value in the final design.

In addition to branch 1, the branch 2 dimension of the crossed branches is also a sensitive parameter to the antenna characteristics. Similar to L_{b1}, we also sweep the branch 2 length L_{b2} from 18 mm to 22 mm. Simulated results of different L_{b2} values are shown in Figure 8. Figure 8(a) shows that the working frequency goes down when L_{b2} varies from 18 mm to 22 mm. Figure 8(b) shows that the axial ratio remains unchanged when L_{b2} varies, which means that the circular polarization characteristic of the antenna is not sensitive to branch 2 dimension. So the selection of branch 2 length is mainly based on S11 results. We choose $L_{b2} = 21$ mm as the final optimized value.

The meander line is an important part in the antenna design, so the internal's of the meander line d is also a parameter that cannot be ignored. To study how the d value affect's the antenna, several different values were used to simulate in HFSS. The results show that axial ratio is not sensitive to d values, but the return loss of the antenna changed greatly while d varies. Figure 9 shows the different results of S11 in terms of different d values. From the figure we can see that while the value of d goes up, the resonance frequency goes down. This can be obviously seen in terms of the rule longer current path lower resonant frequency. As the interval of the meander line becomes bigger, the total length of the current path get's longer, so the frequency reduce.

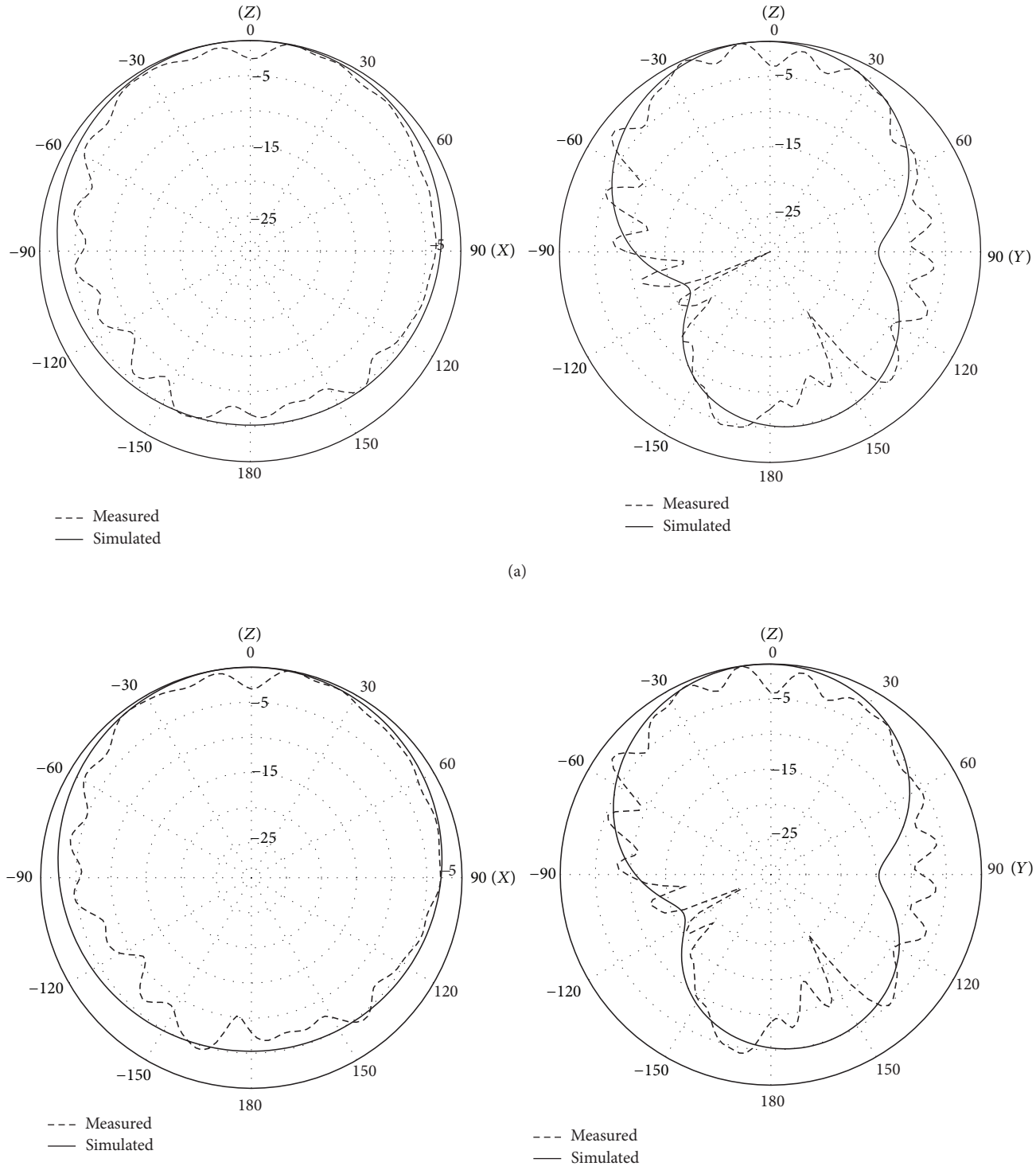

Figure 6: Simulated and measured radiation patterns at 920 MHz and 925 MHz. (a) RHCP gain at 920 MHz. (b) RHCP gain at 925 MHz.

Finally, the dimension of the ground plane of the antenna is also a significant parameter that will have great impact on the antenna performance, including both return loss and axial ratio. So the parameter L should be designed carefully in order to get a perfect antenna. Several values were tried in the simulation in order to get the appropriate length of L. The simulated results of return loss and axial ratio of different L values are shown in Figure 10. Figure 10(a) shows that L

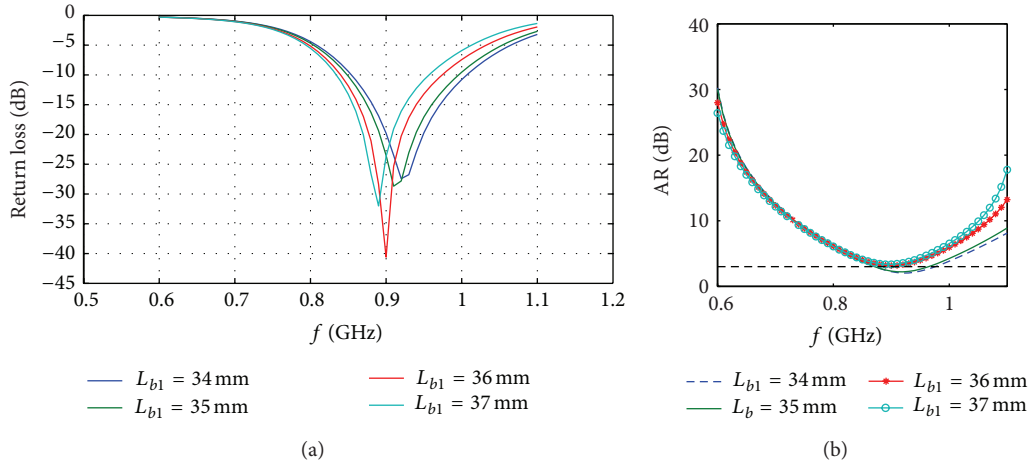

Figure 7: Comparison of S11 and AR of the antenna with different L_{b2}. (a) S11. (b) Axial ratio.

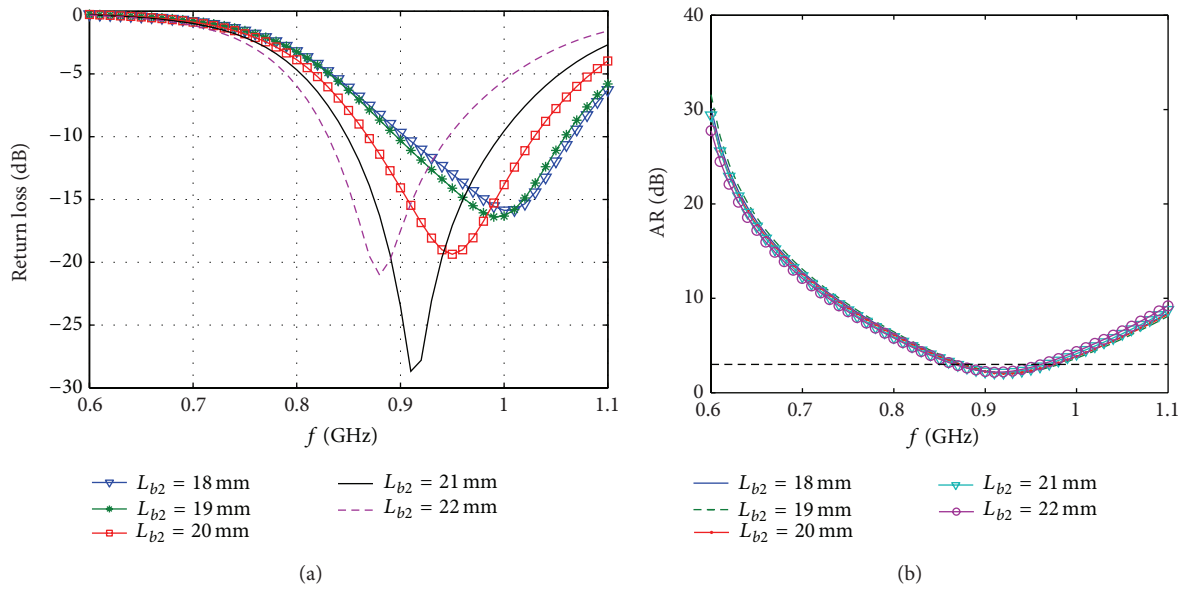

Figure 8: Comparison of S11 and AR of the antenna with different L_{b2}. (a) S11. (b) Axial ratio.

mainly affects the impedance bandwidth. Figure 10(b) shows that the frequency of AR < 3 dB will shift when L varies. While L changes from 100 mm to 150 mm, the frequency of AR < 3 dB goes down quickly. Taking into account the S11, AR performance, and fabrication considerations, L = 120 mm is finally chosen as the optimized value in the antenn design.

In addition to the parameters mentioned above, the dimensions of the clearance at the corner of the ground plane also affect the resonance frequency slightly. So the parameters W_g and L_g should be designed carefully to get good impedance match.

From the analysis above, we can conclude that the axial ratio is mainly affected by the branch 1 length and ground length and all the dimensions of the antenna part have effects on the return loss characteristic.

5. Conclusion

In this paper, a design of compact and circular polarized RFID reader antennae for portable terminal applications is proposed. The antenna has the compactness and circularly polarization at the same time by introducing the meandering line structure and crossed branch. Both simulation and measurement results show that the return loss and AR cover the whole Chinese RFID frequency band. This antenna could find its application in handheld terminals for mobile RFID reader system.

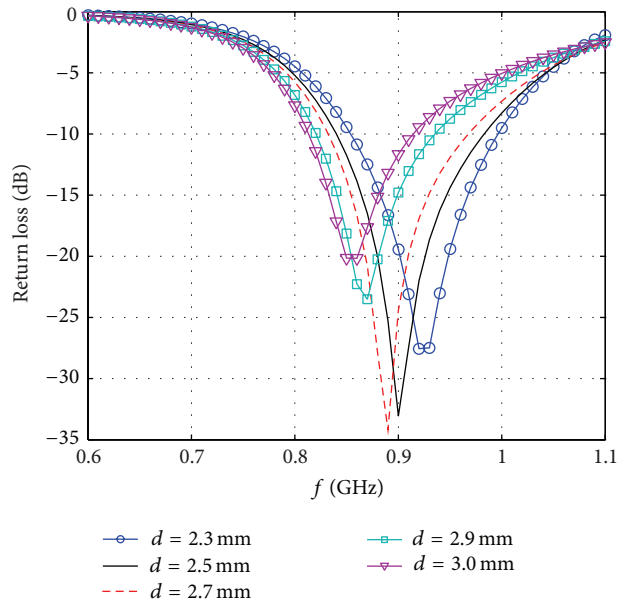

Figure 9: Comparison of S11 of the antenna with different d.

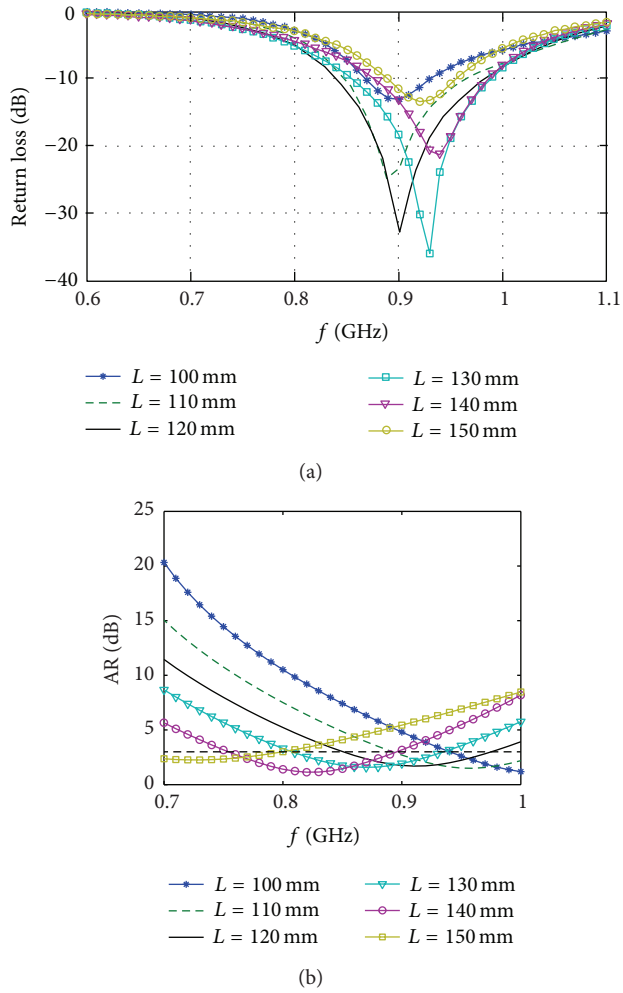

Figure 10: Comparison of S11 and AR of the antenna with different L. (a) S11. (b) Axial ratio.

Acknowledgments

This work is supported by the Fundamental Research Funds for the Central Universities, the National Natural Science Foundation of China under Grant no. 61201026, and the Beijing Natural Science Foundation (4133091).

References

[1] Y. Yao, Y. Sui, X. Chen, and J. Yu, "Planar antenna for RFID tags on metal platform," in *Proceedings of the International Workshop on Antenna Technology: Small Antennas, Novel Structures and Innovative Metamaterials (iWAT '11)*, pp. 408–411, March 2011.

[2] X. Qing, C. K. Goh, and Z. N. Chen, "A broadband uhf near-field rfid antenna," *IEEE Transactions on Antennas and Propagation*, vol. 58, no. 12, pp. 3829–3838, 2010.

[3] G. Marrocco, "The art of UHF RFID antenna design: impedance-matching and size-reduction techniques," *IEEE Antennas and Propagation Magazine*, vol. 50, no. 1, pp. 66–79, 2008.

[4] S.-H. Jeong and H.-W. Son, "UHF RFID tag antenna for embedded use in a concrete floor," *IEEE Antennas and Wireless Propagation Letters*, vol. 10, pp. 1158–1161, 2011.

[5] P. V. Nikitin and K. V. S. Rao, "Helical antenna for handheld UHF RFID reader," in *Proceedings of the 4th Annual IEEE International Conference on RFID (RFID '10)*, pp. 166–173, April 2010.

[6] N. Nasimuddin, Z. N. Chen, and X. Qing, "Asymmetric-circular shaped slotted microstrip antennas for circular polarization and RFID applications," *IEEE Transactions on Antennas and Propagation*, vol. 58, no. 12, pp. 3821–3828, 2010.

[7] Z. N. Chen, X. Qing, and H. L. Chung, "A universal UHF RFID reader antenna," *IEEE Transactions on Microwave Theory and Techniques*, vol. 57, no. 5, pp. 1275–1282, 2009.

[8] Y. Yao, J. Yu, and X. Chen, "Compact multi-band planar antenna design," in *Proceedings of the Asia-Pacific Microwave Conference*, pp. 1328–1330, 2012.

[9] J. Lu and Y. Wang, "Internal uniplanar antenna for LTE/GSM/UMTS operation in a tablet computer," *IEEE Transactions on Antennas and Propagation*, vol. 61, no. 5, pp. 2841–2846, 2013.

[10] W. Chen and W. Jhang, "A planar WWAN/LTE antenna for portable devices," *IEEE Antennas and Wireless Propagation Letters*, vol. 12, pp. 19–22, 2013.

Hindawi Publishing Corporation
International Journal of Antennas and Propagation
Volume 2013, Article ID 743468, 8 pages
http://dx.doi.org/10.1155/2013/743468

Research Article

An Advanced Dynamic Framed-Slotted ALOHA Algorithm Based on Bayesian Estimation and Probability Response

Chaowei Wang, Menglong Li, Juyi Qiao, Weidong Wang, and Xiuhua Li

Information & Electronics Technology Lab, Beijing University of Posts and Telecommunications, P.O. Box 116, Beijing 100876, China

Correspondence should be addressed to Menglong Li; limenglong1861816@163.com

Received 23 May 2013; Accepted 12 July 2013

Academic Editor: Yuan Yao

This paper proposes an advanced dynamic framed-slotted ALOHA algorithm based on Bayesian estimation and probability response (BE-PDFSA) to improve the performance of radio frequency identification (RFID) system. The Bayesian estimation is introduced to improve the accuracy of the estimation algorithm for lacking a large number of observations in one query. The probability response is used to adjust responsive probability of the unrecognized tags to make the responsive tag number equal to the frame length. In this way, we can solve the problem of high collision rate with the increase of tag number and improve the throughput of the whole system. From the simulation results, we can see that the algorithm we proposed can greatly improve the stability of RFID system compared with DFSA and other commonly used algorithms.

1. Introduction

In recent years, radio frequency identification (RFID) technology has been widely used in projects on internet of things (IOT) around the world. People try to use RFID technology to improve the efficiency of the processes in the supply chain. According to the market research analyst IDTechEx (Das, 2005), the cumulative sales of RFID tags for the 60 years up to the beginning of 2006 reached 2.4 billion, with 600 million tags being sold in 2005 alone [1]. With the exponential growth of needs for RF tags, more of them would be needed in a range of areas, such as retailing, logistics, animals and farming, library services, and military equipment [2].

A RFID system consists of readers and tags. Each tag has a unique ID, and a reader has its own operational range. When a tag comes into the identification scope of the reader, it will send its ID combined with other information such as manufacturer and product type to the reader. Besides, it can even measure environmental factors such as temperature which can bring a lot of convenience to the related industries [3]. However, as the number of tags grows in one place, more and more tags will communicate with the reader at the same time and interfere with each other. As a result, the reader will not get the correct information from each tag. This is called the tag collision, and it along with the reader collision constitutes the collision problem of RFID system which is demonstrated in Figure 1.

To solve the tag collision problem, lots of related researches have been carried out, and many algorithms have been proposed. The most widely used anticollision algorithms are ALOHA method and Binary Search method [4]. ALOHA algorithm is based on the thought of ALOHA [5] and combined with the characteristics of RFID system. Its core idea is to separate the response time of tags and to make them respond in different time slots in order to avoid collision. Once the collision occurs, the related tags take time-backoff mechanism and wait for next round to respond [6]. However, the channel utilization of this algorithm is not as high as people expect. Its throughput is only 18.4%. Therefore, framed-slotted ALOHA (FSA) was proposed on the basic of ALOHA algorithm. Frame is a kind of time length, and it is divided into several slots. Tags randomly pick one slot to respond, and it can only respond at the beginning of the slot [7]. If two or more tags select the same slot, the collision would happen. Then they all quit this round and wait for the next frame. By computing, FSA can improve theoretical maximum throughput up to 36.8%. But it is still not very ideal in the case of heavy load conditions.

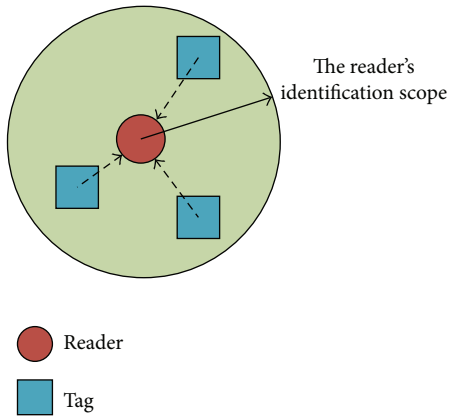

Figure 1: Tag collision problem.

Dynamic framed-slotted ALOHA (DFSA) is an advanced FSA. This algorithm can adjust the size of frame (the number of slots in one frame) dynamically according to the estimation of the tags [8]. As we know, the throughput of the system can reach the maximum when the number of tags is equal to the frame length [9]. So it is really important to find an estimation algorithm of high accuracy. At present, the primary estimation algorithms are minimum tag number estimation algorithm [10], Jae-Ryong Cha algorithm [11], and Harald Vogt algorithm [12]. Although these estimation algorithms play an important role in the way of improving the efficiency of DFSA, they still have two obvious problems. The first one is that it is hard to guarantee the reliability of the algorithm. Currently, the primary estimation algorithms are all traditional statistical methods. Their accuracy is on the basis of a large number of observations. However, in a real RFID system, the reader needs to estimate the number of tags immediately according to the observations in one frame. It is impossible to inquire the tags again and again to get numerous data. As a result, there would be a large error between the actual value and the estimated value. The second problem is the "landslide problem" on identification rate of the tags. When the number of tags is far more than the maximum of frame length (256) [13], the throughput of the system would decline rapidly. We call this phenomenon "landslide problem". To improve the reliability of the whole algorithm, we proposed an advanced estimation algorithm based on the Bayesian estimation and probability response. The advanced algorithm can use a small amount of observations getting a relatively accurate estimation of the tag number. In the case of large tag number, the tags can modify their responsive probability dynamically to make the calculated number of the responsive tags equal to the frame length. In this way, we can improve the throughput of the whole system and solve the two problems mentioned above to a great extent.

The remainder of the paper is organized as follows: in Section 2, a brief description of Bayesian estimation is presented. In Section 3, firstly, the general steps to estimate the tag number are introduced, and then an improved ALOHA algorithm is proposed on two sides (the estimation algorithm based on Bayesian estimation and the mechanism of probability response proposed to further improve the performance of the algorithm). In Section 4, the proposed algorithm is compared with DFSA on several aspects and finally some conclusions are drawn in Section 5.

2. The Bayesian Estimation

Bayesian method is a series of theories proposed by British scholar Bayesian in statistics for inductive inference. With the development for centuries, the theory is widely used in different areas for mathematical analysis. Its basic idea can be expressed as the following example. Assume that $A_1, A_2, \ldots, A_n$ are incompatible events and they are of an event set. Their prior probability is given as $\{P[A_i],\ i = 1, 2, \ldots, n\}$ (prior distribution). After the event B happens, we can reassess the probability of $A_1, A_2, \ldots, A_n$ by the following equation:

$$p(A_i \mid B) = \frac{p(B \mid A_i)\, p(A_i)}{p(B)} = \frac{p(B \mid A_i)\, p(A_i)}{\sum_i p(B \mid A_i)\, p(A_i)}. \tag{1}$$

From (1), we can see that Bayesian formula takes both prior information and new information from the test into account which reflects the transformation from prior distribution to posterior distribution. Therefore, compared with those algorithms that only consider a part of information, Bayesian estimation can make our estimation more accurate in the case without a large amount of statistical data.

The most important issue in Bayesian estimation is how to determine the prior distribution. Many Bayesian scholars have proposed several different methods, but they still have not found a general way for all the cases. For tag collision problem, as the probability of the tags to select time slots is constant and it is only decided by the size of frame, we can calculate prior probability of different cases in advance. So we can use taking Bayesian estimation into our tag number estimation algorithm without a large number of calculations to get prior distribution and can obtain a relatively accurate result.

Assume that distribution density of population X is $p(x, \theta)$, $\theta \in \Theta$. Because θ is a random variable and prior distribution of θ is already known, $p(x, \theta)$ needs to be changed as $p(x \mid \theta)$. If $X = (X_1, \ldots, X_n)^T$ is the sample selected from population X and the sample value is $x = (x_1, \ldots, x_n)^T$, the joint probability density of sample X is

$$q(x_1, \ldots, x_n \mid \theta) = \prod_{i=1}^{n} p(x_i \mid \theta). \tag{2}$$

So, the joint probability density of sample X and θ is

$$\begin{aligned} f(x, \theta) &= q(x \mid \theta)\, \pi(\theta) \\ &= m(x)\, h(\theta \mid x). \end{aligned} \tag{3}$$

Then, we can get

$$m(x) = \sum_{\Theta} q(x_1 \ldots, x_n \mid \theta)\, \pi(\theta). \tag{4}$$

We call $h(\theta \mid x)$ the posterior distribution of θ when sample $X = x$. In (4), $m(x)$ is the boundary distribution of (X, θ) about sample X. If θ is the continuous random variable, then we can get

$$m(x) = \int_{\Theta} q(x_1, \ldots, x_n \mid \theta)\, \pi(\theta)\, d\theta. \tag{5}$$

3. The Advanced DFSA Based on Bayesian Estimation and Probability Response

3.1. General Steps to Estimate Tag Number and Frame Length. In DFSA, suppose that the number of slots in one frame is L, the number of tags is n, and each tag has the same probability to select each slot in one frame ($p = 1/L$). According to the statistical principles, the probability that r tags select the same slot can be expressed as

$$B_{n,1/L(r)} = \binom{n}{r} \left(\frac{1}{L}\right)^r \left(1 - \frac{1}{L}\right)^{n-r}. \tag{6}$$

After one frame, the mathematical expectation of successful identification slot ($r = 1$, only one tag selects the slot), empty slot ($r = 0$, no tag selects the slot), and collision slot ($r \geq 2$, more than one tag select the slot) can be expressed as:

$$\begin{aligned} a_1^{L,n} &= L \times B_{n,1/L(1)} = n\left(1 - \frac{1}{L}\right)^{n-1}, \\ a_0^{L,n} &= L \times B_{n,1/L(0)} = L\left(1 - \frac{1}{L}\right)^{n}, \\ a_k^{L,n} &= L - a_0^{L,n} - a_1^{L,n}. \end{aligned} \tag{7}$$

Therefore, if we know the frame length and tag number, we can calculate the number of slots in different statuses. In turn, if we can get the result $[a_0, a_1, a_k]$ inquired by the reader after one frame, the tag number can be estimated by (7). So, the efficiency of the system is

$$S = \frac{a_1^{L,n}}{L} = \frac{n}{L}\left(1 - \frac{1}{L}\right)^{n-1}. \tag{8}$$

To get the maximum of S, we take derivation of (8):

$$\begin{aligned} \frac{dS}{dn} &= \frac{1}{L}\left(1 - \frac{1}{L}\right)^{n-1} + \frac{n}{L}\left(1 - \frac{1}{L}\right)^{n-1} \ln\left(1 - \frac{1}{L}\right) \\ &= \frac{1}{L}\left(1 - \frac{1}{L}\right)^{n-1} \left[1 + n \ln\left(1 - \frac{1}{L}\right)\right] = 0, \\ L &= \frac{1}{1 - e^{1/n}}. \end{aligned} \tag{9}$$

When n is large enough, we can get:

$$L \approx \frac{1 + 1/n}{1 + 1/n - 1} = n + 1 \tag{10}$$

So, on one side, when the size of frame is approximately equal to the tag number, the throughput of the system will reach its maximum. On the other side, considering the size of frame can only be $L = 2^i$, $i = 1, 2, \ldots 8$, we should set L closest to our estimated value to get the maximum of throughput.

3.2. The Advanced Estimation Algorithm Based on Bayesian Estimation. The advantage of the Bayesian estimation is that it can get a relatively accurate statistical result without a large number of observations. As we cannot get much data from one query in the process of tag number estimation, the accuracy of estimation result always has large errors. So we bring the Bayesian estimation into our estimation algorithm. The results from the simulation show that our advanced algorithm can improve the performance of the system to a great extent. The details of the algorithm will be introduced in the following paragraphs.

In DFSA, the tag number has some randomness. So the tag number can be regarded as a random variable instead of an uncertain constant. That is to say, the tag number meets the requirements of random variables, and it is a discrete random variable.

Suppose the tag number is n and the initial length of the frame is L. When the read cycle begins, tags start to select slot from the frame. This process obeys binomial distribution of $B(n, 1/L)$. So the probability of one slot in a frame to be an empty slot, readable slot, or collision slot is

$$\begin{aligned} p_e &= \left(1 - \frac{1}{L}\right)^n, \\ p_s &= \frac{n}{L}\left(1 - \frac{1}{L}\right)^{n-1}, \\ p_c &= 1 - \left(1 - \frac{1}{L}\right)^n - \frac{n}{L}\left(1 - \frac{1}{L}\right)^{n-1}. \end{aligned} \tag{11}$$

In the definition process, $p(n)$ is the priori probability density of tag number to be estimated, and n is from the sample set which is the observations of the number of slots in different statuses. We use $J = \{j(0), j(1), \ldots, j(M)\}$ to express the sample set. $j(m) = \langle j_e, j_s, j_c \rangle$ is the observations of the number of empty slots, readable slots, and collision slots after the initial frame length of the system. The sample value space is E^d, and the value space of tag number to be estimated is Θ. $\lambda(\tilde{n}, n)$ is the loss function when $\tilde{n}$ is the estimation of n. In the RFID system, we take $\lambda(\tilde{n}, n) = (\tilde{n} - n)^2$.

Then, the total expected risk is

$$R = \sum_{E^d} \sum_{\Theta} \lambda(\tilde{n}, n)\, p(n \mid j)\, p(j). \tag{12}$$

We are definite that the conditional risk under the sample j is

$$R(\tilde{n} \mid j) = \sum_{\Theta} \lambda(\tilde{n}, n)\, p(n \mid j). \tag{13}$$

For $R(\tilde{n} \mid j) \geq 0$, the minimal $R(\tilde{n} \mid j)$ is the minimum of R according to Bayesian decision. That is to say,

$$n^* = \arg\min R(\tilde{n} \mid j). \tag{14}$$

The way to get the minimum of $R(\tilde{n} \mid j)$ is derived as follows:

$$\begin{aligned} R(\tilde{n} \mid j) &= \sum_{\Theta} \lambda(\tilde{n}, n)\, p(n \mid j) \\ &= \sum_{\Theta} (\tilde{n} - n)^2 p(n \mid j) \\ &= \sum_{\Theta} \left[\tilde{n} - E(n \mid j) + E(n \mid j) - n\right]^2 p(n \mid j) \\ &= \sum_{\Theta} \left[\tilde{n} - E(n \mid j)\right]^2 p(n \mid j) \\ &\quad + \sum_{\Theta} \left[E(n \mid j) - n\right]^2 p(n \mid j) \\ &\quad + 2 \sum_{\Theta} \left[E(n \mid j) - n\right] \left[\tilde{n} - E(n \mid j)\right] p(n \mid j). \end{aligned} \tag{15}$$

In (15),

$$E(n \mid j) = \sum_{\Theta} n p(n \mid j). \tag{16}$$

So,

$$\begin{aligned} &2 \sum_{\Theta} \left[E(n \mid j) - n\right] \left[\tilde{n} - E(n \mid j)\right] p(n \mid j) \\ &= 2 \sum_{\Theta} \left[E(n \mid j) - n\right] p(n \mid j) \left[\tilde{n} - E(n \mid j)\right] \\ &= \left[E(n \mid j) - E(n \mid j)\right] \left[\tilde{n} - E(n \mid j)\right] \\ &= 0. \end{aligned} \tag{17}$$

Then,

$$\begin{aligned} R(\tilde{n} \mid j) &= \sum_{\Theta} \lambda(\tilde{n}, n)\, p(n \mid j) \\ &= \sum_{\Theta} \left[\tilde{n} - E(n \mid j)\right]^2 p(n \mid j) \\ &\quad + \sum_{\Theta} \left[E(n \mid j) - n\right]^2 p(n \mid j). \end{aligned} \tag{18}$$

Because $\sum_{\Theta} [E(n \mid j) - n]^2 p(n \mid j)$ has nothing to do with $\tilde{n}$, the minimum of $R(\tilde{n} \mid j)$ is only decided by $\sum_{\Theta} [\tilde{n} - E(n \mid j)]^2 p(n \mid j)$. Only when $\tilde{n} = E(n \mid j)$, $\sum_{\Theta} [\tilde{n} - E(n \mid j)]^2 p(n \mid j) = 0$, and we can get the minimum of $R(\tilde{n} \mid j)$. Therefore, the optimal estimation is

$$n^* = \sum_{\Theta} n p(n \mid j). \tag{19}$$

The conditional probability under the observation of $j(m) = \langle j_e, j_s, j_c \rangle$ [14] is

$$\begin{aligned} p(n \mid j) &= C_L^{j_e} p_e^{j_e} \cdot C_{L-j_e}^{j_s} p_s^{j_s} \cdot C_{L-j_e-j_s}^{j_c} p_c^{j_c} \\ &= \frac{L!}{(L-j_e)!\, j_e!} \cdot \frac{(L-j_e)!}{(L-j_e-j_s)!\, j_s!} \\ &\quad \cdot \frac{(L-j_e-j_s)!}{(L-j_e-j_s-j_c)!\, j_c!} p_e^{j_e} p_s^{j_s} p_c^{j_c} \\ &= \frac{L!}{j_e!\, j_s!\, j_c!} \left(1 - \frac{1}{L}\right)^{n \cdot j_e} \left(\frac{n}{L}\right)^{j_s} \left(1 - \frac{1}{L}\right)^{(n-1) \cdot j_s} \\ &\quad \cdot \left[1 - \left(1 - \frac{1}{L}\right)^n - \frac{n}{L}\left(1 - \frac{1}{L}\right)^{n-1}\right]^{j_c}. \end{aligned} \tag{20}$$

Suppose that the value space of tag number n is $n \in [1, N]$. After normalization processing of (20), we can get

$$\overline{p}(n \mid j) = \frac{\left(L!/j_e!\, j_s!\, j_c!\right) p_e^{j_e} p_s^{j_s} p_c^{j_c}}{\sum_{n=1}^{N} \left(L!/j_e!\, j_s!\, j_c!\right) p_e^{j_e} p_s^{j_s} p_c^{j_c}}. \tag{21}$$

From (19) and (21), the optimal estimation of tag number is

$$\begin{aligned} n^* &= \sum_{n=1}^{N} n \overline{p}(n \mid j) \\ &= \sum_{n=1}^{N} \left(n \cdot \frac{\left(L!/j_e!\, j_s!\, j_c!\right) p_e^{j_e} p_s^{j_s} p_c^{j_c}}{\sum_{n=1}^{N} \left(L!/j_e!\, j_s!\, j_c!\right) p_e^{j_e} p_s^{j_s} p_c^{j_c}} \right). \end{aligned} \tag{22}$$

3.3. The Mechanism of Probability Response. The advanced DFSA based on Bayesian estimation and probability response (BE-PDFSA) can effectively solve the general problem in process of tag identification. By importing the Bayesian estimation, we can estimate the tag number accurately. On the basis of accurate estimation, we can adjust the frame length rationally according to (10). However, the frame length can only be selected from $\{2, 4, 8, 16, 32, 64, 128, 256\}$ because of the limitation of the reader. So we bring in the mechanism of probability response to change the responsive probability of the tags dynamically according to the estimated tag number and frame length which can be selected.

What is more, in the case of large tag number, the throughput of the system would drop rapidly with the increase of tag number which is called the "landslide problem". The mechanism of probability response can also solve this problem by adjusting the responsive probability of the tags dynamically.

The specific process can be described as follows.

Since we have defined the estimated tag number as n^*, therefore the number of unrecognized tags is denoted as $n^\#$ in the rest of paper, which can be calculated by $n^\# = n^* - j_s$. If the frame length which is closest to $n^\#$ is d_i, we set the responsive probability of the unrecognized tags to be $d_i/n^\#$. If $d_i \geq n^\#$, the responsive probability will be higher than 1 which means the number of slots is more than the tag number. In

this case, the collision rate will not be so high. However, the responsive probability can only be no higher than 1, so we set the responsive probability to be 1 which means all the tags will respond in this frame. If $d_i < n^{\#}$, the tag number will be more than the number of slots in one frame. The collision rate will increase with the increase of the tag number. By importing the mechanism of probability response, the number of responsive tags will be d_i in theory instead of $n^{\#}$, and the throughput of the system will be increased. In the case of large tag number, the inequality will change to $d_i \ll n^{\#}$. The max frame length of the reader is 256 ($d_{\max}$), and the collision rate will increase rapidly. However, the mechanism of probability response can effectively solve the "landslide problem" by decreasing the number of responsive tags to the frame length. The tags which are not selected will wait for the next frame and repeat the upper process.

3.4. Working Process of the Whole Algorithm. By importing the Bayesian estimation and the mechanism of probability response, BE-PDFSA can improve the performance of the whole system significantly. Bayesian estimation is mainly used in the process of tag estimation to get an accurate estimation of the tag number. The mechanism of probability response is used in the process of response to further reduce the collision rate of the system especially in the case of large tag number. In this way, we can try our best to make the number of tags to respond in one frame equal to the frame length we select in order to maximize the throughput of the whole system and minimize the collision rate. In order to let everyone have a clearer understanding of the whole process, the proposed algorithm procedure can be divided into the following four steps.

Step 1. Setting the initial frame length L and sending the request command to tags asking for their information.

Step 2. All the tags randomly select one slot to respond and finish the identification of one frame.

Step 3. Count the result of this frame (j_e, j_s, j_c) and use the result to estimate the tag number (n^*) through our estimation algorithm.

Step 4. Calculate the number of unrecognized tags $n^{\#}$ ($n^{\#} = n^* - j_s$). Select the value of frame length d_i from {2, 4, 8, 16, 32, 64, 128, 256} which is the closest to the unrecognized tag number $n^{\#}$ and adjust the responsive probability of the tags to be $d_i/n^{\#}$. Then, turn to Step 2.

If the query result from the reader is $\langle j_e = d_i,\ j_s = 0,\ j_c = 0\rangle$ for continuously three times, the algorithm will judge that all the tags are recognized and quit the cycle.

We can see it more clearly from Figure 2.

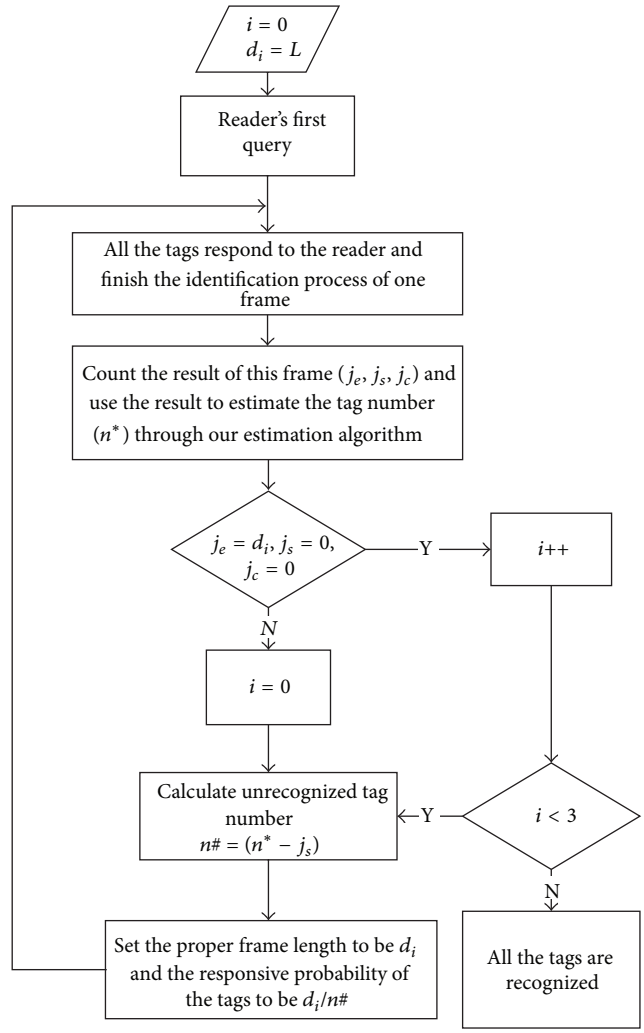

Figure 2: Process of the whole algorithm.

4. Simulation Results and Analysis

4.1. Settings of the Simulation Scene. In RFID system, the aim of using anticollision algorithm is to improve the recognition rate of the tags, to reduce resource consumption, and most importantly to improve the efficiency of the whole system. For the key steps of DFSA, the accuracy of the estimation algorithm is the most important. Here, we introduce error rate to measure the performance of the algorithm. Suppose the tag number is n and the estimated tag number is n^*, then the error rate can be expressed as

$$e = \frac{|n^* - n|}{n}. \tag{23}$$

After the tag estimation process, the algorithm adjusts the responsive probability of the unrecognized tags and the frame length based on the estimated tag number. For the whole system, the resource consumption and the throughput of the system are important parameters. So in the simulation, the total number of slots used in the system is defined as the resource consumption, and the throughput of the system has been given as in (8).

In addition, the slot collision rate and slot idle rate also reflect the degree of the utilization of system resources. Suppose that the value space of tag number in the communication range of the reader is $n \in [1, 1000]$, the max frame length of

Table 1: Settings of the simulation parameters.

Parameters	Tag anticollision algorithm
Reader number	1
Tag number	1–1000
Data transmission rate (Kb/s)	100
Data channel frequency (MHz)	915
Initial frame length	$L_{\text{ini}} = \{16, 32, 64, 128\}$
Number of slots occupied for identification	1
Frame length doubled threshold	Collision rate $p_s \in [0.5, 1]$
Frame length half threshold	Collision rate $p_s \in [0, 0.5]$ & idle rate $p_i \in [0.5, 1]$
Frame length hold threshold	Collision rate $p_s \in [0, 0.5]$ & idle rate $p_i \in [0, 0.5]$
Antenna polarity	Omni

the reader is 256, and the value space of optional frame length is $A = \{N_i, N_i = 2^i\}$ $(i \leq 8)$.

Because we still use the dynamic framed-slotted ALOHA algorithm (DFSA) in the main identification procedure of the system, DFSA adjusts the frame length of the next frame dynamically based on the current collision rate, idle rate, and the successful identification rate of the slot. The relevant configurations of the simulation is same as that in [15].

The specific settings of the simulation parameters are given in Table 1.

4.2. Simulation Results and Analysis. The algorithm can be divided into two parts: tag number estimation and tag identification. So we also compare the algorithm in two sides. We will compare the algorithm we proposed with the minimum tag number estimation algorithm and Jae-Ryong Cha algorithm on the side of error rate. For the tag identification algorithm, we will compare Bayesian estimation probability DFSA (BE-PDFSA) with DFSA algorithm in resource consumption, system throughput, system collision rate, and system idle rate.

From Figure 3, we can see that with the same initial frame length, the performance of Minimum tag number estimation is the worst, considering the least factors. When the tag number reaches 1000, its error rate is nearly 70%. However, the performance of BE-PDFSA is far better than other algorithms. Especially when the frame length is longer than 128, the error rate of the other two algorithms gradually increases with the increase of tag number, and its value is basically higher than 0.3. On the contrary, the Bayesian estimation algorithm is relatively stable, and its error rate stays around 0.1 mostly. So the estimation algorithm we proposed shows the characteristic of high robustness.

From Figure 4, we can see that as the tag number increases, the total source consumption of DFSA and BE-PDFSA all has the upward trend. However, the source consumption of BE-PDFSA is less than that of DFSA, and there will be a growing gap in consumption between the two algorithms with the increase of tag number. When the tag number reaches 1000, the source consumption of BE-PDFSA is about 1/7 of DFSA. According to (10), in the view of source consumption, the performance of BE-PDFSA is far better than DFSA especially in the case of large tag number.

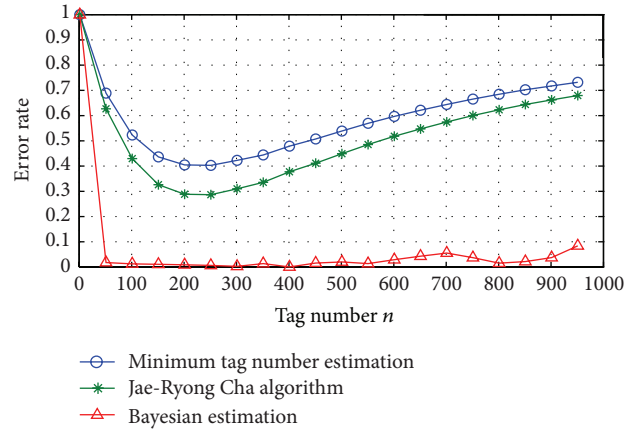

Figure 3: Comparison of error rate for algorithms.

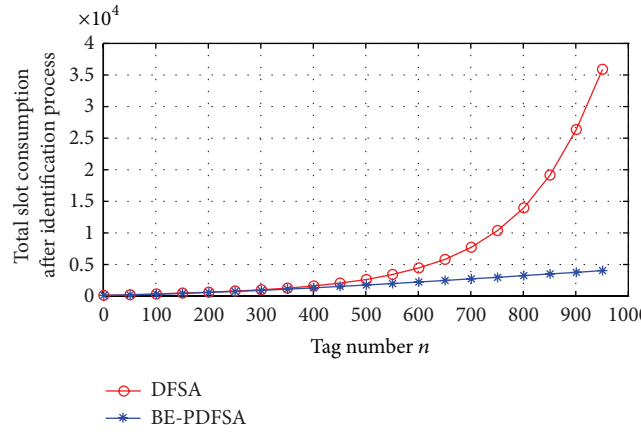

Figure 4: Comparison of total source consumption in identification process.

In Figure 5, the trend of throughput of the two algorithms is almost the same. The throughput of BE-PDFSA reaches a maximum when the tag number is about 100. The number of tags when DFSA reaches its maximum is about 200, but it is still less than that of BE-PDFSA. After reaching the maximum, the throughput of DFSA decreases sharply, though our algorithm decreases relatively slowly and becomes stable.

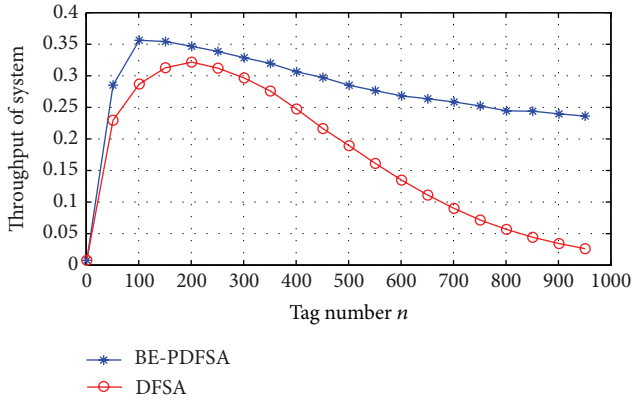

Figure 5: Comparison of throughput for algorithms.

When the tag number is 1000, the throughput of BE-PDFSA can stay around 0.25 which is much larger than that of DFSA. We can see the stability and reliability of our algorithm.

Figure 6 shows the comparison of probability of failure in identification process. Figure 6(a) is the comparison of collision rate for BE-PDFSA and DFSA. With the increase of tag number, the collision rate of DFSA grows nearly in linear. However, BE-PDFSA shows a better performance. Although its collision rate also increases with the increase of tag number, the slope of the curve is smaller than that of DFSA, and the curve becomes stable in the end. That is because with the increase of tag number, more and more tags will respond to the reader at the same time which will cause the increase in collision rate. After using the Bayesian estimation and probability response, the number of tags to respond and the number of slots are as close as they can which slows down the increase of collision rate. On the other side, from Figure 6(b), BE-PDFSA also shows better performance in idle rate. So combined with Figure 6(a), we can see our algorithm improving the stability of DFSA after importing Bayesian estimation and probability response.

5. Conclusion

In this paper, we propose an improved dynamic framed-slotted ALOHA algorithm based on Bayesian estimation and probability response. The Bayesian estimation can improve the accuracy of estimation algorithm by taking advantage of statistical properties in identification process of tags. The mechanism of probability response can adjust the responsive probability of tags especially when the tag number is larger than the max frame length to reduce collision rate and improve the throughput of the whole system.

In general, this algorithm solves the problem that there would be a big error in traditional process of tag estimation because of lacking observations. At the same time, by using the optimal conditions of system throughput, we propose the mechanism of probability response to make the theoretical number of tags to respond be the same as the frame length to improve the efficiency of the system and save the source of the whole system. Finally, the simulation results show the stability of our algorithm and prove the improvement in the performance of the algorithm.

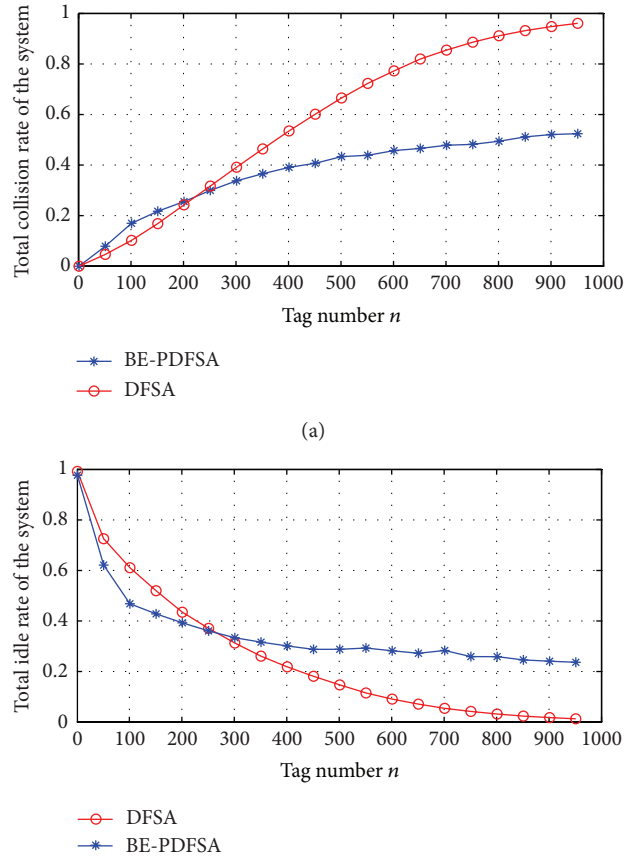

Figure 6: (a) Comparison of collision rate for algorithms in identification process. (b) Comparison of idle rate for algorithms in identification process.

Acknowledgments

This work is supported in part by the Fundamental Research Funds for the Central Universities (2012RC0307), NSFC Grant (61271186), and Beijing Municipal Commission of Education (the service cloud platform of new cultural form based on mobile internet).

References

[1] E. W. T. Ngai, K. K. L. Moon, F. J. Riggins, and C. Y. Yi, "RFID research: an academic literature review (1995–2005) and future research directions," *International Journal of Production Economics*, vol. 112, no. 2, pp. 510–520, 2008.

[2] Y. Zhang, M. G. Amin, and S. Kaushik, "Localization and tracking of passive RFID tags based on direction estimation," *International Journal of Antennas and Propagation*, vol. 2007, Article ID 17426, 9 pages, 2007.

[3] R. Want, "An introduction to RFID technology," *IEEE Pervasive Computing*, vol. 5, no. 1, pp. 25–33, 2006.

[4] L. Zhu and T.-S. P. Yum, "A critical survey and analysis of RFID anti-collision mechanisms," *IEEE Communications Magazine*, vol. 49, no. 5, pp. 214–221, 2011.

[5] A. L. McBride, "An overview of unslotted Aloha in a VSAT network," in *Proceedings of the IEEE Global Telecommunications Conference: Communications Broadening Technology Horizons (GLOBECOM '86)*, pp. 1479–1488, 1986.

[6] R. Metcalfe, "Steady state analysis of a slotted and controlled Aloha system with blocking," in *Proceedings of the 6th Hawaii Conference System Science*, 1973.

[7] V. Namboodiri, M. DeSilva, K. Deegala, and S. Ramamoorthy, "An extensive study of slotted Aloha-based RFID anti-collision protocols," *Computer Communications*, vol. 35, no. 16, pp. 1955–1966, 2012.

[8] J.-B. Eom and T.-J. Lee, "Accurate tag estimation for dynamic framed-slotted ALOHA in RFID systems," *IEEE Communications Letters*, vol. 14, no. 1, pp. 60–62, 2010.

[9] F. C. Schoute, "Dynamic frame length ALOHA," *IEEE Transactions on Communications*, vol. 31, no. 4, pp. 565–568, 1983.

[10] D. M. Dobkin, *The RF in RFID-Passive UHF RFID in Practice*, Newnes, Burlington, Mass, USA, 2008.

[11] J.-R. Cha and J.-H. Kim, "Novel anti-collision algorithms for fast object identification in RFID system," in *Proceedings of the 11th International Conference on Parallel and Distributed Systems Workshops (ICPADS '05)*, vol. 2, pp. 63–67, July 2005.

[12] H. Vogt, "Efficient object identification with passive RFID tags," in *Proceedings of the International Conference on Pervasive Computing*, pp. 1–16, Zurich, Switzerland, 2002.

[13] H. Vogt, "Multiple object identification with passive RFID tags," in *Proceedings of the IEEE International Conference on Systems, Man and Cybernetics*, pp. 651–656, Hammamet, Tunisia, October 2002.

[14] W.-T. Chen, "An accurate tag estimate method for improving the performance of an RFID anticollision algorithm based on dynamic frame length ALOHA," *IEEE Transactions on Automation Science and Engineering*, vol. 6, no. 1, pp. 9–15, 2009.

[15] K. Ali, H. Hassanein, and A.-E. M. Taha, "RFID anti-collision protocol for dense passive tag environments," in *Proceedings of the 32nd IEEE Conference on Local Computer Networks (LCN '07)*, pp. 819–824, Dublin, Ireland, October 2007.

Hindawi Publishing Corporation
International Journal of Antennas and Propagation
Volume 2013, Article ID 961042, 5 pages
http://dx.doi.org/10.1155/2013/961042

Research Article

A Compact RFID Reader Antenna for UHF Near-Field and Far-Field Operations

Lai Xiao zheng,[1] Xie Zeming,[2] and Cen Xuanliang[2]

[1] *School of Computer Science & Engineering, South China University of Technology, Guangzhou 510006, China*
[2] *School of Electronic & Information, South China University of Technology, Guangzhou 510641, China*

Correspondence should be addressed to Lai Xiao zheng; laixz@scut.edu.cn

Received 17 February 2013; Revised 8 July 2013; Accepted 9 July 2013

Academic Editor: Yuan Yao

A compact loop antenna is presented for mobile ultrahigh frequency (UHF) radio frequency identification (RFID) application. This antenna, printed on a 0.8 mm thick FR4 substrate with a small size of 31 mm × 31 mm, achieves good impedance bandwidth from 897 to 928 MHz, which covers USA RFID Band (902–928 MHz). The proposed loop configuration, with a split-ring resonator (SRR) coupled inside it, demonstrates strong and uniform magnetic field distribution in the near-field antenna region. Its linearly polarized radiation pattern provides available far-field gain. Finally, the reading capabilities of antenna are up to 56 mm for near-field and 1.05 m for far-field UHF RFID operations, respectively.

1. Introduction

Radio frequency identification (RFID) technology has been rapidly developed for automated identification and tracking of objects in warehouse, supply chain, industry, and commerce [1]. Currently, mobile UHF RFID technology has received much attention owing to its advantages in cost, portability, and item-level applications. Mobile UHF RFID service is defined as a compact UHF RFID reader into a mobile phone. Anyone with it can directly identify the RFID tag attached product and access mobile internet by wireless communication for searching, verifying, and managing product information [2].

The challenge of mobile UHF RFID reader is that the reader antenna must be miniaturized into the mobile phone and have both near-field and far-field operation for various objects and applications [3]. Electromagnetically far-field operation is commonly used to achieve long reading range, and typical UHF RFID reader antenna works with a pure far-field characteristic [4]. Inductively near-field operation is usually used for objects surrounded by metals or liquids [5]. Recently, a group of loop-type antennas have been considered with a pure near-field characteristic [6–13]. Few papers about UHF reader antenna for both near-field and far-field operations are presented, but they have too large size to integrate in the mobile phone: one has a dimension of 184× 174 mm^2 [14], and another smaller antenna is 72.3×72.3 mm^2 [15].

In order to address the size constraint problem, we have designed a loop antenna with both near-field and far-field characteristics. But it has too narrow bandwidth of 13.5 MHz (915.5–929 MHz) [16]. The United States Federal Communications Commission (FCC) designates 902–928 MHz as the special frequency allocation for UHF RFID band. Most of the countries approve a part of USA band for RFID operation, for example, China band (920–925 MHz), Korea band (917–924 MHz), Australia band (918–926 MHz), and so on [17].

Therefore, we present a novel folded-dipole loop antenna with split-ring resonator (SRR) structure in this paper. An SRR element is coupled inside the folded-dipole loop and formed by a concentric metal ring with a split. The antenna prototype is fabricated and achieves a measured matching bandwidth of 31 MHz (897–928 MHz), which covers the USA RFID band (902–928 MHz). Simulation and measurement show that the proposed antenna has strong surface current distribution, uniform magnetic near-field distribution, and

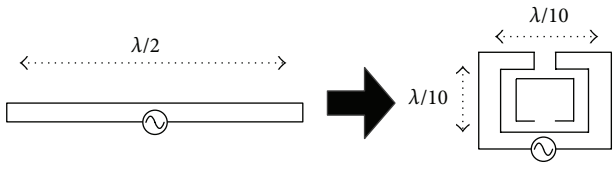

Figure 1: Size comparison of folded-dipole loop with SRR loading.

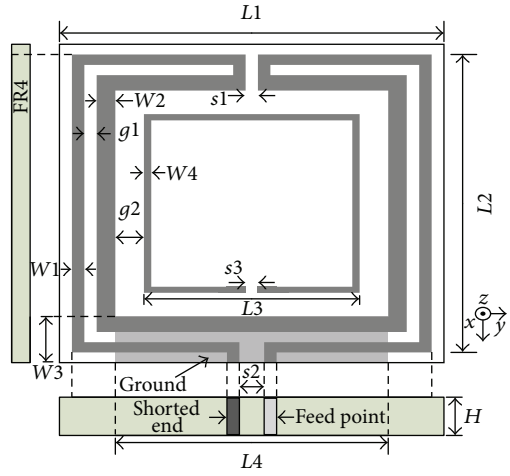

Figure 2: Geometry of the proposed antenna.

available far-field gain. The reading capability of prototype is up to 56 mm with near-field RFID tag and up to 1.05 m with conventional far-field RFID tag.

2. Antenna Design

Loop antennas are commonly used for communication and RFID systems [18–22]. At LF and HF bands, a physically large loop is still a very small electrical fraction compared to the operating wavelength. So, the conventional RFID antenna design at LF and HF bands is to use a multiturn loop. However, it is not suggested at UHF band because the multiturn loop or spiral inductor has poor far-field gain. The other way is to use folded-dipole loop [23]. The folded-dipole loop antenna has good size reduction and exhibits better far-field gain than multiturn loop.

In this paper, a novel folded-dipole antenna with parasitic element is proposed, as shown in Figure 1. The bent folded dipole forms a large outer loop with a split, and a single spilt ring combines a small inner loop. The inductive loading is created by the ring, while the capacitive effect is determined by the split of the ring. Both inductive and capacitive loadings act as an LC tank circuit, which can enhance the magnetic resonance, and realize antenna size reduction. As shown in Figure 1, the total length of proposed antenna is miniaturized as the same resonance condition as the conventional folded-dipole antenna of half wavelength.

In Figure 2, the geometry of antenna was designed on an FR-4 substrate (dielectric constant $\varepsilon_r = 4.4$, loss tangent $\delta = 0.02$, and thickness $H = 1.6$ mm), and the whole antenna

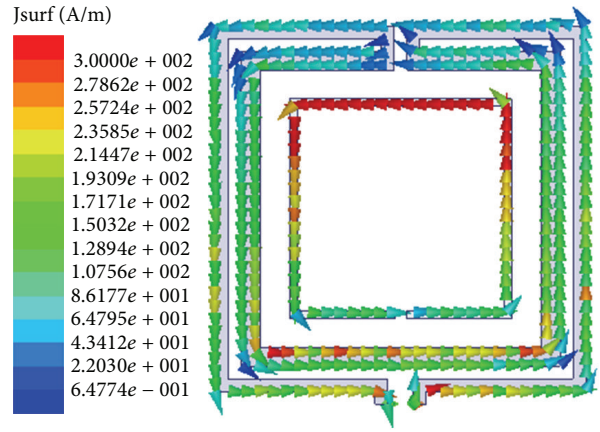

Figure 3: Antenna surface current distribution.

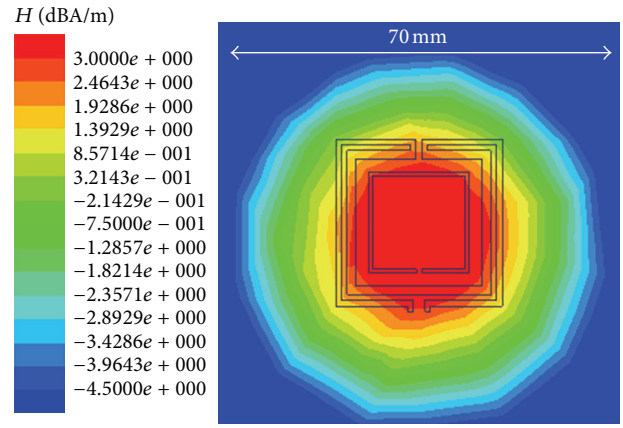

Figure 4: Near-field magnetic distribution (xy-plane, $z = 10$ mm).

size is $L1$ (31 mm) $\times L1$ (31 mm). On the top view of substrate, the dimensions of folded-dipole loop are $L2 = 29$ mm, $s1 = 1.0$ mm, $s2 = 2.0$ mm, $W1 = 1.0$ mm, $W2 = 1.5$ mm, and $g1 = 1.0$ mm. The dimensions of SRR are $g2 = 3.3$ mm, $s3 = 0.9$ mm, and $W4 = 1.2$ mm. On the bottom view, the dimensions of the ground are $L3 = 22$ mm and $W3 = 4.5$ mm.

The antenna was simulated at the centre frequency of interesting band (915 MHz), by using Ansoft High Frequency Structure Simulator (HFSS) software. The simulation result of antenna surface current distribution is shown in Figure 3. It can be seen that the current remains in-phase at both the outer loop and inner SRR and the current along SRR is larger in amplitude relative to that along the outside folded-dipole loop. The in-phase current presented a uniform and strong magnetic field distribution at xy-plane and $z = 10$ mm, as shown in Figure 4. Thus, the tags with inductive coupling can be interrogated in the near-field antenna region.

3. Results and Discussion

A prototype of the proposed antenna was fabricated, as shown in Figure 5. The entire area of prototype is just 31 ×

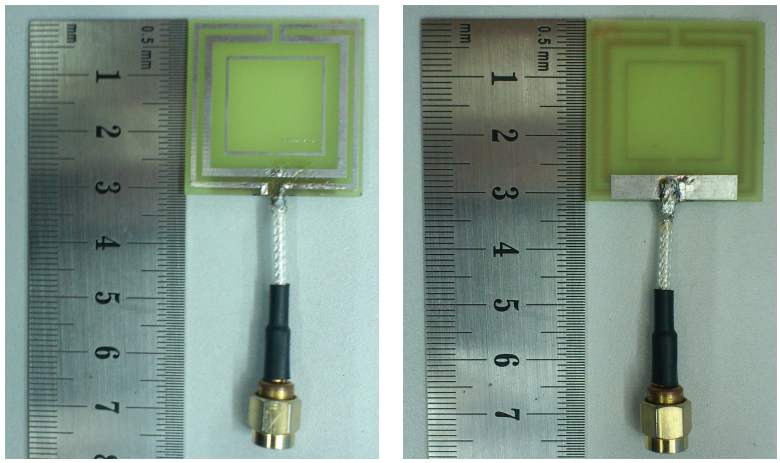

(a) (b)

Figure 5: Photograph of antenna prototype. (a) Top view, (b) bottom view.

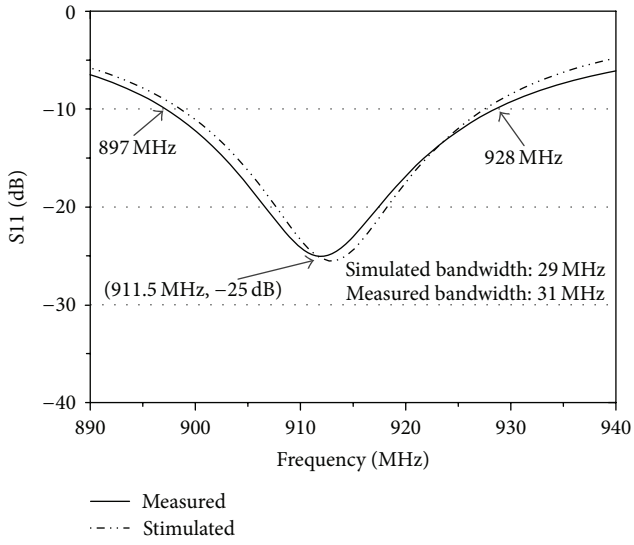

Figure 6: Reflection coefficient for proposed antenna.

31 mm^2, as a coin of one CNY. The simulated and measured matching bandwidth of the proposed antenna is shown in Figure 6. There is good agreement between simulation and measurement. The measured bandwidth of the prototype is 31 MHz (897–928 MHz), under the condition of reflection coefficient less than −10 dB. It completely covers the USA RFID band (902–928 MHz).

The schematic view of near-field reading test is presented in Figure 7(a). As shown in Figure 7(c), the proposed antenna prototype is fabricated on the test stand, and the near-field button tag, attached to polyfoam, is parallel to the surface of antenna. The read range between antenna and tag is achieved along the positive Z-axis. As shown in Figure 7(d), the Impinj UHF button of 13∗10 mm^2 dimension was taken as the reference tag, and the Impinj Technology Speedway R420 reader was used for measurement [24].

Table 1: Comparison of near-field read-range.

Environment	Transmission power at 10 dBm	Transmission power at 20 dBm
Air	30 mm	48 mm
Water container	42 mm	56 mm
Paper	33 mm	36 mm
Plant surface (corn)	37 mm	38 mm
Hand skin (human)	24 mm	29 mm

The read capability of near-field antenna includes read width and read-range. With Impinj UHF button parallel to the prototype, the maximum read width of xy-plane is 70 mm at $z = 10$ mm, as shown in Figure 7(b). It agrees well with the simulated results of magnetic field distribution in Figure 4.

Furthermore, the near-field read-range of test scene in Figure 7(a) is measured under a different transmission power and different environment. As shown in Table 1, we can see the measured results with Impinj UHF button tag attached on different objects, including air, liquids, paper, plant, and human body. The maximum read-range of near-field test can reach 56 mm with the tag attached to water container, along the positive Z-axis under the transmission power level of 20 dBm. The read-range in the other environment is similar to that in the air. This is a major advantage of the near-field RFID operation.

The simulated and measured radiation patterns of the proposed antenna are presented in Figure 8. The measured radiation patterns were obtained by the anechoic chamber. Figures 8(a) and 8(b) show the radiation patterns at 915 MHz in the two orthogonal planes (E-plane and H-plane). The far-field gain of proposed antenna achieves −2.0 dBi at the bidirectional X-axis and negative Z-axis, which shows that the proposed antenna can be acceptable for far-field RFID operation.

To examine the far-field performance, the experiment of far-field reading distance has been performed by using Impinj

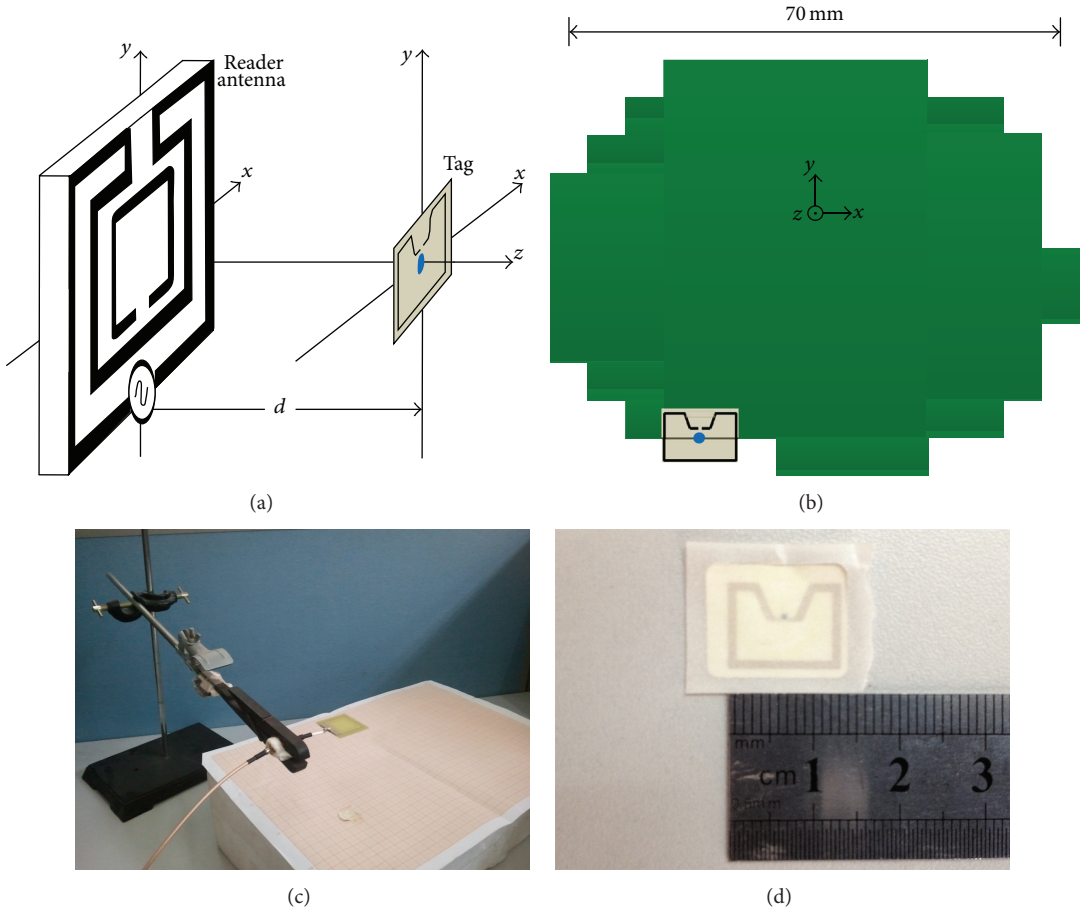

Figure 7: Near-field measurement. (a) Schematic view. (b) Read width at xy-plane and $z = 10$ mm. (c) Test scene. (d) Impinj UHF button.

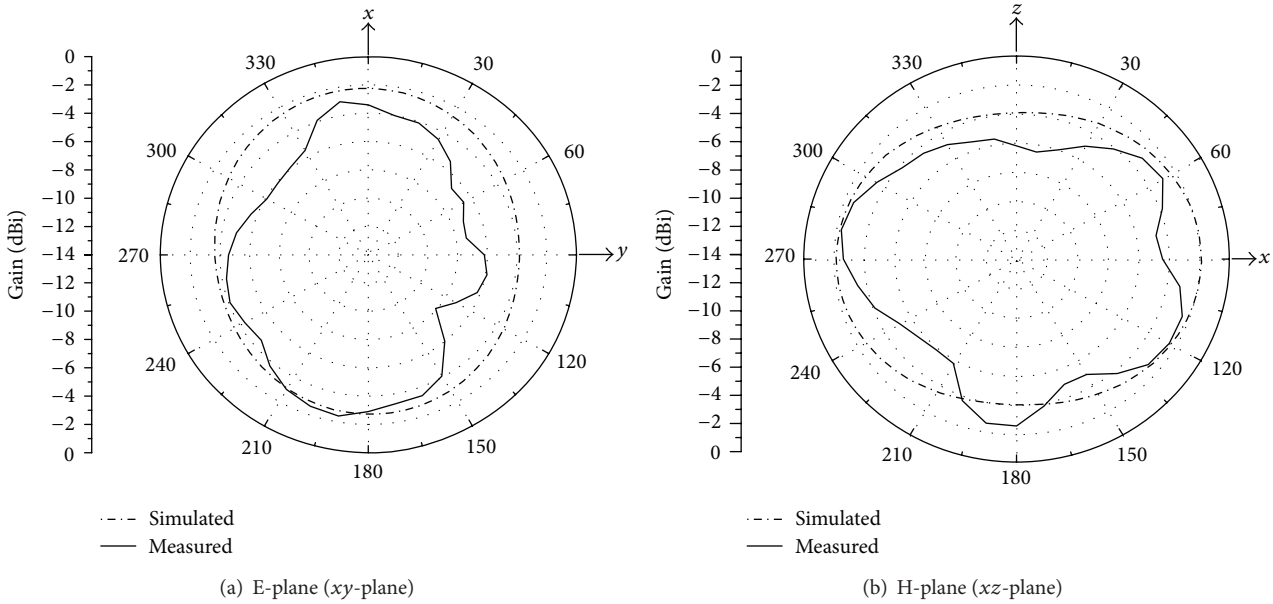

Figure 8: Simulated and measured far-field radiation patterns.

R420 reader. It is shown that the proposed antenna, with conventional dipole tag in the air, has a maximum reading distance of 1.05 m, at the transmission power level of 20 dBm (0.1 W). But the different environment seriously affects the far-field reading performance. When the tag is attached to water container or conducting plate (human body), the far-field reading distance reduces rapidly.

4. Conclusions

In this paper, a folded-dipole loop antenna with SRR has been investigated for mobile UHF RFID applications. The coupled SRR element miniaturizes this antenna to a compact size of 31 mm × 31 mm. Simulation and measurement of antenna implemented sufficient impedance bandwidth (897–928 MHz), uniform magnetic near-field distribution, and suitable far-field gain. Experiments by proposed antenna have shown good capability of both near-field and far-field tag reading. Such a compact antenna is suitable for both near-field and far-field UHF RFID operations.

Acknowledgments

This paper is supported by the National High Technology Research and Development Program (863 program) of China (2008AA04A103), Science and Technology Planning Project of Guangdong Province (2011B080701068), and National Natural Science Foundation of China (61101015 & 60971052).

References

[1] K. Finkenzeller, *RFID Handbook, Radio-Frequency Identification Fundamentals and Applications*, Wiley, New York, NY, USA, 2nd edition, 2004.

[2] J. Chae and S. Oh, "Information Report on Mobile RFID in Korea," ISO/IEC JTC1/SC 31/WG4 N0922, Information paper, ISO/IEC JTC1 SC31 WG4 SG 5, 2005.

[3] P. V. Nikitin, K. V. S. Rao, and S. Lazar, "An overview of near field UHF RFID," in *Proceedings of the IEEE International Conference on RFID*, pp. 166–174, Grapevine, Tex, USA, March 2007.

[4] B. Glover and H. Bhatt, *RFID Essentials*, O'Reilly, Sebastopol, Calif, USA, 2006.

[5] F. Fuschini, C. Piersanti, L. Sydanheimo, L. Ukkonen, and G. Falciasecca, "Electromagnetic analyses of near field UHF RFID systems," *IEEE Transactions on Antennas and Propagation*, vol. 58, no. 5, pp. 1759–1770, 2010.

[6] X. Qing, C. K. Goh, and Z. N. Chen, "Segmented loop antenna for UHF near-field RFID applications," *Electronics Letters*, vol. 45, no. 17, pp. 872–873, 2009.

[7] X. Z. Lai, Z. M. Xie, Q. Q. Xie, and J. W. Chao, "A Srr-based near field RFID antenna," *Progress in Electromagnetics Research C*, vol. 33, pp. 133–144, 2012.

[8] X. Qing, Z. N. Chen, and C. K. Goh, "UHF near-field RFID reader antenna with capacitive couplers," *Electronics Letters*, vol. 46, no. 24, pp. 1591–1592, 2010.

[9] X. Li, J. Liao, Y. Yuan, and D. Yu, "Eye-shaped segmented reader antenna for near-field UHF RFID applications," *Progress in Electromagnetics Research*, vol. 114, pp. 481–493, 2011.

[10] H.-W. Liu, K.-H. Wu, and C.-F. Yang, "UHF reader loop antenna for near-field RFID applications," *Electronics Letters*, vol. 46, no. 1, pp. 10–11, 2010.

[11] X. Li and Z. Yang, "Dual-printed-dipoles reader antenna for UHF near-field RFID applications," *IEEE Antennas and Wireless Propagation Letters*, vol. 10, pp. 239–242, 2011.

[12] X. Qing, C. K. Goh, and Z. N. Chen, "A broadband uhf near-field rfid antenna," *IEEE Transactions on Antennas and Propagation*, vol. 58, no. 12, pp. 3829–3838, 2010.

[13] C. F. Huang and Y. F. Huang, "Design of RFID reader antenna for exclusively reading single one in tag assembling production," *International Journal of Antennas and Propagation*, vol. 2012, Article ID 162684, 5 pages, 2012.

[14] B. Shrestha, A. Elsherbeni, and L. Ukkonen, "UHF RFID reader antenna for near-field and far-field operations," *IEEE Antennas and Wireless Propagation Letters*, vol. 10, pp. 1274–1277, 2011.

[15] A. L. Borja, A. Belenguer, J. Cascon, and J. R. Kelly, "A reconfigurable passive UHF reader loop antenna for near-field and far-field RFID applications," *IEEE Antennas and Wireless Propagation Letters*, vol. 11, pp. 580–583, 2012.

[16] X. Z. Lai, Z. M. Xie, and X. L. Cen, "Compact loop antenna for near-field and far-field UHF RFID applications," *Progress in Electromagnetics Research C*, vol. 37, pp. 171–182, 2013.

[17] UHF for RFID Regulations, http://www.gs1.org/docs/epcglobal/UHF_Regulations.pdf.

[18] Z. Xing, L. Wang, C. Wu, J. Li, and M. Zhang, "Characteristics and application of a novel loop antenna to UHF RFID receivers," *International Journal of Antennas and Propagation*, vol. 2011, Article ID 480717, 7 pages, 2011.

[19] Y.-W. Chi and K.-L. Wong, "Internal compact dual-band printed loop antenna for mobile phone application," *IEEE Transactions on Antennas and Propagation*, vol. 55, no. 5, pp. 1457–1462, 2007.

[20] D.-O. Kim, C.-Y. Kim, and D.-G. Yang, "Flexible Hilbert-curve loop antenna having a triple-band and omnidirectional pattern for WLAN/WiMAX applications," *International Journal of Antennas and Propagation*, vol. 2012, Article ID 687256, 9 pages, 2012.

[21] C.-W. Chiu, C.-H. Chang, and Y.-J. Chi, "Multiband folded loop antenna for smart phones," *Progress in Electromagnetics Research*, vol. 102, pp. 213–226, 2010.

[22] H. Lee and H. Lee, "Isolation improvement technique for two closely spaced loop antennas using MTM absorber cells," *International Journal of Antennas and Propagation*, vol. 2012, Article ID 736065, 7 pages, 2012.

[23] Y.-T. Im, J.-H. Kim, and W.-S. Park, "Matching techniques for miniaturized UHF RFID loop antennas," *IEEE Antennas and Wireless Propagation Letters*, vol. 8, pp. 266–270, 2009.

[24] UHF Gen 2 for item-level tagging, http://www.impinj.com/Documents/Applications/White_Papers/Technology/UHF_Gen_2_for_Item-level_Tagging/.